16

Human eye sensitivity and photometric quantities

The recipient of the light emitted by most visible-spectrum LEDs is the human eye. In this chapter, the characteristics of human vision and of the human eye and are summarized, in particular as these characteristics relate to human eye sensitivity and photometric quantities.

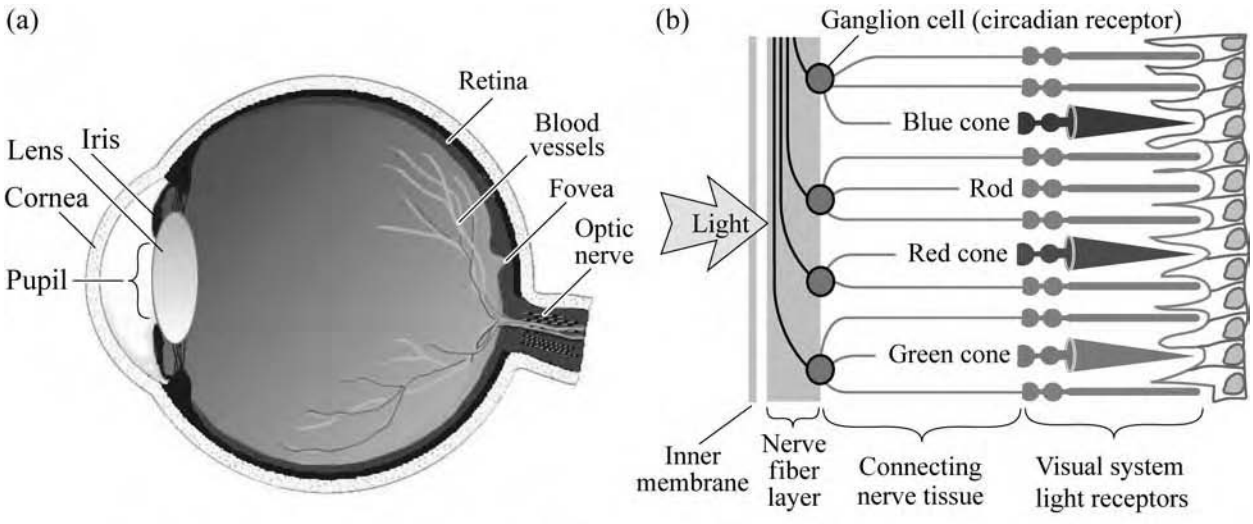

Fig. 16.1. (a) Cross section through a human eye. (b) Schematic view of the retina including rod and cone light receptors (adapted from Encyclopedia Britannica, 1994).

16.1 Light receptors of the human eye

Figure 16.1 (a) shows a schematic illustration of the human eye (Encyclopedia Britannica, 1994). The inside of the eyeball is clad by the retina, which is the light-sensitive part of the eye. The illustration also shows the fovea, a cone-rich central region of the retina which affords the high acuteness of central vision. Figure 16.1 (b) shows the cell structure of the retina including the light-sensitive ***rod cells*** and ***cone cells***. Also shown are the ganglion cells and nerve fibers that transmit the visual information to the brain. Rod cells are more abundant and more light sensitive than cone cells. Rods are sensitive over the entire visible spectrum. There are three types of cone

cells, namely cone cells sensitive in the red, green, and blue spectral range. The cone cells are therefore denoted as the red-sensitive, green-sensitive, and blue-sensitive cones, or simply as the red, green, and blue cones.

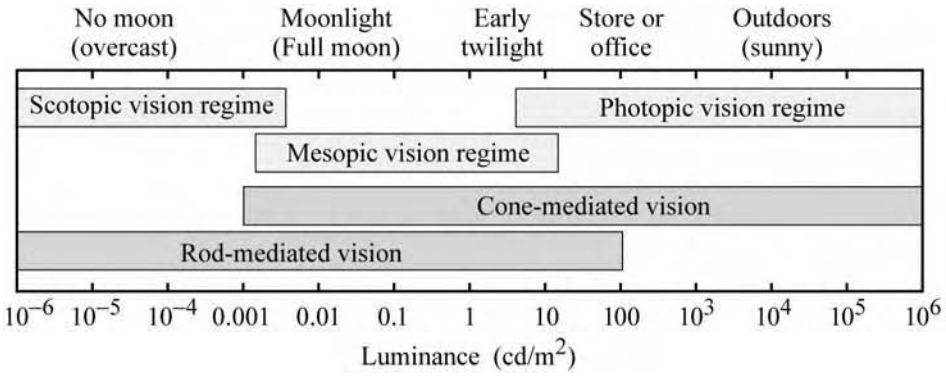

Fig. 16.2. Approximate ranges of vision regimes and receptor regimes (after Osram Sylvania, 2000).

Three different vision regimes are shown in Fig. 16.2 along with the receptors relevant to each of the regimes (Osram Sylvania, 2000). ***Photopic vision*** relates to human vision at high ambient light levels (e.g. during daylight conditions) when vision is mediated by the cones. The photopic vision regime applies to luminance levels > 3 cd/m^2. ***Scotopic vision*** relates to human vision at low ambient light levels (e.g. at night) when vision is mediated by rods. Rods have a much higher sensitivity than the cones. However, the sense of color is essentially lost in the scotopic vision regime. At low light levels such as in a moonless night, objects lose their colors and only appear to have different gray levels. The scotopic vision regime applies to luminance levels < 0.003 cd/m^2. ***Mesopic vision*** relates to light levels between the photopic and scotopic vision regime (0.003 cd/m^2 < mesopic luminance < 3 cd/m^2).

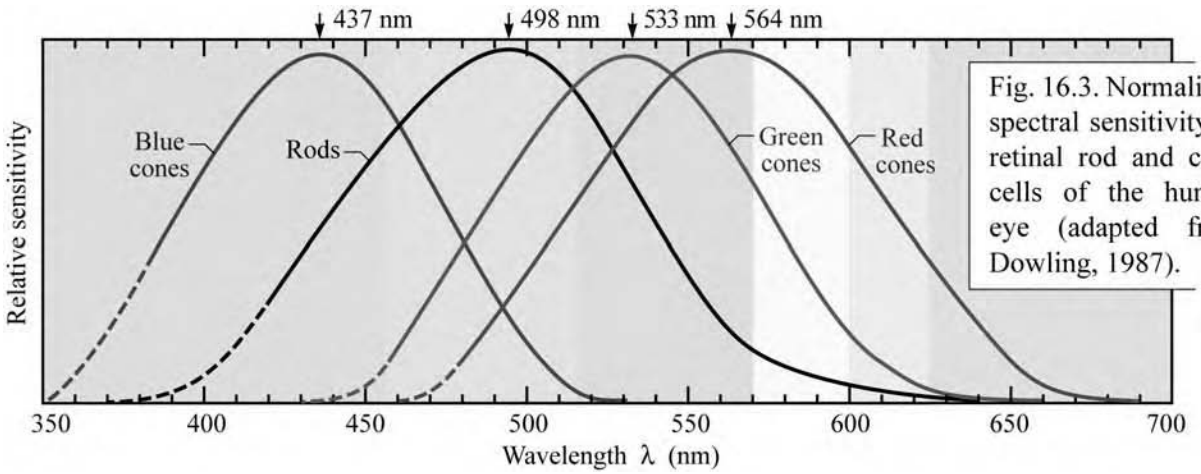

Fig. 16.3. Normalized spectral sensitivity of retinal rod and cone cells of the human eye (adapted from Dowling, 1987).

The approximate spectral sensitivity functions of the rods and three types or cones are shown in Fig. 16.3 (Dowling, 1987). Inspection of the figure reveals that night-time vision (scotopic vision) is weaker in the red spectral range and thus stronger in the blue spectral range as compared to day-time vision (photopic vision). The following discussion mostly relates to the photopic vision regime.

16.2 Basic radiometric and photometric units

The physical properties of electromagnetic radiation are characterized by ***radiometric units***. Using radiometric units, we can characterize light in terms of physical quantities; for example, the number of photons, photon energy, and ***optical power*** (in the lighting community frequently called the ***radiant flux***). However, the radiometric units are irrelevant when it comes to light perception by a human being. For example, infrared radiation causes no luminous sensation in the eye. To characterize the light and color sensation by the human eye, different types of units are needed. These units are called ***photometric units***.

The ***luminous intensity***, which is a photometric quantity, represents the light intensity of an optical source, as perceived by the human eye. The luminous intensity is measured in units of ***candela*** (cd), which is a base unit of the International System of Units (SI unit). The present definition of luminous intensity is as follows: *a monochromatic light source emitting an optical power of (1/683) watt at 555 nm into the solid angle of 1 steradian (sr) has a luminous intensity of 1 candela (cd).*

The unit *candela* has great historical significance. All light intensity measurements can be traced back to the candela. It evolved from an older unit, the ***candlepower***, or simply, the ***candle***. The original, now obsolete, definition of one candela was the light intensity emitted by a plumber's candle, as shown in Fig. 16.4, which had a specified construction and dimensions:

one standardized candle emits a luminous intensity of 1.0 cd

.

Fig. 16.4. Plumber's candle, as used by plumbers in the nineteenth century to melt lead solder when joining water pipes.

The luminous intensity of a light source can thus be characterized by giving the number of standardized candles that, when combined, would emit the same luminous intensity. Note that *candlepower* and *candle* are non-SI units that are no longer current and rarely used at the present time.

The ***luminous flux***, which is also a photometric quantity, represents the light power of a source as perceived by the human eye. The unit of luminous flux is the ***lumen*** (lm). It is defined as follows: *a monochromatic light source emitting an optical power of (1/683) watt at 555 nm has a luminous flux of 1 lumen (lm).* The lumen is an SI unit.

A comparison of the definitions for the candela and lumen reveals that 1 candela equals 1 lumen per steradian or cd = lm/sr. Thus, an isotropically emitting light source with luminous intensity of 1 cd has a luminous flux of 4π lm = 12.57 lm.

The ***illuminance*** is the luminous flux incident per unit area. The illuminance measured in ***lux*** (lux = lm/m^2). It is an SI unit used when characterizing illumination conditions. Table 16.1 gives typical values of the illuminance in different environments.

Table 16.1. Typical illuminance in different environments.

Illumination condition	**Illuminance**
Full moon	1 lux
Street lighting	10 lux
Home lighting	30 to 300 lux
Office desk lighting	100 to 1 000 lux
Surgery lighting	10 000 lux
Direct sunlight	100 000 lux

The ***luminance*** of a ***surface source*** (i.e. a source with a non-zero light-emitting surface area such as a display or an LED) is the ratio of the luminous intensity emitted in a certain direction (measured in cd) divided by the *projected surface area* in that direction (measured in m^2). The luminance is measured in units of cd/m^2. In most cases, the direction of interest is normal to the chip surface. In this case, the luminance is the luminous intensity emitted along the chip-normal direction divided by the chip area.

The *projected surface area* mentioned above follows a cosine law, i.e. the projected area is given by $A_{\text{projected}} = A_{\text{surface}} \cos\Theta$, where Θ is the angle between the direction considered and the surface normal. The light-emitting surface area and the projected area are shown in Fig. 16.5. The luminous intensity of LEDs with lambertian emission pattern also depends on the angle Θ

according to a cosine law. Thus the luminance of lambertian LEDs is a constant, independent of angle.

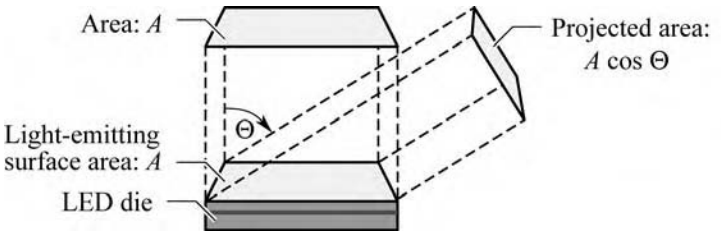

Fig. 16.5. Area of LED, A, and projected area, $A\cos\Theta$, used for the definition of the luminance of an LED.

For LEDs, it is desirable to maximize luminous intensity and luminous flux while keeping the LED chip area minimal. Thus the luminance is a measure of how efficiently the valuable semiconductor wafer area is used to attain, at a given injection current, a certain luminous intensity.

There are several units that are used to characterize the luminance of a source. The names of these common units are given in Table 16.2.

Typical luminances of displays, organic LEDs, and inorganic LEDs are given in Table 16.3. The table reveals that displays require a comparatively low luminance because the observer directly views the display from a close distance. This is not the case for high-power inorganic LEDs used for example in traffic light and illumination applications.

Photometric and the corresponding radiometric units are summarized in Table 16.4.

Table 16.2. Conversion between common SI and non-SI units for luminance.

Unit	**Common name**
1 cd/cm^2	1 stilb
$(1/\pi)$ cd/cm^2	1 lambert
1 cd/m^2	1 nit

Unit	**Common name**
$(1/\pi)$ cd/m^2	1 apostilb
$(1/\pi)$ cd/ft^2	1 foot-lambert

Table 16.3. Typical values for the luminance of displays, LEDs fabricated from organic materials, and inorganic LEDs.

Device	**Luminance** (cd/m^2)
Display	100 (operation)
Display	250–750 (max. value)

Device	**Luminance** (cd/m^2)
Organic LED	100–10 000
III–V LED	1 000 000–10 000 000

Table 16.4. Photometric and corresponding radiometric units.

Photometric unit	Dimension	Radiometric unit	Dimension
Luminous flux	lm	Radiant flux (optical power)	W
Luminous intensity	lm / sr = cd	Radiant intensity	W / sr
Illuminance	lm / m^2 = lux	Irradiance (power density)	W / m^2
Luminance	lm / (sr m^2) = cd / m^2	Radiance	W / (sr m^2)

Exercise: ***Photometric units***. A 60 W incandescent light bulb has a luminous flux of 1000 lm. Assume that light is emitted isotropically from the bulb.

(a) What is the luminous efficiency (i.e. the number of lumens emitted per watt of electrical input power) of the light bulb?
(b) What number of standardized candles emit the same luminous intensity?
(c) What is the illuminance, E_{lum}, in units of lux, on a desk located 1.5 m below the bulb?
(d) Is the illuminance level obtained under (c) sufficiently high for reading?
(e) What is the luminous intensity, I_{lum}, in units of candela, of the light bulb?
(f) Derive the relationship between the illuminance at a distance r from the light bulb, measured in *lux*, and the luminous intensity, measured in *candela*.
(g) Derive the relationship between the illuminance at a distance r from the light bulb, measured in *lux*, and the luminous flux, measured in *lumen*.
(h) The definition of the cd involves the optical power of (1/683) W. What, do you suppose, is the origin of this particular power level?

Solution: (a) 16.7 lm/W. (b) 80 candles. (c) E_{lum} = 35.4 lm/m^2 = 35.4 lux. (d) Yes.
(e) 79.6 lm/sr = 79.6 cd. (f) $E_{lum}\, r^2 = I_{lum}$. (g) $E_{lum}\, 4\pi r^2 = \Phi_{lum}$.
(h) Originally, the unit of luminous intensity had been defined as the intensity emitted by a real candle. Subsequently the unit was defined as the intensity of a light source with specified wavelength and optical power. When the power of that light source is (1/683) W, it has the same intensity as the candle. Thus this particular power level has a historical origin and results from the effort to maintain continuity.

16.3 Eye sensitivity function

The conversion between radiometric and photometric units is provided by the ***luminous efficiency function*** or ***eye sensitivity function***, $V(\lambda)$. In 1924, the CIE introduced the photopic eye sensitivity function $V(\lambda)$ for point-like light sources where the viewer angle is 2° (CIE, 1931). This function is referred to as the ***CIE 1931 V(λ) function***. It is the current photometric standard in the United States.

A *modified* $V(\lambda)$ function was introduced by Judd and Vos in 1978 (Vos, 1978; Wyszecki and Stiles, 1982, 2000) and this modified function is here referred to as the ***CIE 1978 V(λ) function***. The modification was motivated by the underestimation of the human eye sensitivity in the blue and violet spectral region by the CIE 1931 $V(\lambda)$ function. The modified function $V(\lambda)$ has higher values in the spectral region below 460 nm. The CIE has endorsed the CIE 1978 $V(\lambda)$

function by stating “the spectral luminous efficiency function for a point source may be adequately represented by the Judd modified $V(\lambda)$ function” (CIE, 1988) and “the Judd modified $V(\lambda)$ function would be the preferred function in those conditions where luminance measurements of short wavelengths consistent with color normal observers is desired” (CIE, 1990).

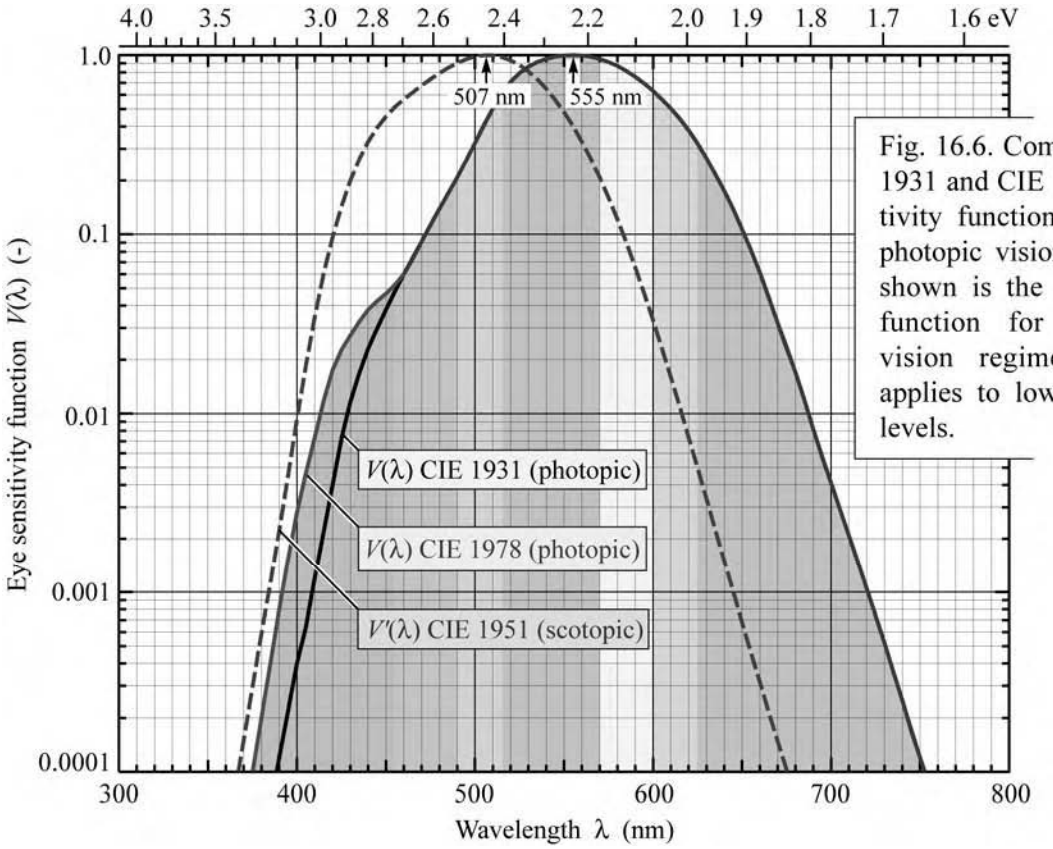

Fig. 16.6. Comparison of CIE 1931 and CIE 1978 eye sensitivity functions $V(\lambda)$ for the photopic vision regime. Also shown is the eye sensitivity function for the scotopic vision regime, $V'(\lambda)$, that applies to low ambient light levels.

The CIE 1931 $V(\lambda)$ function and the CIE 1978 $V(\lambda)$ function are shown in Fig. 16.6. The photopic eye sensitivity function has maximum sensitivity in the green spectral range at 555 nm, where $V(\lambda)$ has a value of unity, i.e. $V(555\ \text{nm}) = 1$. Inspection of the figure also reveals that the CIE 1931 $V(\lambda)$ function underestimated the eye sensitivity in the blue spectral range ($\lambda < 460$ nm). Numerical values of the CIE 1931 and CIE 1978 $V(\lambda)$ function are tabulated in Appendix 16.1.

Also shown in Fig. 16.6 is the scotopic eye sensitivity function $V'(\lambda)$. The peak sensitivity in the scotopic vision regime occurs at 507 nm. This value is markedly shorter than the peak sensitivity in the photopic vision regime. Numerical values of the CIE 1951 $V'(\lambda)$ function are tabulated in Appendix 16.2.

Note that even though the CIE 1978 $V(\lambda)$ function is preferable, it is not the standard, mostly for practical reasons such as possible ambiguities created by changing standards. Wyszecki and Stiles (2000) note that even though the CIE 1978 $V(\lambda)$ function is not a standard, it has been used in several visual studies. The CIE 1978 $V(\lambda)$ function, which can be considered the most accurate description of the eye sensitivity in the photopic vision regime, is shown in Fig. 16.7.

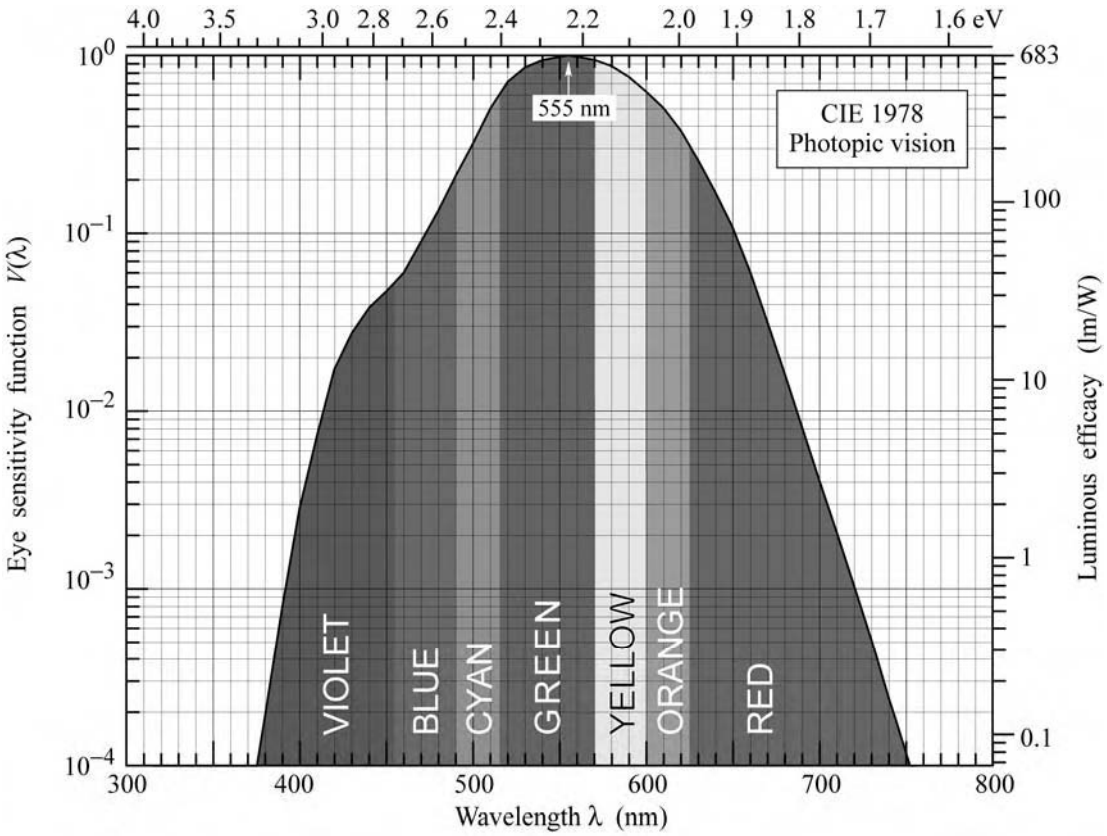

Fig. 16.7. Eye sensitivity function, $V(\lambda)$, (left-hand ordinate) and luminous efficacy, measured in lumens per watt of optical power (right-hand ordinate). $V(\lambda)$ is maximum at 555 nm (after 1978 CIE data).

The eye sensitivity function has been determined by the ***minimum flicker method***, which is the classic method for luminance comparison and for the determination of $V(\lambda)$. The stimulus is a light-emitting small circular area, alternatingly illuminated (with a frequency of 15 Hz) with the standard color and the comparison color. Since the hue-fusion frequency is lower than 15 Hz, the hues fuse. However, the brightness-fusion frequency is higher than 15 Hz and thus if the two colors differ in brightness, then there will be visible flicker. The human subject's task is to adjust the target color until the flicker is minimal.

Any desired chromaticity can be obtained with an infinite variety of spectral power

distributions $P(\lambda)$. One of these distributions has the greatest possible luminous efficacy. This limit can be obtained in only one way, namely by the mixture of suitable intensities emitted by two monochromatic sources (MacAdam, 1950). The maximum attainable luminous efficacy obtained with a single monochromatic pair of emitters is shown in Fig. 16.8. The maximum luminous efficacy of *white* light depends on the color temperature; it is about 420 lm/W for a color temperature of 6500 K and can exceed 500 lm/W for lower color temperatures. The exact value depends on the exact location within the white area of the chromaticity diagram.

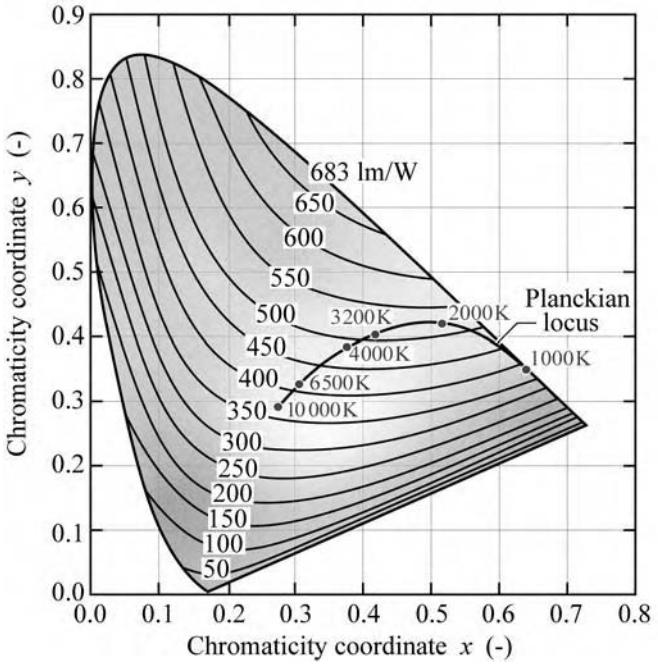

Fig. 16.8. Relation of maximum possible luminous efficacy (lumens per optical watt) and chromaticity in the CIE 1931 *x*, *y* chromaticity diagram (adapted from MacAdam, 1950).

16.4 Colors of near-monochromatic emitters

For wavelengths ranging from 390 to 720 nm, the eye sensitivity function $V(\lambda)$ is greater than 10^{-3}. Although the human eye is sensitive to light with wavelengths < 390 nm and > 720 nm, the sensitivity at these wavelengths is extremely low. Therefore, the wavelength range $390\ \text{nm} \le \lambda \le 720\ \text{nm}$ can be considered the *visible wavelength range*. The relationship between color and wavelength within the visible wavelength range is given in Table 16.5. This relationship is valid for monochromatic or near-monochromatic light sources such as LEDs. Note that color is, to some extent, a subjective quantity. Also note that the transition between different colors is continuous.

Table 16.5. Colors and associated typical LED peak wavelength ranges

Color	Wavelength
Ultraviolet	< 390 nm
Violet	390–455 nm
Blue	455–490 nm
Cyan	490–515 nm
Green	515–570 nm

Color	Wavelength
Yellow	570–600 nm
Amber	590–600 nm
Orange	600–625 nm
Red	625–720 nm
Infrared	> 720 nm

.

16.5 Luminous efficacy and luminous efficiency

The ***luminous flux***, Φ_{lum}, is obtained from the radiometric light power using the equation

$$\Phi_{\text{lum}} = 683 \frac{\text{lm}}{\text{W}} \int_{\lambda} V(\lambda)\, P(\lambda)\, \mathrm{d}\lambda \tag{16.1}$$

where $P(\lambda)$ is the power spectral density, i.e. the light power emitted per unit wavelength, and the prefactor 683 lm/W is a normalization factor. The optical power emitted by a light source is then given by

$$P = \int_{\lambda} P(\lambda)\, \mathrm{d}\lambda \ . \tag{16.2}$$

High-performance single-chip visible-spectrum LEDs can have a luminous flux of about 10–100 lm at an injection current of 100–1 000 mA.

The ***luminous efficacy of optical radiation*** (also called the ***luminosity function***), measured in units of lumens per watt of optical power, is the conversion efficiency from optical power to luminous flux. The luminous efficacy is defined as

$$\text{Luminous efficacy} = \frac{\Phi_{\text{lum}}}{P} = \left[683 \frac{\text{lm}}{\text{W}} \int_{\lambda} V(\lambda)\, P(\lambda)\, \mathrm{d}\lambda \right] \Big/ \left[\int_{\lambda} P(\lambda)\, \mathrm{d}\lambda \right] . \tag{16.3}$$

For strictly monochromatic light sources ($\Delta\lambda \to 0$), the luminous efficacy is equal to the eye sensitivity function $V(\lambda)$ multiplied by 683 lm/W. However, for multicolor light sources and especially for white light sources, the luminous efficacy needs to be calculated by integration over all wavelengths. The luminous efficacy is shown on the right-hand ordinate of Fig. 16.4.

The ***luminous efficiency of a light source***, also measured in units of lm/W, is the luminous

flux of the light source divided by the electrical input power.

$$\text{Luminous efficiency} = \Phi_{\text{lum}} / (I\,V) \tag{16.4}$$

where the product ($I\,V$) is the electrical input power of the device. Note that in the lighting community, luminous efficiency is often referred to as *luminous efficacy of the source*.

Inspection of Eqs. (16.3) and (16.4) reveals that the luminous efficiency is the product of the luminous efficacy and the electrical-to-optical power conversion efficiency. The luminous efficiency of common light sources is given in Table 16.6.

Table 16.6. Luminous efficiencies of different light sources. (a) Incandescent sources. (b) Fluorescent sources. (c) High-intensity discharge (HID) sources.

Light source		**Luminous efficiency**
Edison's first light bulb (with C filament)	(a)	1.4 lm/W
Tungsten filament light bulbs	(a)	15–20 lm/W
Quartz halogen light bulbs	(a)	20–25 lm/W
Fluorescent light tubes and compact bulbs	(b)	50–80 lm/W
Mercury vapor light bulbs	(c)	50–60 lm/W
Metal halide light bulbs	(c)	80–125 lm/W
High-pressure sodium vapor light bulbs	(c)	100–140 lm/W

The luminous efficiency is a highly relevant figure of merit for visible-spectrum LEDs. It is a measure of the perceived light power normalized to the electrical power expended to operate the LED. For light sources with a perfect electrical-power-to-optical-power conversion, the luminous source efficiency is equal to the luminous efficacy of radiation.

Exercise: ***Luminous efficacy and luminous efficiency of LEDs***. Consider a red and an amber LED emitting at 625 and 590 nm, respectively. For simplicity, assume that the emission spectra are monochromatic ($\Delta\lambda \to 0$). What is the luminous efficacy of the two light sources? Calculate the luminous efficiency of the LEDs, assuming that the red and amber LEDs have an external quantum efficiency of 50%. Assume that the LED voltage is given by $V = E_g / e = h\nu / e$.

Assume next that the LED spectra are thermally broadened and have a gaussian lineshape with a linewidth of $1.8\,kT$. Again calculate the luminous efficacy and luminous efficiency of the two light sources. How accurate are the results obtained with the approximation of monochromaticity?

Some LED structures attain excellent power efficiency by using small light-emitting areas (current injection in a small area of chip) and advanced light-output-coupling structures (see, for example, Schmid *et al*., 2002). However, such devices have low luminance because only a small

fraction of the chip area is injected with current. Table 16.7 summarizes frequently used figures of merit for light-emitting diodes.

Table 16.7. Summary of photometric, radiometric, and quantum performance measures for LEDs.

Figure of merit	Explanation	Unit
Luminous efficacy	Luminous flux per optical unit power	lm/W
Luminous efficiency	Luminous flux per input electrical unit power	lm/W
Luminous intensity efficiency	Luminous flux per sr per input electrical unit power	cd/W
Luminance	Luminous flux per sr per chip unit area	cd/m^2
Power efficiency	Optical output power per input electrical unit power	%
Internal quantum efficiency	Photons emitted in active region per electron injected	%
External quantum efficiency	Photons emitted from LED per electron injected	%
Extraction efficiency	Escape probability of photons emitted in active region	%

16.6 Brightness and linearity of human vision

Although the term ***brightness*** is frequently used, it lacks a standardized scientific definition. The frequent usage is due to the fact that the general public can more easily relate to the term *brightness* than to photometric terms such as *luminance* or *luminous intensity*. Brightness is an attribute of visual perception and is frequently used as synonym for *luminance* and (incorrectly) for the radiometric term *radiance*.

To quantify the brightness of a source, it is useful to differentiate between point and surface area sources. For *point sources*, brightness (in the photopic vision regime) can be approximated by the luminous intensity (measured in cd). For *surface sources*, brightness (in the photopic vision regime) can be approximated by the luminance (measured in cd/m^2). However, due to the lack of a formal standardized definition of the term brightness, it is frequently avoided in technical publications.

Standard CIE photometry assumes human vision to be ***linear*** within the photopic regime. It is clear that an isotropically emitting blue point source and an isotropically emitting red point source each having a luminous flux of, e.g., 5 lm, have the same luminous intensity. Assuming *linearity* of photopic vision, both sources still have the same luminous intensity as the luminous fluxes of the sources are increased from 5 to, e.g., 5000 lm.

However, if the luminous fluxes of the two sources are reduced so that the mesopic or scotopic vision regime is entered, the blue source will appear brighter than the red source due to

the shift of the eye sensitivity function to shorter wavelengths in the scotopic regime.

It is important to keep in mind that the linearity of human vision within the photopic regime is an *approximation*. Linearity clearly simplifies photometry. However, human subjects may feel discrepancies between the experience of brightness and measured luminance of a light source, especially for colored light sources if the luminous flux is changed over orders of magnitude.

16.7 Circadian rhythm and circadian sensitivity NO

The human wake-sleep rhythm has a period of approximately 24 hours and the rhythm therefore is referred to as the ***circadian rhythm*** or ***circadian cycle***, with the name being derived from the Latin words *circa* and *dies* (and its declination *diem*), meaning *approximately* and *day*, respectively. Light has been known for a long time to be the synchronizing clock (*zeitgeber*) of the human circadian rhythm. For reviews on the development of the understanding of the circadian rhythm including the identification of light as the dominant trigger for the endogenous *zeitgeber*, see Pittendrigh (1993) and Sehgal (2004).

The wake-sleep rhythm of humans is synchronized by the intensity and spectral composition of light. Sunlight is the natural *zeitgeber*. During mid-day hours sunlight has high intensity, a high color temperature, and a high content of blue light. During evening hours, intensity, color temperature, and blue content of sunlight strongly decrease. Humans have adapted to this variation and the circadian rhythm is most likely synchronized by the following three factors: intensity, color temperature, and blue content.

Exposure to inappropriately high intensities of light in the late afternoon or evening can upset the regular wake-seep rhythm and lead to sleeplessness and even serious illnesses such as cancer (Brainard *et al*., 2001; Blask *et al*, 2003). It is therefore highly advisable to limit exposure to high intensity light in the late afternoon and evening hours, to not be counterproductive to the natural circadian rhythm (Schubert, 1997).

It was believed for a long time that rod cells and the three types of cone cells are the only optically sensitive cells in the human eye. However, Brainard *et al*. (2001) postulated that an unknown photoreceptor in the human eye would control the circadian rhythm. Evidence presented by Berson *et al*. (2002) and Hattar *et al*., (2002) indicates that retinal ganglion cells have an optical sensitivity as well. For a schematic illustration of ganglion cells, see Fig. 16.1. The spectral sensitivity of mammalian ganglion cells was measured and the responsivity curve is shown in Fig. 16.9. Inspection of the figure reveals a ganglion-cell peak-sensitivity at 484 nm, i.e. in the blue spectral range.

Berson *et al*. (2002) presented evidence that the photosensitive ganglion cells are instrumental in the control of the circadian rhythm. Due to their sensitivity in the blue spectral range, it can be hypothesized that the blue sky occurring near mid-day is a strong factor in synchronizing the endogenous circadian rhythm. The photosensitive ganglion cells have therefore been referred to as *blue-sky receptors*.

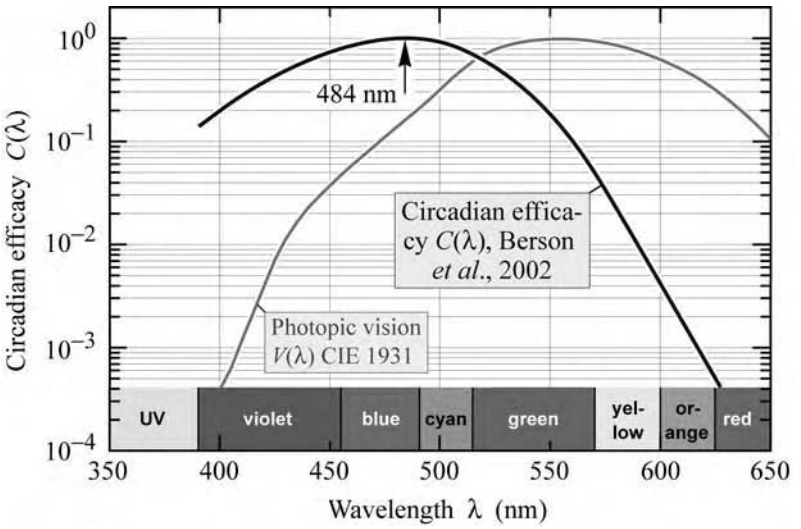

Fig. 16.9. Circadian efficacy curve derived from retinal ganglion cell photoresponse measurements. The ganglion cells on which the measurements were performed originated from mammals. The figure reveals the significant difference between circadian and visual sensitivity (adapted from Berson *et al*., 2002).

Inspection of the spectral sensitivity of the ganglion cells shown in Fig. 16.9 reveals the huge difference of red light and blue light for circadian efficacy: The efficacy of blue light in synchronizing the circadian rhythm can be three orders of magnitude greater than the efficacy of red light. This particular role of blue light should be taken into account in lighting design and the use of artificial lighting by consumers.

References

Berson D. M., Dunn F. A., and Takao M. "Phototransduction by retinal ganglion cells that set the circadian clock" *Science* **295**, 1070 (2002)

Brainard G. C., Hanifin J. P., Greeson J. M., Byrne B., Glickman G., Gerner E., and Rollag M. D. "Action spectrum for melatonin regulation in humans: Evidence for a novel circadian photoreceptor" *J. Neuroscience* **21,** 6405 (2001)

Blask D. E., Dauchy R. T., Sauer L. A., Krause J. A., Brainard G. C. "Growth and fatty acid metabolism of human breast cancer (MCF-7) xenografts in nude rats: Impact of constant light-induced nocturnal melatonin suppression" *Breast Cancer Research and Treatment* **79**, 313 (2003)

CIE *Commission Internationale de l'Eclairage Proceedings* (Cambridge University Press, Cambridge, 1931)

CIE *Proceedings* **1**, Sec. 4; **3**, p. 37; Bureau Central de la CIE, Paris (1951)

CIE data of 1931 and 1978 available at http://cvision.ucsd.edu and http://www.cvrl.org (1978). The CIE 1931 $V(\lambda)$ data were modified by D. B. Judd and J. J. Vos in 1978. The Judd–Vos-modified eye-sensitivity function is frequently referred to as $V_M(\lambda)$; *see* J. J. Vos "Colorimetric and photometric properties of a 2-deg fundamental observer" *Color Res. Appl.* **3**, 125 (1978)

CIE publication 75-1988 *Spectral Luminous Efficiency Functions Based Upon Brightness Matching for Monochromatic Point Sources with 2° and 10° Fields* ISBN 3900734119 (1988)

CIE publication 86-1990 *CIE 1988 2° Spectral Luminous Efficiency Function for Photopic Vision* ISBN 3900734232 (1990)

Dowling J. E. *The retina: An Approachable Part of the Brain* (Harvard University Press, Cambridge, Massachusetts, 1987)

Encyclopedia Britannica, Inc. Illustration of human eye adopted from 1994 edition of the encyclopedia (1994)

Hattar S., Liao H.-W., Takao M., Berson D. M., and Yau K.-W. "Melanopsin-containing retinal ganglion cells: Architecture, projections, and intrinsic photosensitivity" *Science* **295**, 1065 (2002)

MacAdam D. L. "Maximum attainable luminous efficiency of various chromaticities" *J. Opt. Soc. Am.* **40**, 120 (1950)

Osram Sylvania Corporation *Lumens and mesopic vision* Application Note FAQ0016-0297 (2000)

Pittendrigh C. S. "Temporal organization: Reflections of a Darwinian clock-watcher" *Ann. Rev. Physiol.* **55**, 17 (1993)

Schmid W., Scherer M., Karnutsch C., Plobl A., Wegleiter W., Schad S., Neubert B., and Streubel K. "High-efficiency red and infrared light-emitting diodes using radial outcoupling taper" *IEEE J. Sel. Top. Quantum Electron.* **8**, 256 (2002)

Schubert E. F. The author of this book noticed in 1997 that working after 8 PM under bright illumination conditions in the office allowed him to fall asleep only very late, typically after midnight. The origin of sleeplessness was traced back to high-intensity office lighting conditions. Once the high intensity of the office lighting was reduced, the sleeplessness vanished (1997)

Sehgal A., editor *Molecular Biology of Circadian Rhythms* (John Wiley and Sons, New York, 2004)

Vos J. J. "Colorimetric and photometric properties of a 2-deg fundamental observer" *Color Res. Appl.* **3**, 125 (1978)

Wyszecki G. and Stiles W. S. *Color Science – Concepts and Methods, Quantitative Data and Formulae* 2nd edition (John Wiley and Sons, New York, 1982)

Wyszecki G. and Stiles W. S. *Color Science – Concepts and Methods, Quantitative Data and Formulae* 2nd edition (John Wiley and Sons, New York, 2000)

Appendix 16.1

Tabulated values of the 2º degree CIE 1931 photopic eye sensitivity function and the CIE 1978 Judd–Vos-modified photopic eye sensitivity function for point sources (after CIE, 1931 and CIE, 1978).

λ (nm)	CIE 1931 $V(\lambda)$	CIE 1978 $V(\lambda)$
360	3.9170 E–6	0.0000E–4
365	6.9650 E–6	0.0000E–4
370	1.2390 E–5	0.0000E–4
375	2.2020 E–5	0.0000E–4
380	3.9000 E–5	2.0000E–4
385	6.4000 E–5	3.9556E–4
390	1.2000 E–4	8.0000E–4
395	2.1700 E–4	1.5457E–3
400	3.9600 E–4	2.8000E–3
405	6.4000 E–4	4.6562E–3
410	1.2100 E–3	7.4000E–3
415	2.1800 E–3	1.1779E–2
420	4.0000 E–3	1.7500E–2
425	7.3000 E–3	2.2678E–2
430	1.1600 E–2	2.7300E–2
435	1.6840 E–2	3.2584E–2
440	2.3000 E–2	3.7900E–2
445	2.9800 E–2	4.2391E–2
450	3.8000 E–2	4.6800E–2
455	4.8000 E–2	5.2122E–2
460	6.0000 E–2	6.0000E–2
465	7.3900 E–2	7.2942E–2
470	9.0980 E–2	9.0980E–2
475	0.11260	0.11284
480	0.13902	0.13902
485	0.16930	0.16987
490	0.20802	0.20802
495	0.25860	0.25808
500	0.32300	0.32300
505	0.40730	0.40540
510	0.50300	0.50300
515	0.60820	0.60811
520	0.71000	0.71000
525	0.79320	0.79510
530	0.86200	0.86200
535	0.91485	0.91505
540	0.95400	0.95400
545	0.98030	0.98004
550	0.99495	0.99495
555	1.00000	1.00000
560	0.99500	0.99500
565	0.97860	0.97875
570	0.95200	0.95200
575	0.91540	0.91558
580	0.87000	0.87000
585	0.81630	0.81623
590	0.75700	0.75700
595	0.69490	0.69483
600	0.63100	0.63100
605	0.56680	0.56654
610	0.50300	0.50300
615	0.44120	0.44172
620	0.38100	0.38100
625	0.32100	0.32052
630	0.26500	0.26500
635	0.21700	0.21702
640	0.17500	0.17500
645	0.13820	0.13812
650	0.10700	0.1.0700
655	8.1600 E–2	8.1652E–2
660	6.1000 E–2	6.1000E–2
665	4.4580 E–2	4.4327E–2
670	3.2000 E–2	3.2000E–2
675	2.3200 E–2	2.3454E–2
680	1.7000 E–2	1.7000E–2
685	1.1920 E–2	1.1872E–2
690	8.2100 E–3	8.2100E–3
695	5.7230 E–3	5.7723E–3
700	4.1020 E–3	4.1020E–3
705	2.9290 E–3	2.9291E–3
710	2.0910 E–3	2.0910E–3
715	1.4840 E–3	1.4822E–3
720	1.0470 E–3	1.0470E–3
725	7.4000 E–4	7.4015E–4
730	5.2000 E–4	5.2000E–4
735	3.6110 E–4	3.6093E–4
740	2.4920 E–4	2.4920E–4
745	1.7190 E–4	1.7231E–4
750	1.2000 E–4	1.2000E–4
755	8.4800 E–5	8.4620E–5
760	6.0000 E–5	6.0000E–5
765	4.2400 E–5	4.2446E–5
770	3.0000 E–5	3.0000E–5
775	2.1200 E–5	2.1210E–5
780	1.4990 E–5	1.4989E–5
785	1.0600 E–5	1.0584E–5
790	7.4657 E–6	7.4656E–6
795	5.2578 E–6	5.2592E–6
800	3.7029 E–6	3.7028E–6
805	2.6078 E–6	2.6076E–6
810	1.8366 E–6	1.8365E–6
815	1.2934 E–6	1.2950E–6
820	9.1093 E–7	9.1092E–7
825	6.4153 E–7	6.3564E–7

Appendix 16.2

Tabulated values of the CIE 1951 eye sensitivity function of the scotopic vision regime, $V'(\lambda)$ (after CIE, 1951).

λ (nm)	CIE 1951 $V'(\lambda)$		
380	5.890e-004	585	8.990e-002
385	1.108e-003	590	6.550e-002
390	2.209e-003	595	4.690e-002
395	4.530e-003	600	3.315e-002
400	9.290e-003	605	2.312e-002
405	1.852e-002	610	1.593e-002
410	3.484e-002	615	1.088e-002
415	6.040e-002	620	7.370e-003
420	9.660e-002	625	4.970e-003
425	1.436e-001	630	3.335e-003
430	1.998e-001	635	2.235e-003
435	2.625e-001	640	1.497e-003
440	3.281e-001	645	1.005e-003
445	3.931e-001	650	6.770e-004
450	4.550e-001	655	4.590e-004
455	5.130e-001	660	3.129e-004
460	5.670e-001	665	2.146e-004
465	6.200e-001	670	1.480e-004
470	6.760e-001	675	1.026e-004
475	7.340e-001	680	7.150e-005
480	7.930e-001	685	5.010e-005
485	8.510e-001	690	3.533e-005
490	9.040e-001	695	2.501e-005
495	9.490e-001	700	1.780e-005
500	9.820e-001	705	1.273e-005
505	9.980e-001	710	9.140e-006
510	9.970e-001	715	6.600e-006
515	9.750e-001	720	4.780e-006
520	9.350e-001	725	3.482e-006
525	8.800e-001	730	2.546e-006
530	8.110e-001	735	1.870e-006
535	7.330e-001	740	1.379e-006
540	6.500e-001	745	1.022e-006
545	5.640e-001	750	7.600e-007
550	4.810e-001	755	5.670e-007
555	4.020e-001	760	4.250e-007
560	3.288e-001	765	3.196e-007
565	2.639e-001	770	2.413e-007
570	2.076e-001	775	1.829e-007
575	1.602e-001	780	1.390e-007
580	1.212e-001		

17

Colorimetry

The assessment and quantification of color is referred to as ***colorimetry*** or the "science of color". Colorimetry is closely associated with human color vision. Both colorimetry and human vision have attracted a great deal of interest that spans many centuries. For a thorough and entertaining review of the history of colorimetry including early attempts to understand color, we recommended the collection of historical reprints complied by MacAdam (1993).

The human sense of vision is very different from the human sense of hearing. If we hear two frequencies simultaneously, e.g. two frequencies generated by a musical instrument, we will be able to recognize the musical tone as having two distinct frequencies. This is not the case for optical signals and the sense of vision. Mixing two monochromatic optical signals will appear to us as one color and we are unable to recognize the original dichromatic composition of that color.

17.1 Color-matching functions and chromaticity diagram

Light causes different levels of excitation of the red, green, and blue cones. However, the sensation of color and luminous flux caused a particular light source varies slightly among different individuals. Furthermore, the sensation of color is, to some extent, a subjective quantity. For these reasons, *The International Commission for Illumination* (*Commission Internationale de l'Eclairage*, CIE) has *standardized the measurement of color* by means of ***color-matching functions*** and the ***chromaticity diagram*** (CIE, 1931).

How are color-matching functions obtained? Consider two lights lying side by side: One being monochromatic and the other one being a mixture of three primary lights with color red, green, and blue, as shown in Fig. 17.1. A human subject will be able to make the two lights appear identical (i.e. "match" them) by adjusting the relative intensities of the red, green, and blue light. The three color-matching functions are obtained from a series of such matches, in which the subject sets the intensities of the three primary lights required to match a series of monochromatic lights across the visible spectrum.

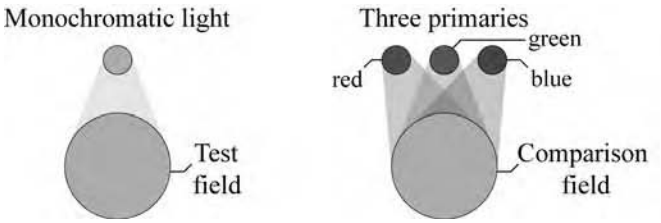

Fig. 17.1. Principle of color matching: A monochromatic test light (imaged on the "test field") is color-matched by mixing three adjustable primary lights, red, green, and blue (imaged on the "comparison field").

Subsequently, the measured set of color-matching functions is mathematically transformed into a new set of color-matching functions for which the green color-matching function, $\bar{y}(\lambda)$, is chosen to be identical to the eye sensitivity function, $V(\lambda)$, i.e.

$$\boxed{\bar{y}(\lambda) = V(\lambda)}\,. \tag{17.1}$$

The CIE 1931 and CIE 1978 color-matching functions $\bar{x}(\lambda)$, $\bar{y}(\lambda)$, and $\bar{z}(\lambda)$ are shown in Fig. 17.2. The numerical values of these color-matching functions are tabulated in Appendices 17.1 and 17.2, respectively. The three color-matching functions reflect the fact that human color vision possesses ***trichromacy***, that is, the color of any light source can be described by just three variables. Note that $\bar{x}(\lambda)$, $\bar{y}(\lambda)$, and $\bar{z}(\lambda)$ are dimensionless quantities. Also note that neither the color-matching functions nor the chromaticity diagram is unique (see, for example, Judd, 1951 or Vos, 1978). In fact there have been several different versions of the color-matching functions and of the chromaticity diagram.

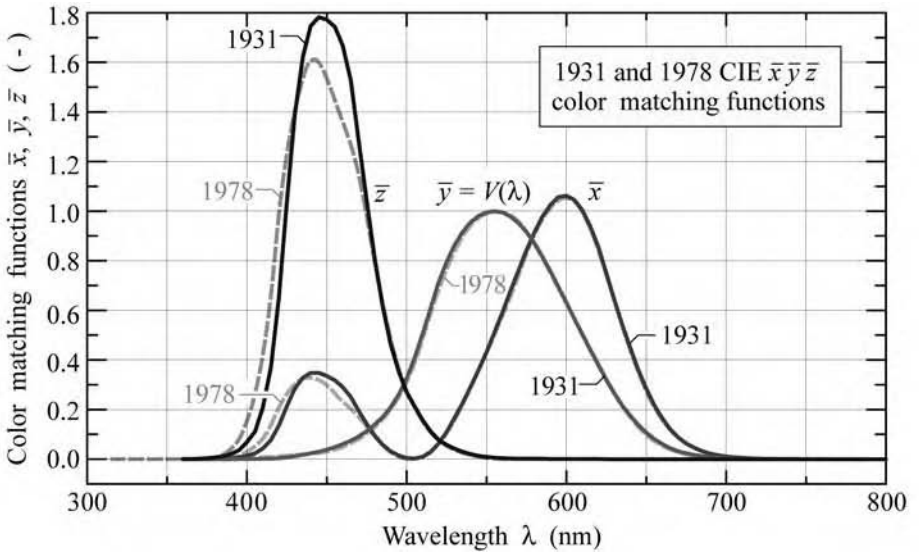

Fig. 17.2. CIE (1931) and CIE (1978) $\bar{x}\bar{y}\bar{z}$ color-matching functions. The $\bar{y}$ color-matching function is identical to the eye sensitivity function $V(\lambda)$. Note that the CIE 1931 color-matching functions are the currently valid official standard in the United States.

For a given power-spectral density $P(\lambda)$, the degree of stimulation required to match the color of $P(\lambda)$ is given by

$$X = \int_\lambda \bar{x}(\lambda)\, P(\lambda)\, \mathrm{d}\lambda \tag{17.2}$$

$$Y = \int_\lambda \bar{y}(\lambda)\, P(\lambda)\, \mathrm{d}\lambda \tag{17.3}$$

$$Z = \int_\lambda \bar{z}(\lambda)\, P(\lambda)\, \mathrm{d}\lambda \tag{17.4}$$

where X, Y, and Z are the ***tristimulus values*** that give the stimulation (i.e. power) of each of the three primary red, green, and blue lights needed to match the color of $P(\lambda)$. Large values of X, Y, and Z indicate red, green, and blue colors of the spectrum $P(\lambda)$, respectively.

Because of the distinct similarity of the three retinal-cone-sensitivity functions on one hand, and the color-matching functions on the other hand (both groups of functions have three peaks), each tristimulus value represents the *approximate* (but not *exact*) degree of stimulation that each type of retinal cone experiences when illuminated by a light source with spectrum $P(\lambda)$.

Inspection of Eqs. (17.2)–(17.4) suggests that the unit of the tristimulus values is "watt". However, the tristimulus values are usually given as dimensionless quantities. The prefactor "watt^{-1}" in front of the integral can be included so that the tristimulus values become dimensionless. If only *ratios* of tristimulus values are employed, as below, the prefactors and units cancel and thus become irrelevant.

The ***chromaticity coordinates*** x and y are calculated from the tristimulus values according to

$$x = \frac{X}{X + Y + Z} \tag{17.5}$$

$$y = \frac{Y}{X + Y + Z} \,. \tag{17.6}$$

Thus, the value of a chromaticity coordinate is the stimulation of each primary light (or of each type of retinal cone) divided by the entire stimulation ($X + Y + Z$). The value of the z chromaticity coordinate is calculated analogously, that is

$$z = \frac{Z}{X + Y + Z} = 1 - x - y \,. \tag{17.7}$$

Note that the z chromaticity value can be obtained from x and y, so that there is no new information provided by the z chromaticity coordinate. Therefore, the z coordinate is redundant

and, for this reason, does not need to be used.

The (x, y) chromaticity diagram is shown in Fig. 17.3. Reddish and greenish colors are found for large values of x and y, respectively. Bluish colors are found for large values of z, which is, according to Eq. (17.7), for low values of x and y, or near the origin of the chromaticity diagram.

The chromaticity diagram of Fig. 17.4 shows a detailed attribution of colors to their locations in the chromaticity diagram. The assignment of colors was given by Gage *et al*. (1977).

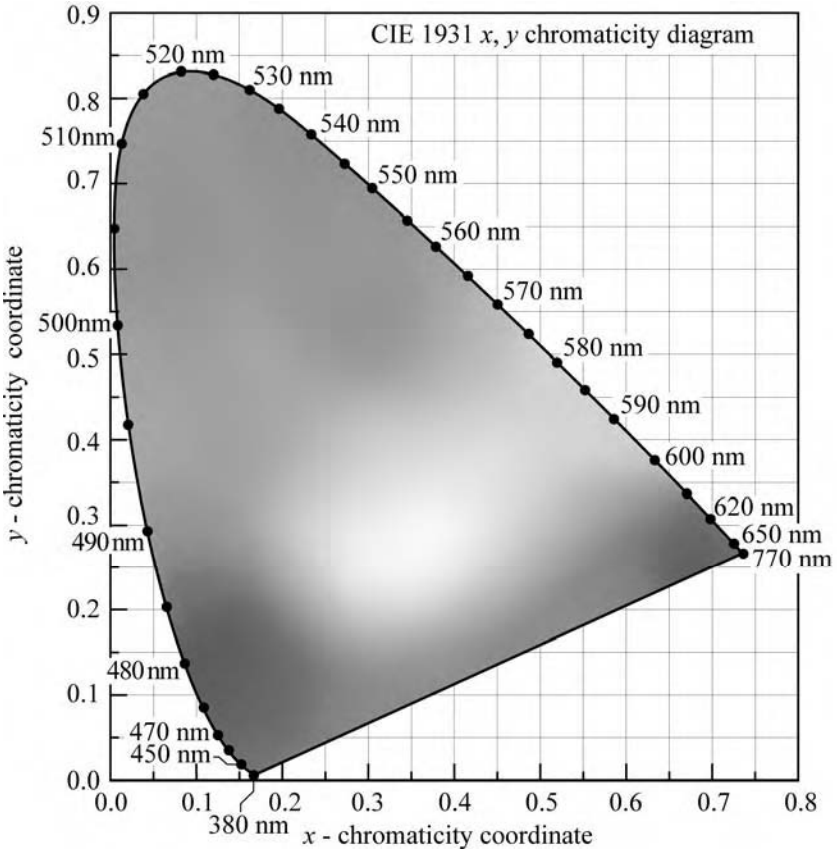

Fig. 17.3. CIE 1931 (x, y) chromaticity diagram. Monochromatic colors are located on the perimeter and white light is located in the center of the diagram.

An assignment of common colors in the chromaticity diagram is given in Fig. 17.5. The figure also shows the ***equal-energy point*** located in the center of the chromaticity diagram at (x, y, z) = (1/3, 1/3, 1/3). The optical spectrum corresponding to the equal-energy point has a constant spectral distribution, i.e. the optical energy per wavelength interval $d\lambda$ is constant across the visible spectrum. Such a spectrum also results in equal tristimulus values, i.e. $X = Y = Z$.

Monochromatic or pure colors are found on the perimeter of the chromaticity diagram. White light is found in the center of the chromaticity diagram. All colors can be characterized in terms of their location in the chromaticity diagram.

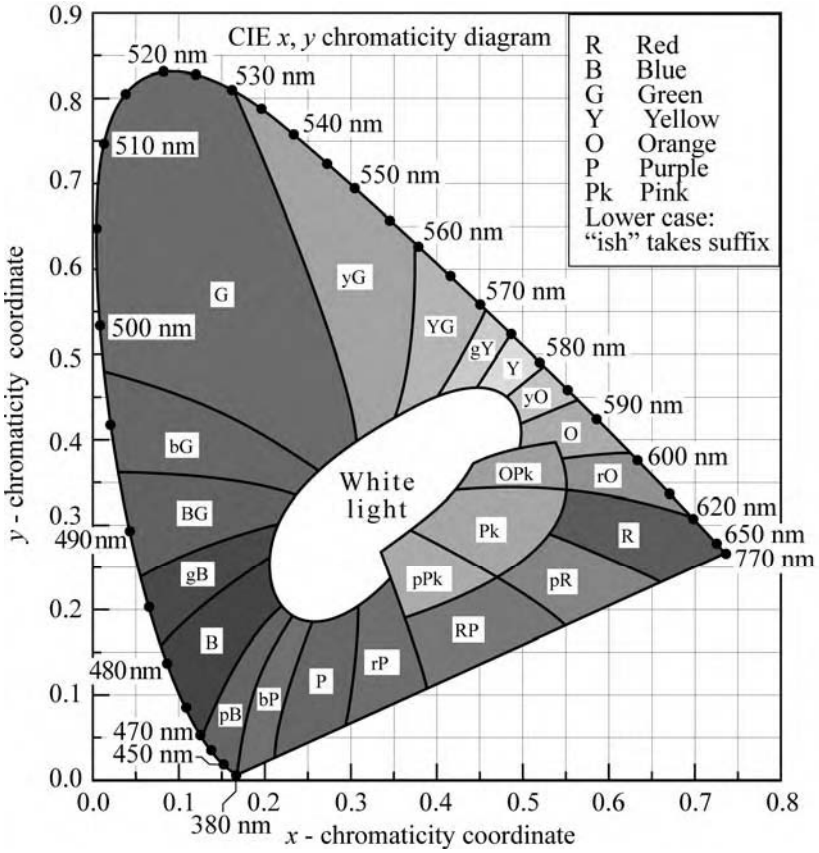

Fig. 17.4. 1931 CIE chromaticity diagram with areas attributed to distinct colors (after Gage *et al*., 1977).

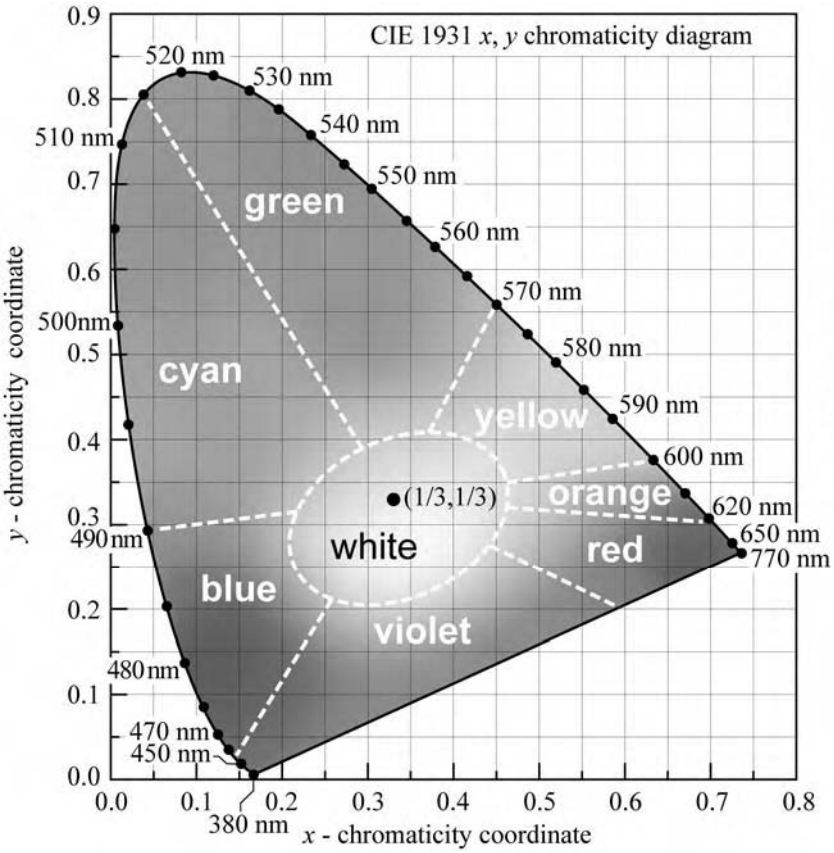

Fig. 17.5. CIE 1931 (x, y) chromaticity diagram. Monochromatic colors are located on the perimeter. Color saturation decreases towards the center of the diagram. White light is located in the center. Also shown are the regions of distinct colors. The equal-energy point is located at the center and has the coordinates (x, y) = (1/3, 1/3).

MacAdam (1943) analyzed the color differences of closely spaced points in the chromaticity diagram. The author found that two chromaticity points must have a *minimum geometrical distance* to yield a perceptible difference in color. Colors within a certain small region in the chromaticity diagram appear identical to human subjects. MacAdam showed that these regions have the shape of an ellipses. Such ellipses, now known as the ***MacAdam ellipses***, are shown in Fig. 17.6 (MacAdam, 1943, 1993; Wright, 1943). Inspection of the figure shows that ellipses in the blue and green regions are very different in size. Thus, the geometric distance between two points in the (x, y) chromaticity diagram does *not* scale linearly with the color difference.

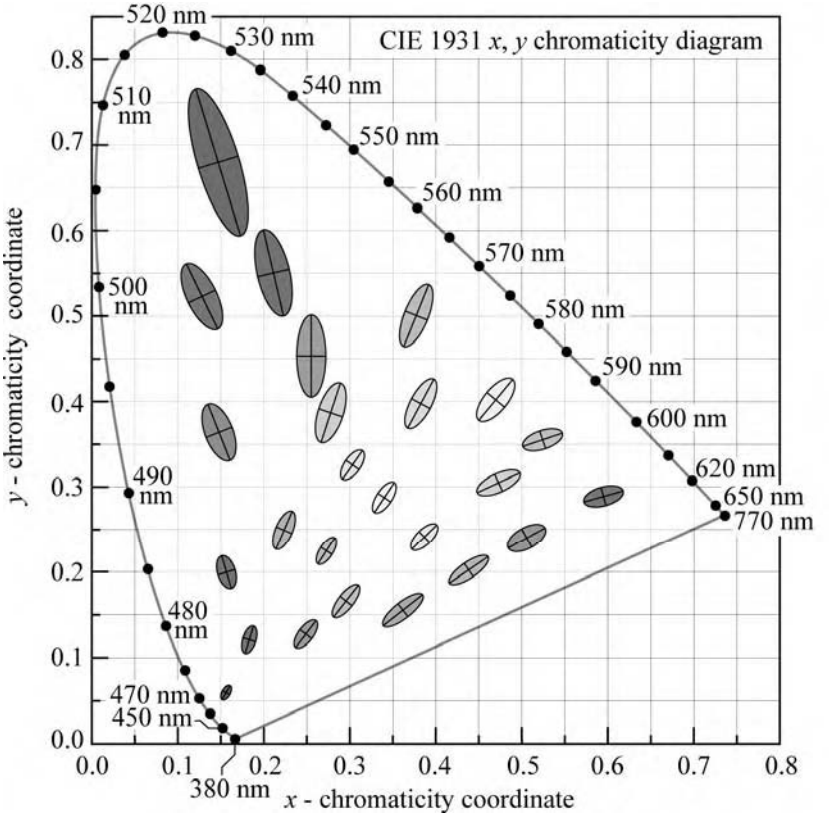

Fig. 17.6. MacAdam ellipses plotted in the CIE 1931 (x, y) chromaticity diagram. The axes of the ellipses are ten times their actual lengths (after MacAdam, 1943; Wright, 1943; MacAdam, 1993).

The total number of differentiable chromaticities can be obtained by dividing the area of the chromaticity diagram through the average area of the MacAdam ellipses. This calculation yields the result that humans can discern approximately 50 000 distinct chromaticities. If possible variations in luminance (brightness) are taken into account, the number of differentiable colors increases to a value greater than 10^6.

In the chromaticity diagram, it is very desirable for the color difference to be proportional to the geometric difference. This has motivated the *uniform* chromaticity diagram. In 1960, the CIE introduced the (u, v) and in 1976 the (u', v') ***uniform chromaticity coordinates*** (Wyszecki and

Stiles, 2000). These coordinates form the ***uniform chromaticity diagram***. The uniform chromaticity coordinates are calculated from the tristimulus values according to

$$u = \frac{4X}{X + 15Y + 3Z} \qquad v = \frac{6Y}{X + 15Y + 3Z} \qquad \text{(CIE, 1960)} \qquad (17.8)$$

and

$$u' = \frac{4X}{X + 15Y + 3Z} \qquad v' = \frac{9Y}{X + 15Y + 3Z} \qquad \text{(CIE, 1976)}\,. \qquad (17.9)$$

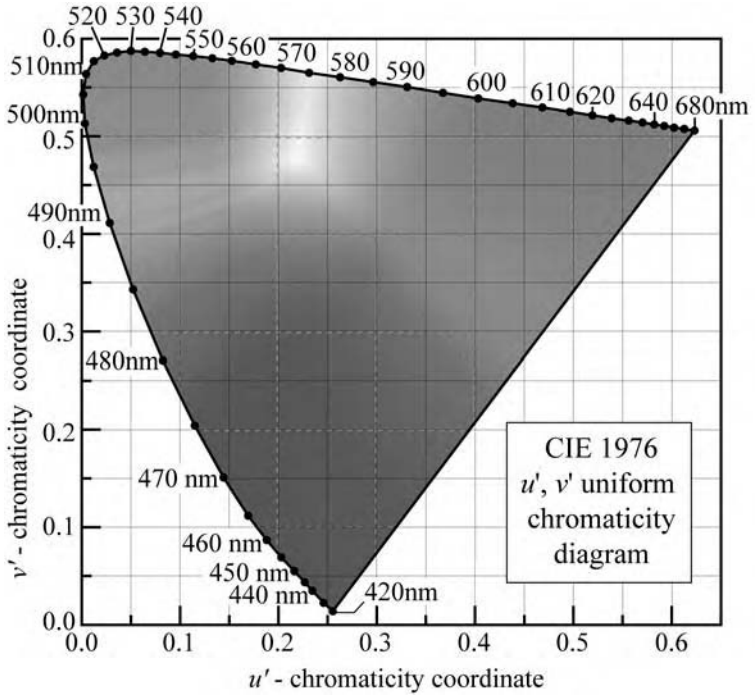

Fig. 17.7. CIE 1976 (u', v') uniform chromaticity diagram calculated using the CIE 1931 2° standard observer.

The CIE 1976 (u', v') uniform chromaticity diagram is shown in Fig. 17.7. The (u, v) and (u', v') uniform chromaticity coordinates can be calculated from the (x, y) chromaticity coordinates according to

$$u = u' = \frac{4x}{-2x + 12y + 3} \qquad (17.10)$$

and

$$v = \frac{6y}{-2x + 12y + 3} \qquad v' = \frac{9y}{-2x + 12y + 3}\,. \qquad (17.11)$$

Conversely, one obtains

$$x = \frac{9u'}{6u' - 16v' + 12} \qquad y = \frac{2v'}{3u' - 8v' + 6} \tag{17.12}$$

and

$$x = \frac{3u}{2u - 8v + 4} \qquad y = \frac{2v}{2u - 8v + 4} \; . \tag{17.13}$$

The color differences between two points in the (x, y) chromaticity diagram are spatially very non-uniform, that is, the color changes much more rapidly in one direction, e.g. the x-direction, compared with the other direction, e.g. the y-direction. This deficiency of the (x, y) chromaticity diagram is strongly reduced, although not eliminated, in the (u, v) and (u', v') uniform chromaticity diagrams. As a result, the *color difference* between two locations in the uniform chromaticity diagram is (approximately) directly proportional to the *geometrical distance* between these points.

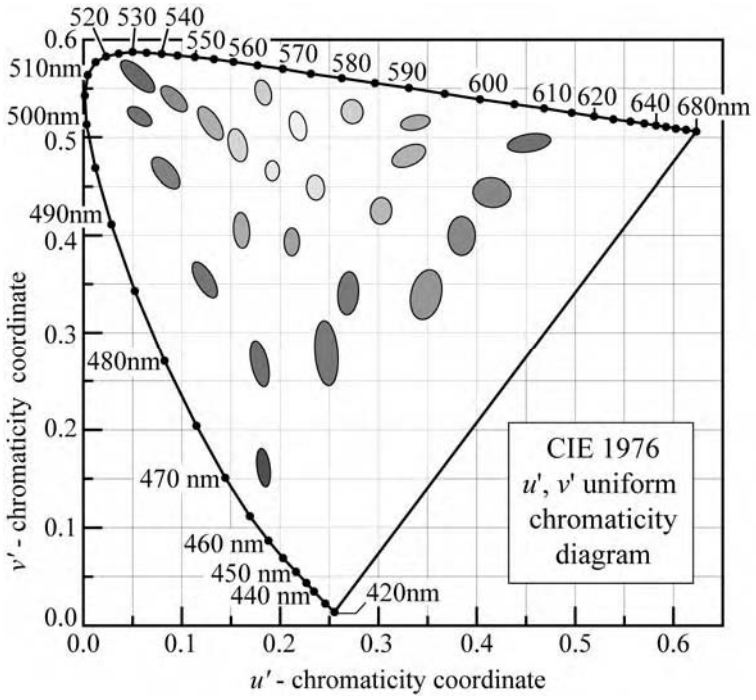

Fig. 17.8. MacAdam ellipses transformed to uniform CIE 1976 (u', v') chromaticity coordinates. For clarity, the axes of the transformed ellipses are ten times their actual lengths. Transformed ellipses are not ellipses in a strict mathematical sense, but their shapes closely resemble those of ellipses. The areas of the transformed ellipses in the (u', v') diagram are much more similar than the MacAdam ellipses in the (x, y) diagram.

The 1943 MacAdam ellipses in the (x, y) chromaticity diagram can be transformed to the uniform (u', v') chromaticity diagram. This transformation is shown in Fig. 17.8, which reveals that the areas of non-discernable colors are much more uniform in shape and area than the

MacAdam ellipses in the (x, y) chromaticity diagram.

Note that the transformation from the (x, y) to the (u', v') coordinate system is mathematically *non-linear*, and thus ellipses in the (x, y) chromaticity diagram do *not* transform into ellipses in the (u', v') coordinate system. However, if the ellipses in the (x, y) chromaticity diagram are sufficiently small in size, non-linear distortions are small as well, so that the transformed regions are very close to ellipses.

17.2 Color purity

Monochromatic sources ($\Delta\lambda \to 0$) are located on the perimeter of the chromaticity diagram. However, as the spectral linewidth of a light source gets broader, the color location in the chromaticity diagram moves towards the center of the chromaticity diagram. If the spectral width of a light source becomes comparable to the entire visible range, the light source is *white* and thus located near the center of the chromaticity diagram.

The ***dominant wavelength*** of a test light source is defined as the wavelength (i.e. monochromatic color) located on the perimeter of the chromaticity diagram that appears to be closest to the color of the test light source. The dominant wavelength is determined by drawing a straight line from the equal-energy point to the (x, y) chromaticity coordinate of the test light source, and by extending the straight line to the perimeter of the chromaticity diagram. The intersection point is the dominant wavelength of the light source. The procedure is schematically shown in Fig. 17.9.

The ***color purity*** or ***color saturation*** of a light source is the distance in the chromaticity diagram between the (x, y) color-coordinate point of the test source and the coordinate of the equal-energy point divided by the distance between the equal-energy point and the dominant-wavelength point. The color purity is thus given by

$$\text{color purity} \;=\; \frac{a}{a \;+\; b} \;=\; \frac{\sqrt{(x - x_{ee})^2 \;+\; (y - y_{ee})^2}}{\sqrt{(x_d - x_{ee})^2 \;+\; (y_d - y_{ee})^2}} \tag{17.14}$$

where a and b are shown in Fig. 17.9 and (x, y), (x_{ee}, y_{ee}), and (x_d, y_d) represent the chromaticity coordinates of the light source under test, of the equal-energy reference illuminant, and of the dominant-wavelength point, respectively. Thus the color purity is the relative distance of a light source under test from the center of the chromaticity diagram. Generally, the color purity is 100% for monochromatic light sources ($\Delta\lambda \to 0$) located on the perimeter of the chromaticity

diagram and near 0% for white illuminants.

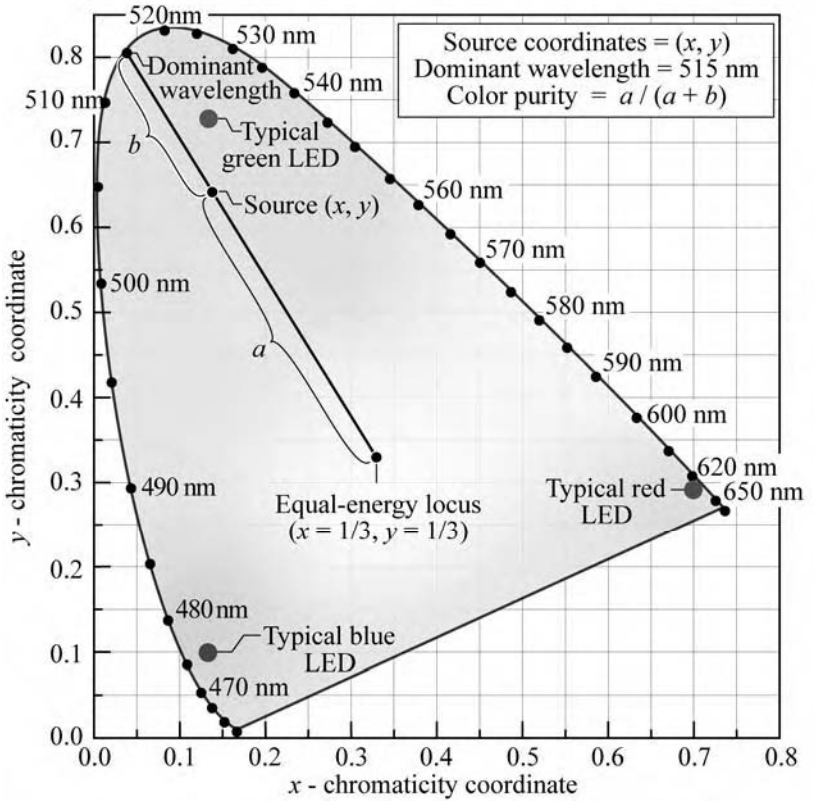

Fig. 17.9. Chromaticity diagram showing the determination of the *dominant wavelength* and *color purity* of a light source with chromaticity coordinates (x, y) using the equal-energy locus $(x = 1/3, y = 1/3)$ as the white-light reference. Also shown are typical locations of blue, green, and red LEDs.

Note that the dominant wavelength and color purity are an alternative way to uniquely characterize the location of an emitter on the chromaticity diagram. Dominant wavelength and color purity are quite intuitive quantities (more so than the numerical (x, y) chromaticity coordinates) and they are therefore frequently preferred.

17.3 LEDs in the chromaticity diagram

Monochromatic light sources ($\Delta\lambda \to 0$) are located on the perimeter of the chromaticity diagram. Light emission from LEDs is monochromatic (single color) to the eye but LEDs are not monochromatic in the strict physical sense since LEDs have a spectral linewidth of about 1.8 kT. Owing to the finite spectral linewidth of LEDs, they are not located on the very perimeter of the chromaticity diagram but are located *close* to the perimeter. When a source emits light distributed over a range of wavelengths, then the chromaticity location moves towards the center of the diagram.

The location of different LEDs on the chromaticity diagram is shown in Fig. 17.10. Inspection of the figure reveals that the location of red and blue LEDs is on the perimeter of the

chromaticity diagram. That is, their color purity is very high, close to 100%. However, blue–green and green LEDs are located off the perimeter closer to the center of the diagram due to the finite linewidth of the emission spectrum and the strong curvature of the chromaticity diagram in the green wavelength range.

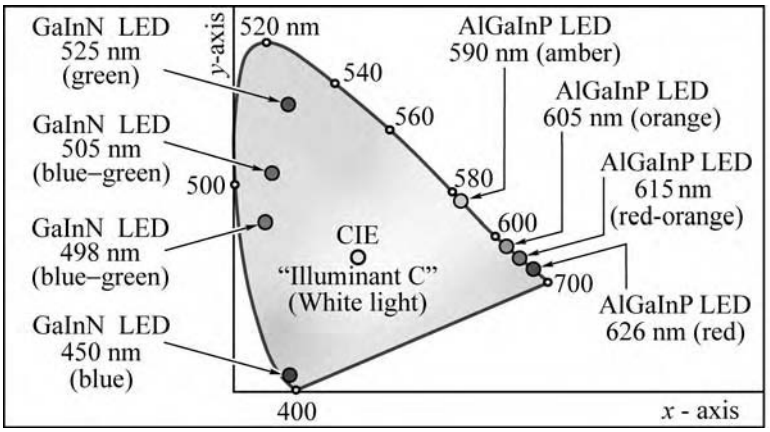

Fig. 17.10. Location of LED light emission on the chromaticity diagram (adapted from Schubert and Miller, 1999).

17.4 Relationship between chromaticity and color

Having completed the discussion of *chromaticity* allows us to revisit the question: What is *color*? One could certainly define a color by its location in the chromaticity diagram (i.e. by its chromaticity). However, the CIE (1986) adopted a more general definition of the term "color" that goes beyond the location in the chromaticity diagram. The CIE's broader definition of color includes ***chromaticity*** as well as ***brightness***. That is, we can keep the chromaticity of a light source the same but change its luminous intensity (brightness); this, according to the CIE definition, changes the color of the source. If, on the other hand, we restrict our considerations to a single brightness level, the terms "chromaticity" and "color" can be used synonymously.

The location of a chromaticity point can be expressed by the *dominant wavelength* and *saturation* (or, alternatively, by *hue* and *saturation*). Thus, the CIE definition of the *color of light* is given by the *dominant wavelength*, *saturation*, *and* ***bright****ness*. The *color of an object* is given by the *dominant wavelength*, *saturation*, *and* ***light****ness*.

References

CIE *Commission Internationale de l'Eclairage Proceedings* (Cambridge University Press, Cambridge, 1931)
CIE data of 1931 and 1978 available at http://cvision.ucsd.edu and http://www.cvrl.org (1978)
CIE data of 1960 relating to the (u, v) chromaticity coordinates can be found in CIE, 1986
CIE data of 1976 relating to the (u', v') chromaticity coordinates can be found in CIE, 1986

CIE publication No. 15 (E.1.3.1) 1971: *Colorimetry*; this publication was updated in 1986 to CIE Publication 15.2 *Colorimetry* (CIE, Vienna, Austria, 1986)

Gage S., Evans D., Hodapp M. W., and Sorensen H. *Optoelectronics Applications Manual* 1st edition (McGraw Hill, New York, 1977)

Judd D. B. "Report of US Secretariat Committee on Colorimetry and Artificial Daylight" in *Proceedings of the 12th Session of the CIE* **1**, p. 11 (Bureau Central de la CIE, Paris, 1951)

MacAdam D. L. "Specification of small chromaticity differences" *J. Opt. Soc. Am.* **33**, 18 (1943)

MacAdam D. L. (Editor) *Colorimetry – Fundamentals* (SPIE Optical Engineering Press, Bellingham, Washington, 1993)

Schubert E. F. and Miller J. N "Light-emitting diodes - An introduction" *Encyclopedia of Electrical Engineering*, edited by John G. Webster, Vol. **11**, p. 326 (John Wiley and Sons, New York, March 1999)

Vos J. J. "Colorimetric and photometric properties of a 2-degree fundamental observer" *Color Res. Appl.* **3**, 125 (1978)

Wyszecki G. and Stiles W. S. *Color Science – Concepts and Methods, Quantitative Data and Formulae* 2nd edition (John Wiley and Sons, New York, 2000)

Wright W. D. "The graphical representation of small color differences" *J. Opt. Soc. Am.* **33**, 632 (1943)

Appendix 17.1

Tabulated values of the CIE 1931 two-degree color-matching functions and eye sensitivity function for point sources (after CIE, 1931).

λ (nm)	$\bar{x}(\lambda)$ ***red***	$\bar{y} = V(\lambda)$ ***green***	$\bar{z}(\lambda)$ ***blue***
360	1.2990 E–4	3.9170 E–6	6.0610 E–4
365	2.3210 E–4	6.9650 E–6	1.0860 E–3
370	4.1490 E–4	1.2390 E–5	1.9460 E–3
375	7.4160 E–4	2.2020 E–5	3.4860 E–3
380	1.3680 E–3	3.9000 E–5	6.4500 E–3
385	2.2360 E–3	6.4000 E–5	1.0550 E–2
390	4.2430 E–3	1.2000 E–4	2.0050 E–2
395	7.6500 E–3	2.1700 E–4	3.6210 E–2
400	1.4310 E–2	3.9600 E–4	6.7850 E–2
405	2.3190 E–2	6.4000 E–4	0.11020
410	4.3510 E–2	1.2100 E–3	0.20740
415	7.7630 E–2	2.1800 E–3	0.37130
420	0.13438	4.0000 E–3	0.64560
425	0.21477	7.3000 E–3	1.03905
430	0.28390	1.1600 E–2	1.38560
435	0.32850	1.6840 E–2	1.62296
440	0.34828	2.3000 E–2	1.74706
445	0.34806	2.9800 E–2	1.78260
450	0.33620	3.8000 E–2	1.77211
455	0.31870	4.8000 E–2	1.74410
460	0.29080	6.0000 E–2	1.66920
465	0.25110	7.3900 E–2	1.52810
470	0.19536	9.0980 E–2	1.28764
475	0.14210	0.11260	1.04190
480	9.5640 E–2	0.13902	0.81295
485	5.7950 E–2	0.16930	0.61620
490	3.2010 E–2	0.20802	0.46518
495	1.4700 E–2	0.25860	0.35330
500	4.9000 E–3	0.32300	0.27200
505	2.4000 E–3	0.40730	0.21230
510	9.3000 E–3	0.50300	0.15820
515	2.9100 E–2	0.60820	0.11170
520	6.3270 E–2	0.71000	7.8250 E–2
525	0.10960	0.79320	5.7250 E–2
530	0.16550	0.86200	4.2160 E–2
535	0.22575	0.91485	2.9840 E–2
540	0.29040	0.95400	2.0300 E–2
545	0.35970	0.98030	1.3400 E–2
550	0.43345	0.99495	8.7500 E–3
555	0.51205	1.00000	5.7500 E–3
560	0.59450	0.99500	3.9000 E–3
565	0.67840	0.97860	2.7500 E–3
570	0.76210	0.95200	2.1000 E–3
575	0.84250	0.91540	1.8000 E–3
580	0.91630	0.87000	1.6500 E–3
585	0.97860	0.81630	1.4000 E–3
590	1.02630	0.75700	1.1000 E–3
595	1.05670	0.69490	1.0000 E–3
600	1.06220	0.63100	8.0000 E–4
605	1.04560	0.56680	6.0000 E–4
610	1.00260	0.50300	3.4000 E–4
615	0.93840	0.44120	2.4000 E–4
620	0.85445	0.38100	1.9000 E–4
625	0.75140	0.32100	1.0000 E–4
630	0.64240	0.26500	5.0000 E–5
635	0.54190	0.21700	3.0000 E–5
640	0.44790	0.17500	2.0000 E–5
645	0.36080	0.13820	1.0000 E–5
650	0.28350	0.10700	0.0000 E–5
655	0.21870	8.1600 E–2	0.0000 E–5
660	0.16490	6.1000 E–2	0.0000 E–5
665	0.12120	4.4580 E–2	0.0000 E–5
670	8.7400 E–2	3.2000 E–2	0.0000 E–5
675	6.3600 E–2	2.3200 E–2	0.0000 E–5
680	4.6770 E–2	1.7000 E–2	0.0000 E–5
685	3.2900 E–2	1.1920 E–2	0.0000 E–5
690	2.2700 E–2	8.2100 E–3	0.0000 E–5
695	1.5840 E–2	5.7230 E–3	0.0000 E–5
700	1.1359 E–2	4.1020 E–3	0.0000 E–5
705	8.1109 E–3	2.9290 E–3	0.0000 E–5
710	5.7903 E–3	2.0910 E–3	0.0000 E–5
715	4.1065 E–3	1.4840 E–3	0.0000 E–5
720	2.8993 E–3	1.0470 E–3	0.0000 E–5
725	2.0492 E–3	7.4000 E–4	0.0000 E–5
730	1.4400 E–3	5.2000 E–4	0.0000 E–5
735	9.9995 E–4	3.6110 E–4	0.0000 E–5
740	6.9008 E–4	2.4920 E–4	0.0000 E–5
745	4.7602 E–4	1.7190 E–4	0.0000 E–5
750	3.3230 E–4	1.2000 E–4	0.0000 E–5
755	2.3483 E–4	8.4800 E–5	0.0000 E–5
760	1.6615 E–4	6.0000 E–5	0.0000 E–5
765	1.1741 E–4	4.2400 E–5	0.0000 E–5
770	8.3075 E–5	3.0000 E–5	0.0000 E–5
775	5.8707 E–5	2.1200 E–5	0.0000 E–5
780	4.1510 E–5	1.4990 E–5	0.0000 E–5
785	2.9353 E–5	1.0600 E–5	0.0000 E–5
790	2.0674 E–5	7.4657 E–6	0.0000 E–5
795	1.4560 E–5	5.2578 E–6	0.0000 E–5
800	1.0254 E–5	3.7029 E–6	0.0000 E–5
805	7.2215 E–6	2.6078 E–6	0.0000 E–5
810	5.0859 E–6	1.8366 E–6	0.0000 E–5
815	3.5817 E–6	1.2934 E–6	0.0000 E–5
820	2.5225 E–6	9.1093 E–7	0.0000 E–5
825	1.7765 E–6	6.4153 E–7	0.0000 E–5

Appendix 17.2

Tabulated values of the CIE 1978 two-degree color-matching functions and eye sensitivity function for point sources (after CIE, 1978). The functions are also called the Judd–Vos-modified color-matching functions.

λ (nm)	$\bar{x}(\lambda)$ ***red***	$\bar{y} = V(\lambda)$ ***green***	$\bar{z}(\lambda)$ ***blue***
380	2.6899E–3	2.0000E–4	1.2260E–2
385	5.3105E–3	3.9556E–4	2.4222E–2
390	1.0781E–2	8.0000E–4	4.9250E–2
395	2.0792E–2	1.5457E–3	9.5135E–2
400	3.7981E–2	2.8000E–3	1.7409E–1
405	6.3157E–2	4.6562E–3	2.9013E–1
410	9.9941E–2	7.4000E–3	4.6053E–1
415	1.5824E–1	1.1779E–2	7.3166E–1
420	2.2948E–1	1.7500E–2	1.0658
425	2.8108E–1	2.2678E–2	1.3146
430	3.1095E–1	2.7300E–2	1.4672
435	3.3072E–1	3.2584E–2	1.5796
440	3.3336E–1	3.7900E–2	1.6166
445	3.1672E–1	4.2391E–2	1.5682
450	2.8882E–1	4.6800E–2	1.4717
455	2.5969E–1	5.2122E–2	1.3740
460	2.3276E–1	6.0000E–2	1.2917
465	2.0999E–1	7.2942E–2	1.2356
470	1.7476E–1	9.0980E–2	1.1138
475	1.3287E–1	1.1284E–1	9.4220E–1
480	9.1944E–2	1.3902E–1	7.5596E–1
485	5.6985E–2	1.6987E–1	5.8640E–1
490	3.1731E–2	2.0802E–1	4.4669E–1
495	1.4613E–2	2.5808E–1	3.4116E–1
500	4.8491E–3	3.2300E–1	2.6437E–1
505	2.3215E–3	4.0540E–1	2.0594E–1
510	9.2899E–3	5.0300E–1	1.5445E–1
515	2.9278E–2	6.0811E–1	1.0918E–1
520	6.3791E–2	7.1000E–1	7.6585E–2
525	1.1081E–1	7.9510E–1	5.6227E–2
530	1.6692E–1	8.6200E–1	4.1366E–2
535	2.2768E–1	9.1505E–1	2.9353E–2
540	2.9269E–1	9.5400E–1	2.0042E–2
545	3.6225E–1	9.8004E–1	1.3312E–2
550	4.3635E–1	9.9495E–1	8.7823E–3
555	5.1513E–1	1.0000	5.8573E–3
560	5.9748E–1	9.9500E–1	4.0493E–3
565	6.8121E–1	9.7875E–1	2.9217E–3
570	7.6425E–1	9.5200E–1	2.2771E–3
575	8.4394E–1	9.1558E–1	1.9706E–3
580	9.1635E–1	8.7000E–1	1.8066E–3
585	9.7703E–1	8.1623E–1	1.5449E–3
590	1.0230	7.5700E–1	1.2348E–3
595	1.0513	6.9483E–1	1.1177E–3
600	1.0550	6.3100E–1	9.0564E–4
605	1.0362	5.6654E–1	6.9467E–4
610	9.9239E–1	5.0300E–1	4.2885E–4
615	9.2861E–1	4.4172E–1	3.1817E–4
620	8.4346E–1	3.8100E–1	2.5598E–4
625	7.3983E–1	3.2052E–1	1.5679E–4
630	6.3289E–1	2.6500E–1	9.7694E–5
635	5.3351E–1	2.1702E–1	6.8944E–5
640	4.4062E–1	1.7500E–1	5.1165E–5
645	3.5453E–1	1.3812E–1	3.6016E–5
650	2.7862E–1	1.0700E–1	2.4238E–5
655	2.1485E–1	8.1652E–2	1.6915E–5
660	1.6161E–1	6.1000E–2	1.1906E–5
665	1.1820E–1	4.4327E–2	8.1489E–6
670	8.5753E–2	3.2000E–2	5.6006E–6
675	6.3077E–2	2.3454E–2	3.9544E–6
680	4.5834E–2	1.7000E–2	2.7912E–6
685	3.2057E–2	1.1872E–2	1.9176E–6
690	2.2187E–2	8.2100E–3	1.3135E–6
695	1.5612E–2	5.7723E–3	9.1519E–7
700	1.1098E–2	4.1020E–3	6.4767E–7
705	7.9233E–3	2.9291E–3	4.6352E–7
710	5.6531E–3	2.0910E–3	3.3304E–7
715	4.0039E–3	1.4822E–3	2.3823E–7
720	2.8253E–3	1.0470E–3	1.7026E–7
725	1.9947E–3	7.4015E–4	1.2207E–7
730	1.3994E–3	5.2000E–4	8.7107E–8
735	9.6980E–4	3.6093E–4	6.1455E–8
740	6.6847E–4	2.4920E–4	4.3162E–8
745	4.6141E–4	1.7231E–4	3.0379E–8
750	3.2073E–4	1.2000E–4	2.1554E–8
755	2.2573E–4	8.4620E–5	1.5493E–8
760	1.5973E–4	6.0000E–5	1.1204E–8
765	1.1275E–4	4.2446E–5	8.0873E–9
770	7.9513E–5	3.0000E–5	5.8340E–9
775	5.6087E–5	2.1210E–5	4.2110E–9
780	3.9541E–5	1.4989E–5	3.0383E–9
785	2.7852E–5	1.0584E–5	2.1907E–9
790	1.9597E–5	7.4656E–6	1.5778E–9
795	1.3770E–5	5.2592E–6	1.1348E–9
800	9.6700E–6	3.7028E–6	8.1565E–10
805	6.7918E–6	2.6076E–6	5.8626E–10
810	4.7706E–6	1.8365E–6	4.2138E–10
815	3.3550E–6	1.2950E–6	3.0319E–10
820	2.3534E–6	9.1092E–7	2.1753E–10
825	1.6377E–6	6.3564E–7	1.5476E–10

18

Planckian sources and color temperature

White light is a unique color. There are a very large number of optical spectra that can be used to generate white light. Among these spectra, the planckian black-body radiation spectrum forms a unique and very useful standard because it allows us to describe the spectrum with only one parameter, namely the color temperature. Furthermore, natural daylight closely resembles the planckian spectrum.

18.1 The solar spectrum

White light usually has a broad spectrum extending over the entire visible range. An instructive model for white light is sunlight. The sun's optical spectrum is shown in Fig. 18.1, including the spectrum at sea level with the sun at zenith, incident above the earth's atmosphere, and at sunset and sunrise (Jackson, 1975). The spectrum of sunlight extends over the entire visible region. However, the sun's spectrum depends on the time of day, season, altitude, weather, and other factors.

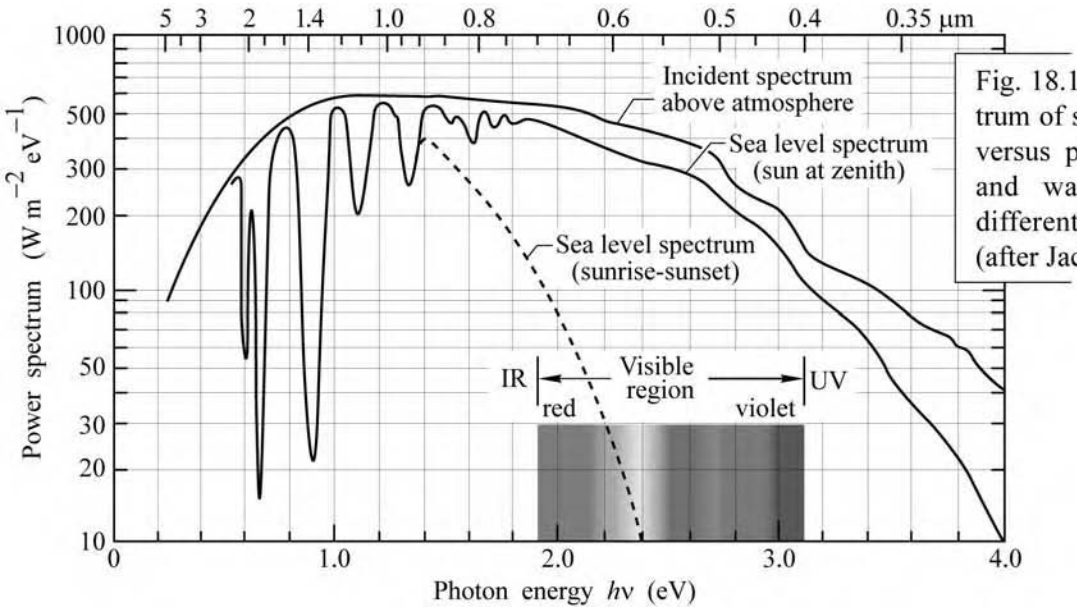

Fig. 18.1. Power spectrum of solar radiation versus photon energy and wavelength for different conditions (after Jackson, 1975).

Exact replication of the solar spectrum for white-light illumination sources would not yield an efficient source due to the large infrared (IR) and ultraviolet (UV) components of the solar spectrum. Thus, "mother nature" does not serve as a good example for an efficient white source. Even if the IR and UV components of the spectrum were to be eliminated, the solar spectrum still would not be optimum, due to the high intensity at the visible-IR and visible-UV boundaries.

18.2 The planckian spectrum

It is desirable to define an independent standard for white light. The ***planckian black-body radiation spectrum*** is used as one such standard. The black-body spectrum is characterized by only one parameter, the temperature of the body. The black-body spectrum was first derived by Max Planck (1900) and is given by

$$I(\lambda) = \frac{2hc^2}{\lambda^5\left[\exp\left(\frac{hc}{\lambda kT}\right) - 1\right]} . \qquad (18.1)$$

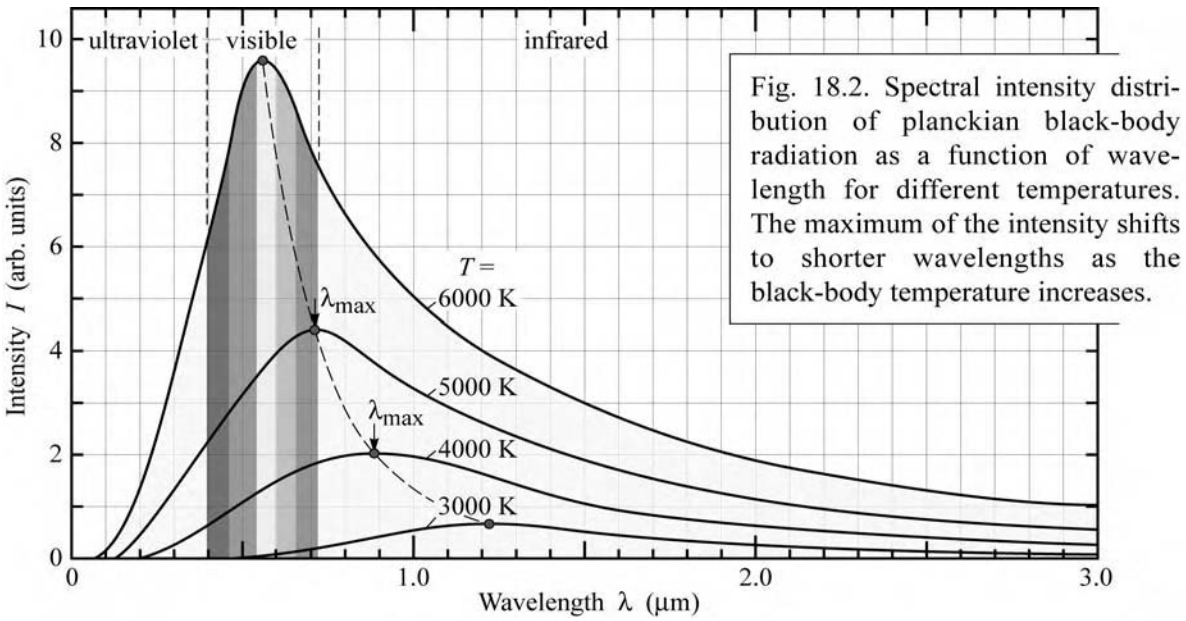

Fig. 18.2. Spectral intensity distribution of planckian black-body radiation as a function of wavelength for different temperatures. The maximum of the intensity shifts to shorter wavelengths as the black-body temperature increases.

The planckian spectrum is shown for different black-body temperatures in Fig. 18.2. The maximum intensity of radiation emanating from a black body of temperature T occurs at a specific wavelength which is given by ***Wien's law***

$$\lambda_{max} = \frac{2880\ \mu m\ K}{T} . \qquad (18.2)$$

At “low” black-body temperatures, e.g. 3 000 K, the radiation occurs mostly in the infrared. As the temperature increases, the maximum of the radiation shifts into the visible wavelength range.

The location of the black-body radiation in the (x, y) chromaticity diagram (called planckian locus) is shown in Fig. 18.3. As the temperature of the black body increases, the chromaticity location moves from the red wavelength range towards the center of the diagram. Typical black-body temperatures in the white region of the chromaticity diagram range between 2 500 and 10 000 K. Also shown in Fig. 18.3 are the locations of several illuminants standardized by the CIE. These standard illuminants include Illuminants A, B, C, D_{65}, and E. The planckian locus and the locations of the black-body temperatures in the (u', v') uniform chromaticity diagram are shown in Fig. 18.4. The (x, y) and in (u', v') chromaticity coordinates of the planckian radiator are tabulated in Appendix 18.1.

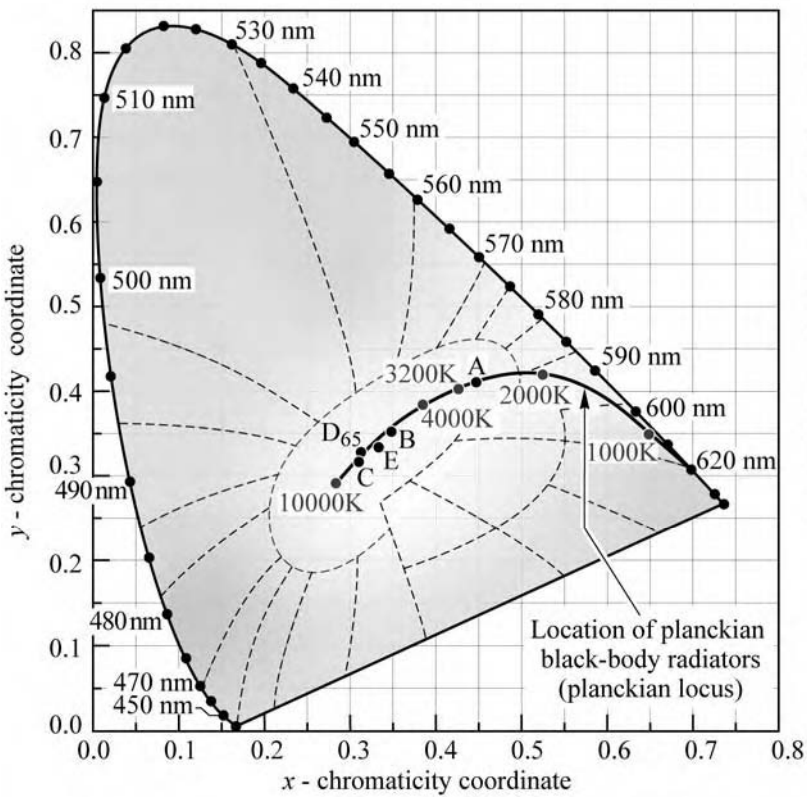

Illuminant A
(x, y) = (0.4476, 0.4074)
(Incandescent source, T = 2856 K)

Illuminant B
(x, y) = (0.3484, 0.3516)
(Direct sunlight, T = 4870 K)

Illuminant C
(x, y) = (0.3101, 0.3162)
(Overcast source, T = 6770 K)

Illuminant D_{65}
(x, y) = (0.3128, 0.3292)
(Daylight, T = 6500 K)

Illuminant E (equal-energy point)
(x, y) = (0.3333, 0.3333)

Fig. 18.3. Chromaticity diagram showing planckian locus, the standardized white Illuminants A, B, C, D_{65}, and E, and their color temperatures (after CIE, 1978).

In both the (x, y) and the (u', v') chromaticity diagrams, the planckian locus starts out in the red, then moves through the orange and yellow, to finally the white region. This sequence of colors is reminiscent of the colors of a real object (e.g. a piece of metal) heated to high

temperatures, indicating that real objects closely follow the chromaticity of Planck's idealized black bodies.

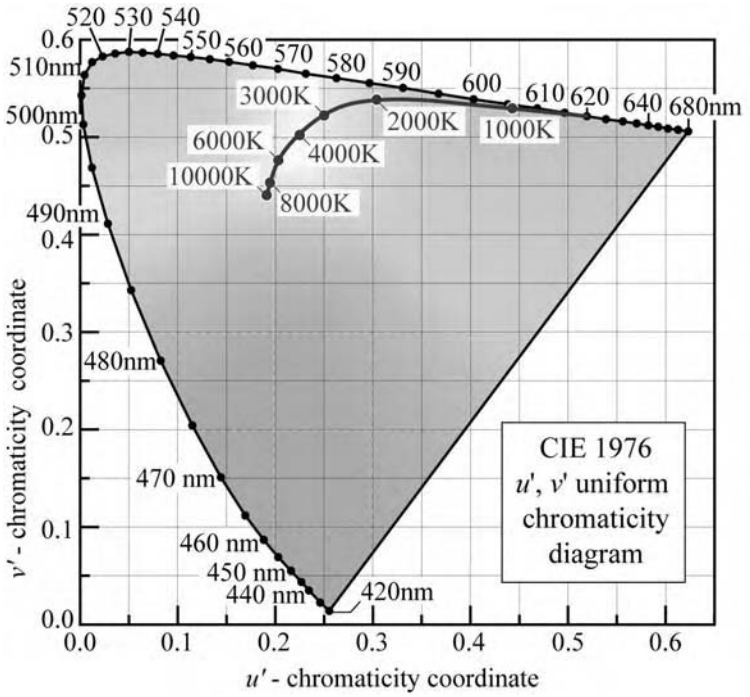

Fig. 18.4. CIE 1976 (u', v') uniform chromaticity diagram calculated using the CIE 1931 2° standard observer and planckian locus.

18.3 Color temperature and correlated color temperature

Color temperature may appear to be a somewhat surprising quantity as *color* and *temperature* don't seem to have a direct relationship with each other. However, the relationship is derived from Planck's black-body radiator. With increasing temperatures, it glows in the red, orange, yellowish white, white, and ultimately bluish white. The ***color temperature*** (CT) of a white light source, given in units of kelvin, is the temperature of a planckian black-body radiator that has the same chromaticity location as the white light source considered.

If the color of a white light source does not fall on the planckian locus, the ***correlated color temperature*** (CCT), also given in units of kelvin, is used. The correlated color temperature of a white light source is defined as the temperature of a planckian black-body radiator whose color is closest to the color of the white light source.

The correlated color temperature of a light source is determined as follows. On the (u', v') uniform chromaticity diagram, the point on the planckian locus that is *closest* to the chromaticity location of the light source is determined (i.e. shortest geometrical distance). The correlated color temperature is the temperature of the planckian black-body radiator at that point. The

determination of the correlated color temperature was discussed in CIE publication No. 17.4 (1987) and by Robertson (1968).

On the (x, y) chromaticity diagram, the correlated color temperature *cannot* be determined by using the shortest distance to the planckian locus due to the non-uniformity of the (x, y) chromaticity diagram. The lines of constant correlated color temperature in the (x, y) chromaticity diagram are shown in Fig. 18.5 (Duggal, 2005).

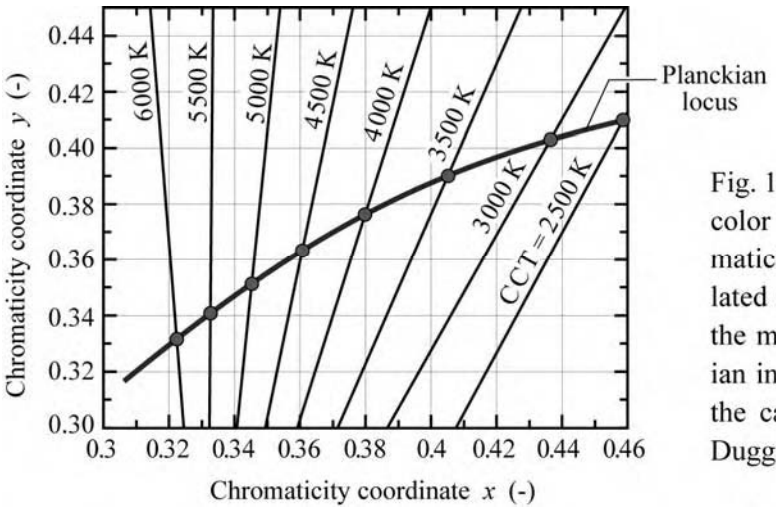

Fig. 18.5. Lines of constant correlated color temperature in the (x, y) chromaticity diagram. Whereas the correlated color temperature follows from the minimum distance to the planckian in the (u', v') diagram, this is not the case in the (x, y) diagram (after Duggal, 2005).

Table 18.1. Correlated color temperatures of common artificial and natural light sources.

Light source	**Correlated color temperature (K)**
Wax candle flame / CIE standard candle flame	1 500 to 2 000 / 2 000
W filament household lamp: 60 W / 100 W	2 800 / 2 850
W filament halogen lamp	2 800 to 3 200
“Warm white” fluorescent tube	3 000
“Cool daylight white” fluorescent tube	4 300
“True daylight” color match fluorescent tube	6 500
Carbon arc white flame	5 000
Xenon arc (unfiltered)	6 000
Summer sunlight (before 9.00 or after 15.00 h)	4 900 to 5 600
Summer sunlight (9.00 to 15.00 h)	5 400 to 5 700
Direct sun	5 700 to 6 500
Overcast daylight	6 500 to 7 200
Clear blue sky	8 000 to 27 000

The chromaticity locations of incandescent light sources are very close to, although not exactly on the planckian locus (Ohno, 2001). For such incandescent light sources, the *color temperature* can be specified. Standard incandescents have color temperatures ranging from 2 000 to 2 900 K. The common warm incandescent light source has a color temperature of 2 800 K. Quartz halogen incandescent lamps have a color temperature ranging from 2 800 to 3 200 K (Ohno, 1997). Other light sources, such as metal-halide sources, are further removed from the planckian locus. For such light sources, the *correlated color temperature* should be used. Bluish white lights have a correlated color temperature of about 8 000 K. Color temperatures and correlated color temperatures of common artificial and natural light sources are given in Table 18.1.

References

CIE publication No. 17.4 *International Lighting Vocabulary* see http://www.cie.co.at (CIE, Vienna, Austria, 1987)

Duggal A. R. "Organic electroluminescent devices for solid-state lighting" in *Organic Electroluminescence* edited by Z. H. Kafafi (Taylor & Francis Group, Boca Raton, Florida, 2005)

Jackson J. D. *Classical Electrodynamics* (John Wiley and Sons, New York, 1975)

Ohno Y. "Photometric standards" Chapter 3 in *OSA/AIP Handbook of Applied Photometry*, 55 (Optical Society of America, Washington DC, 1997)

Ohno Y. "Photometry and radiometry" Chapter 14 in *OSA Handbook of Optics*, *Volume III Review for Vision Optics, Part 2, Vision Optics* (McGraw-Hill, New York, 2001)

Planck M. "On the theory of the law on energy distribution in the normal spectrum (translated from German)" *Verhandlungen der Deutschen Physikalischen Gesellschaft* **2**, 237 (1900)

Robertson R. "Computation of correlated color temperature and distribution temperature" *J. Opt. Soc. Am*. **58**, 1528 (1968)

Appendix 18.1

Color temperature T and (x, y) and (u', v') chromaticity coordinates of a planckian emitter.

T	x	y	u'	v'
1 000 K	0.649	0.347	0.443	0.533
1 200 K	0.623	0.370	0.402	0.538
1 400 K	0.597	0.389	0.369	0.541
1 600 K	0.572	0.402	0.342	0.542
1 800 K	0.549	0.412	0.321	0.542
2 000 K	0.527	0.417	0.303	0.540
2 200 K	0.506	0.420	0.288	0.538
2 400 K	0.487	0.419	0.276	0.535
2 600 K	0.470	0.417	0.266	0.531
2 800 K	0.454	0.414	0.257	0.528
3 000 K	0.439	0.409	0.250	0.524
3 200 K	0.425	0.404	0.243	0.520
3 400 K	0.413	0.399	0.237	0.516
3 600 K	0.402	0.393	0.233	0.512
3 800 K	0.392	0.388	0.228	0.508
4 000 K	0.383	0.382	0.225	0.504
4 200 K	0.374	0.376	0.221	0.500
4 400 K	0.367	0.371	0.218	0.497
4 600 K	0.360	0.366	0.216	0.494
4 800 K	0.353	0.361	0.213	0.490
5 000 K	0.347	0.356	0.211	0.487
5 200 K	0.342	0.351	0.209	0.484
5 400 K	0.337	0.347	0.208	0.481
5 600 K	0.332	0.343	0.206	0.479
5 800 K	0.328	0.339	0.205	0.476
6 000 K	0.324	0.335	0.203	0.473
6 200 K	0.321	0.332	0.202	0.471
6 400 K	0.317	0.328	0.201	0.469
6 500 K	0.315	0.327	0.201	0.468
6 600 K	0.314	0.325	0.200	0.466
6 800 K	0.311	0.322	0.199	0.464
7 000 K	0.308	0.319	0.198	0.462
7 200 K	0.306	0.317	0.198	0.460
7 400 K	0.303	0.314	0.197	0.459
7 600 K	0.301	0.312	0.196	0.457
7 800 K	0.299	0.309	0.196	0.455
8 000 K	0.297	0.307	0.195	0.454
8 500 K	0.292	0.301	0.194	0.450
9 000 K	0.289	0.297	0.193	0.447
9 500 K	0.285	0.293	0.192	0.444
10 000 K	0.282	0.290	0.191	0.441

19

Color mixing and color rendering

19.1 Additive color mixing

The *combination* or *additive mixing* of two or more light sources is employed in a number of applications. In LED displays, three different types of LEDs, usually emitting in the red, green, and blue, are used. The three colors are mixed so that the observer can experience a wide range of colors. Another useful application of color mixing is the generation of white light by two, three, or more complementary colors. A schematic of additive color mixing and a corresponding experiment are shown in Fig. 19.1.

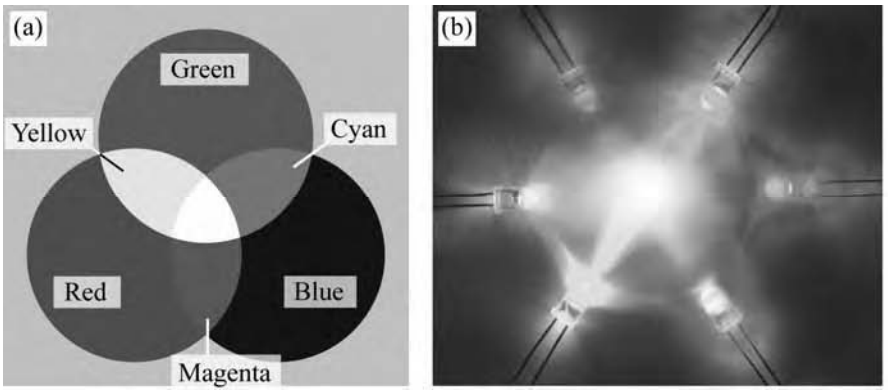

Fig. 19.1. (a) Schematic of additive color mixing of three primary colors. (b) Additive color mixing using LEDs.

Next, we determine the chromaticity coordinates of the mixture of three discrete emission bands. Assume that the three emission bands have spectral power densities $P_1(\lambda)$, $P_2(\lambda)$, and $P_3(\lambda)$ with peak wavelengths of λ_1, λ_2, λ_3, respectively. We assume that each emission band is much narrower than any of the three color-matching functions. We further assume that the three light sources have the chromaticity coordinates (x_1, y_1), (x_2, y_2), and (x_3, y_3). Then the tristimulus values are given by

$$X = \int_\lambda \bar{x}(\lambda) P_1(\lambda)\,\mathrm{d}\lambda + \int_\lambda \bar{x}(\lambda) P_2(\lambda)\,\mathrm{d}\lambda + \int_\lambda \bar{x}(\lambda) P_3(\lambda)\,\mathrm{d}\lambda \approx \bar{x}(\lambda_1) P_1 + \bar{x}(\lambda_2) P_2 + \bar{x}(\lambda_3) P_3 \quad (19.1)$$

$$Y = \int_\lambda \bar{y}(\lambda)\, P_1(\lambda)\, \mathrm{d}\lambda + \int_\lambda \bar{y}(\lambda)\, P_2(\lambda)\, \mathrm{d}\lambda + \int_\lambda \bar{y}(\lambda)\, P_3(\lambda)\, \mathrm{d}\lambda \approx \bar{y}(\lambda_1)\, P_1 + \bar{y}(\lambda_2)\, P_2 + \bar{y}(\lambda_3)\, P_3 \quad (19.2)$$

$$Z = \int_\lambda \bar{z}(\lambda)\, P_1(\lambda)\, \mathrm{d}\lambda + \int_\lambda \bar{z}(\lambda)\, P_2(\lambda)\, \mathrm{d}\lambda + \int_\lambda \bar{z}(\lambda)\, P_3(\lambda)\, \mathrm{d}\lambda \approx \bar{z}(\lambda_1)\, P_1 + \bar{z}(\lambda_2)\, P_2 + \bar{z}(\lambda_3)\, P_3 \quad (19.3)$$

where P_1, P_2, and P_3 are the optical powers emitted by the three sources. Using the abbreviations

$$L_1 = \bar{x}(\lambda_1)\, P_1 + \bar{y}(\lambda_1)\, P_1 + \bar{z}(\lambda_1)\, P_1 \quad (19.4)$$

$$L_2 = \bar{x}(\lambda_2)\, P_2 + \bar{y}(\lambda_2)\, P_2 + \bar{z}(\lambda_2)\, P_2 \quad (19.5)$$

$$L_3 = \bar{x}(\lambda_3)\, P_3 + \bar{y}(\lambda_3)\, P_3 + \bar{z}(\lambda_3)\, P_3 \quad (19.6)$$

the chromaticity coordinates of the mixed light can be calculated from the tristimulus values to yield

$$x = \frac{x_1 L_1 + x_2 L_2 + x_3 L_3}{L_1 + L_2 + L_3} \quad (19.7)$$

$$y = \frac{y_1 L_1 + y_2 L_2 + y_3 L_3}{L_1 + L_2 + L_3}\,. \quad (19.8)$$

Thus, the chromaticity coordinate of the multi-component light *is a linear combination of the individual chromaticity coordinates* weighted by the L_i factors.

The principle of color mixing in the chromaticity diagram is shown in Fig. 19.2. The figure shows the mixing of *two* colors with chromaticity coordinates (x_1, y_1) and (x_2, y_2). For the case of two colors, $L_3 = P_3 = 0$. The mixed color will be located on the straight line connecting the chromaticity coordinates of the two light sources. Thus *any* color (including white) located between the two chromaticity points can be created by mixing the two colors.

Figure 19.2 also shows the mixing of *three* colors, located in the red, green, and blue regions of the chromaticity diagram. The three chromaticity points, connected by a dashed line, are typical points for red, green, and blue LEDs. The area located within the dashed line, called the ***color gamut***, represents all colors that can be created by mixing the three primary colors red, green, and blue. The ability to create a great variety of colors is an important quality for displays. It is desirable that the color gamut provided by the three light sources is as large as possible to create displays able to show brilliant, saturated colors.

The color gamut represents the entire range of colors that can be created from a set of

primary sources. Color gamuts are polygons positioned within the perimeter of the chromaticity diagram. For the case of *three* primary colors, the color gamut is a *triangle*, as shown in Fig. 19.2. All colors created by additive mixtures of the vertex points (primary colors) of a gamut, are necessarily located inside the gamut.

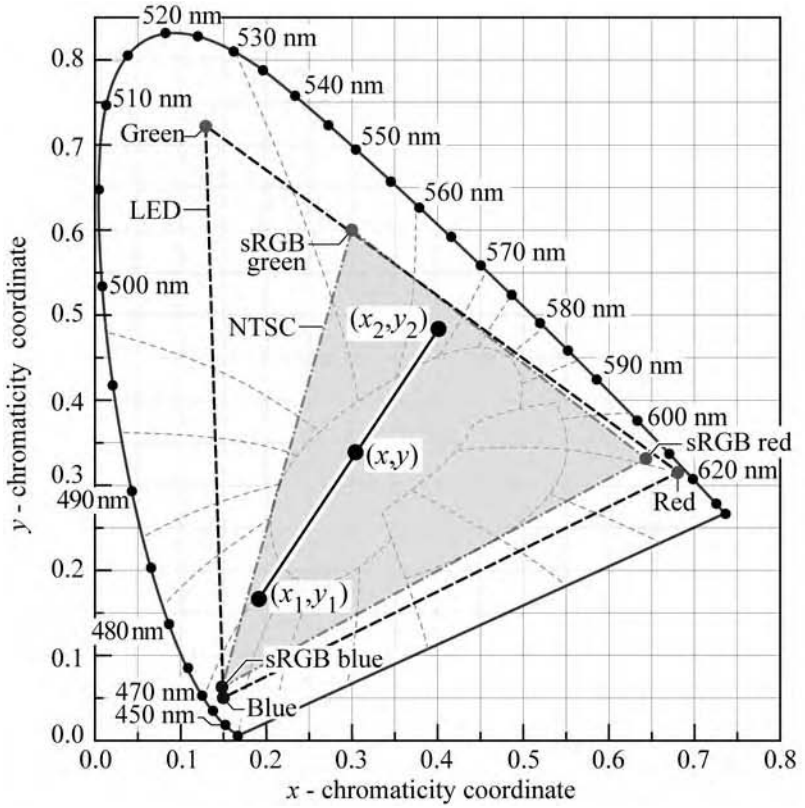

Fig. 19.2. Principle of color mixing illustrated with two light sources with chromaticity coordinates (x_1, y_1) and (x_2, y_2). The resulting color has the coordinates (x, y). Also shown is the triangular area of the chromaticity diagram (color gamut) accessible by additive mixing of a red, green, and blue LED. The locations of the red, green, and blue phosphors of the sRGB display standard (x_r = 0.64, y_r = 0.33, x_g = 0.30, y_g = 0.60, x_b = 0.15, y_b = 0.06) are also shown. The sRGB standard is similar to the NTSC standard.

The insight now gained on color mixing allows one to understand the location of different LEDs in the chromaticity diagram. The perimeter of the chromaticity diagram in the red spectral region is approximately a *straight line*, so that red LEDs, despite their thermal broadening, are located directly on the perimeter of the chromaticity diagram. In contrast, the perimeter is strongly curved in the green region, so that green LEDs, due to their spectral broadening, are displaced from the perimeter towards the center of the chromaticity diagram.

19.2 Color rendering

Another important characteristic of a white light source is its ability to show (i.e. render) the true colors of physical objects, e.g. fruits, plants, or toys, that are being illuminated by the source. The ability to render the colors of an object is measured in terms of the ***color-rendering index*** or ***CRI*** (Wyszecki and Stiles, 1982, 2000; MacAdam, 1993; Berger-Schunn, 1994; CIE, 1995). It is

a measure of the ability of the *illuminant* (i.e. a white illumination source) to faithfully render the colors of physical objects illuminated by the source.

Figure 19.3 shows an example of a physical object (here a painting by the impressionist Auguste Renoir) under illumination with a high-CRI source and with a low-CRI source. Colors appear richer and more vivid under illumination with a high-CRI source. Whereas high color rendering is important in locations such as museums, homes, and offices, it is less so in locations such as streets and parking lots. Finally, the color-rendering index is irrelevant for white light sources used in indicator lamp and signage applications.

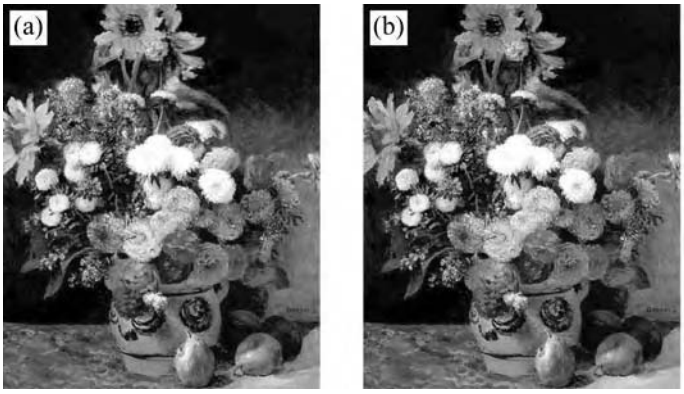

Fig. 19.3. Artwork entitled "Fleurs dans un vase" illuminated with (a) high-CRI source and (b) low-CRI source (Auguste Renoir, French impressionist, 1841–1919) .

The color-rendering ability of a ***test light source*** (to be abbreviated as ***test source***) is evaluated by comparing it with the color-rendering ability of a ***reference light source*** (to be abbreviated as ***reference source***). For the calculation of the CRI, the reference source is chosen as follows (CIE, 1995): (*i*) If the chromaticity point of the test source is located *on* the planckian locus, the reference source is a planckian black-body radiator with the same color temperature as the test source. (*ii*) If the chromaticity point of the test source is located *off* the planckian locus, the reference source is a planckian black-body radiator with the same *correlated* color temperature as the test source. (*iii*) Alternatively, one of the standardized CIE illuminants (e.g. Illuminant D_{65}) can be used as a reference source (CIE, 1995). Ideally, the test source and the reference source have the same chromaticity coordinates and luminous flux.

By convention, the planckian black-body reference source is assumed to have perfect color-rendering properties and thus its color-rendering index is CRI = 100. This convention was agreed upon because natural daylight closely resembles a planckian black-body source and thus rightfully deserves to be established as the standard reference source. Illuminants other than the reference source necessarily have a color-rendering index lower than 100. Because the CRI depends sensitively on the choice of the reference source, the selection of the reference source is

of critical importance when calculating the CRIs of test sources.

Because the emission spectrum of an incandescent lamp closely follows that of a planckian black-body radiator, such lamps have the highest possible CRI and thus the best color-rendering properties of all artificial light sources. Incandescent quartz-halogen lamps are used in locations where color rendering is of prime importance, such as in museums, art galleries, and clothing shops. The drawback of quartz-halogen lamps is high power consumption.

In addition to the test source and the reference source, ***test-color samples*** are instrumental in determining the CRI of a test source. Test-color samples could be derived from real objects, e.g. fruit, flowers, wood, furniture, and clothes. However, in the interest of international standardization, a specific set of 14 test-color samples has been agreed upon for the purpose of determining the CRI. These 14 test-color samples are a subset of a larger collection of test-color samples initially introduced by Albert H. Munsell, a professor who taught at Rochester Institute of Technology (Rochester, NY) in the late 1800s and early 1900s (Munsell, 1905; 2005; Billmeyer, 1987; Long and Luke, 2001). Munsell introduced a color notation – the ***Munsell color system*** – which is a notation for defining a very wide range of colors.

The CRI calculation has been discussed in detail by Wyszecki and Stiles (1982; 2000) and by CIE (1995). The ***CIE general CRI*** is an average calculated according to

$$\mathrm{CRI}_{\mathrm{general}} \quad = \quad \frac{1}{8} \sum_{i=1}^{8} \mathrm{CRI}_i \tag{19.9}$$

where the CRI_i are the ***special CRIs*** for a set of eight test-color samples. The special color-rendering indices are calculated according to

$$\mathrm{CRI}_i \quad = \quad 100 \; - \; 4.6 \, \Delta E_i^* \tag{19.10}$$

where ΔE_i^* represents the quantitative color change that occurs when a test-color sample is illuminated with, first, the reference illumination source (“reference source”), and subsequently with the test illumination source (“test source”). The special color-rendering indices are calculated in such a way that they have a value of 100 if there is no difference in color appearance. The quantitative color change, ΔE_i^*, plays a key role in the calculation of the CRI and the determination of ΔE_i^* will be discussed in detail in the two subsequent sections where we will differentiate between on-planckian-locus and off-planckian-locus test sources.

At the time Eq. (19.10) was established, the pre-factor 4.6 had been chosen in such a way

that the general CRI equals 60 when a “standard warm white” fluorescent lamp was used as a test source and a planckian black-body radiator was used as a reference source. Current fluorescent light sources have higher CRIs, typically in the range 60–85 (Kendall and Scholand, 2001).

The test-color samples mentioned above are defined in terms of their spectral reflectivity. The reflectivity curves of eight internationally agreed-upon test-color samples are shown in Fig. 19.4. The numerical values of the reflectivity of the eight test-color samples are listed in Appendix 19.1. The general color-rendering index is calculated from these eight test-color samples (i = 1–8).

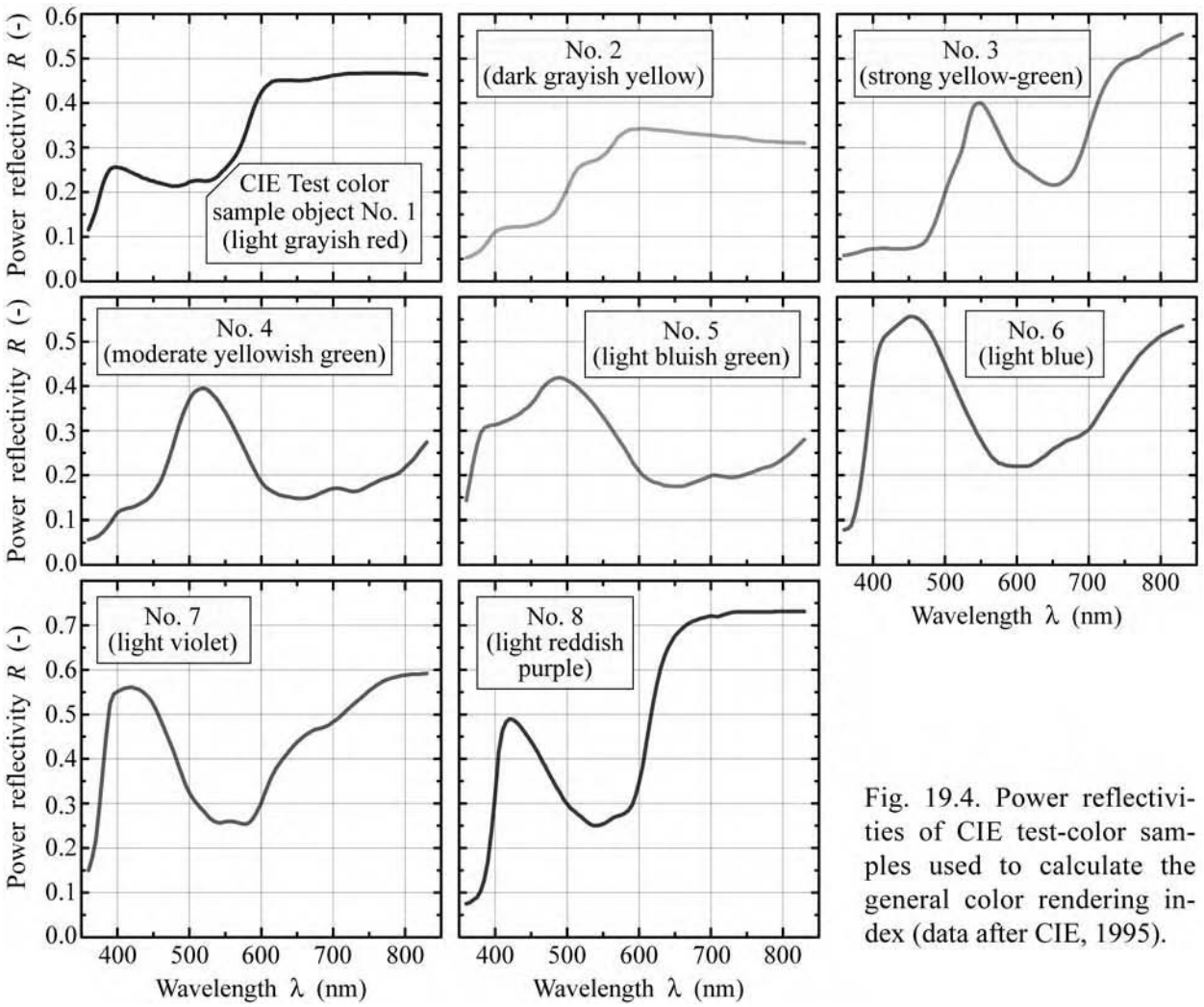

Fig. 19.4. Power reflectivities of CIE test-color samples used to calculate the general color rendering index (data after CIE, 1995).

In addition to the test-color samples (with numbers 1–8) used to calculate the *general* color rendering index, six supplemental test-color samples (with numbers 9–14) are used to further assess the color rendering capabilities of test sources. These supplemental test-color samples

have the following colors: 9 – strong red; 10 – strong yellow; 11 – strong green; 12 – strong purplish blue; 13 – complexion of white person; 14 – leaf of tree. The reflectivity spectra and the numerical values of the reflectivity of the supplemental test-color samples are given in Fig. 19.5 and in Appendix 19.2, respectively. Inspection of the reflectivity curves reveals that the colors of the test-color samples 9–14 have particularly strong colors with relatively narrow peaks. CRI_9 to CRI_{14} are referred to as the ***special color-rendering indices 9–14***.

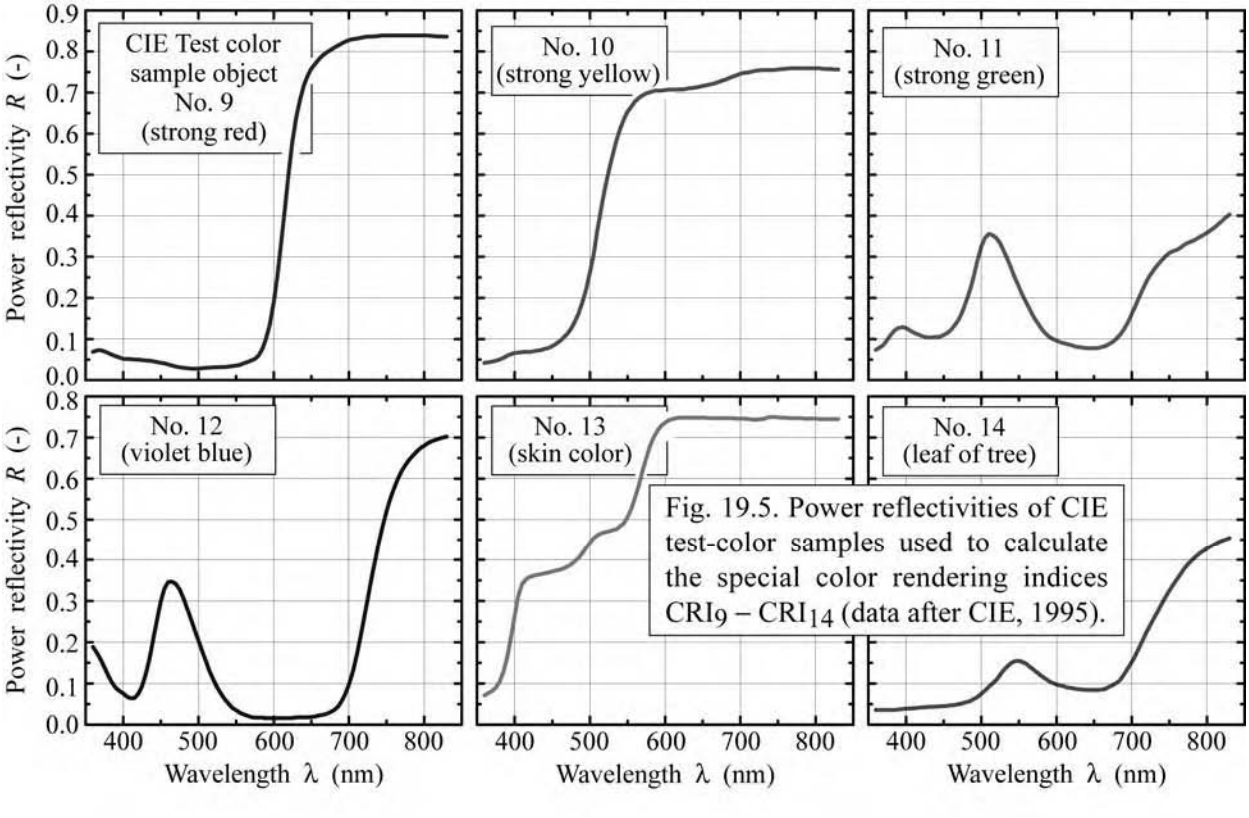

Fig. 19.5. Power reflectivities of CIE test-color samples used to calculate the special color rendering indices CRI_9 – CRI_{14} (data after CIE, 1995).

The meaning of *chromaticity difference* of a test and a reference illumination source and the rendered colors of a test-color sample, when illuminated with the test and reference illumination sources, is illustrated in Fig. 19.6. In the example shown in the figure, the test source is located slightly off the planckian locus. The reference source is a planckian source with the least possible distance from the test-source chromaticity point. As a result, the color temperature of the reference source is equal to the correlated color temperature of the test source. The four chromaticity points shown in Fig. 19.6 enter the calculation of the CRI.

Note, however, that the term “color” as used by the CIE, is not equal to “chromaticity”. The broad CIE definition for color includes hue, saturation, and additionally, brightness (for light) or lightness (for physical objects). Whereas hue and saturation are fully defined by location in the

chromaticity coordinate system, brightness and lightness are not. To allow for a graphical representation of object lightness (or source brightness) a third axis could be added to the chromaticity diagram, as done for illustrative purposes in Fig. 19.7. The *color difference* of a physical object when illuminated with, first, a reference source, and subsequently with a test source, thus consists of the *chromaticity difference* and the *lightness difference*, as represented by the geometrical distance of the two points shown in Fig. 19.7. The reader is cautioned that the representation shown in Fig. 19.7 is for educational purposes and not a standardized CIE representation.

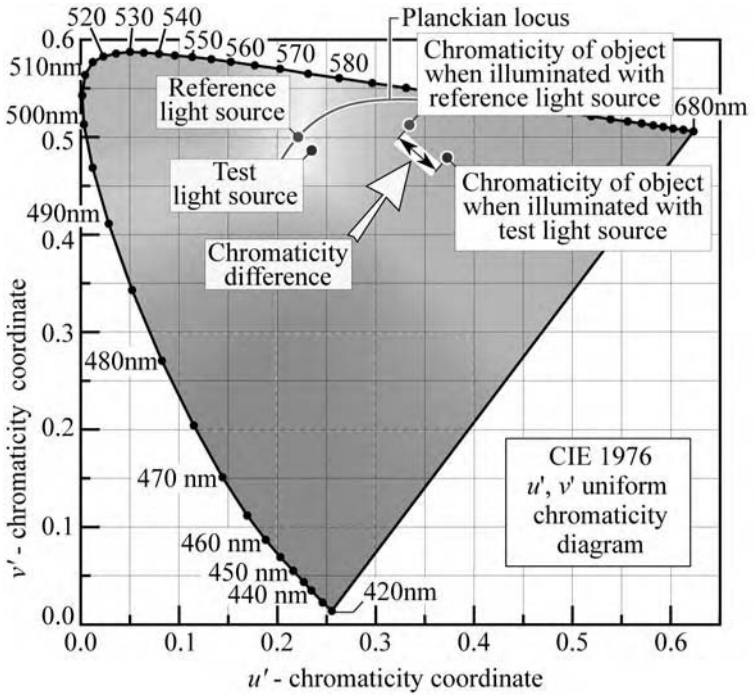

Fig. 19.6. Chromaticity difference resulting from the illumination of an object with a reference and a test light source. In the CIE 1976 u', v' uniform chromaticity diagram, the chromaticity difference is directly proportional to the geometric distance. The reference light source is located on the planckian locus at the correlated color temperature of the test light source.

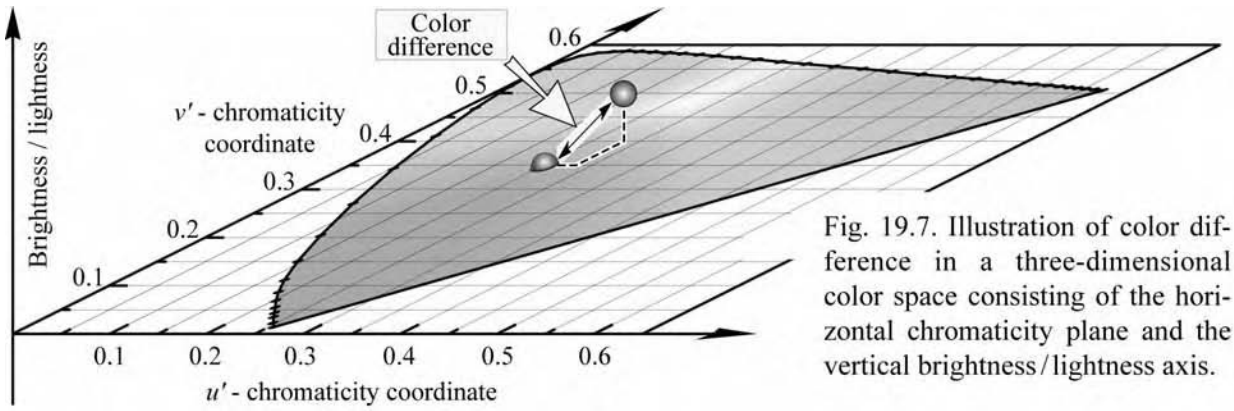

Fig. 19.7. Illustration of color difference in a three-dimensional color space consisting of the horizontal chromaticity plane and the vertical brightness/lightness axis.

Table 19.1. General color-rendering indices (CRIs) of different light sources. (a) Using sunlight as reference source. (b) Using incandescent light with the same correlated color temperature as the reference source. (c) Using Illuminant D_{65} as the reference source (some data after Kendall and Scholand, 2001).

Light source	**Color-rendering index**	
Sunlight	100	(a)
Quartz halogen W filament incandescent light	100	(b)
W filament incandescent light	100	(b)
Fluorescent light	60–95	(b)
Trichromatic white LED	60–95	(b, c)
Tetrachromatic white LED	70–95	(b, c)
Phosphor-based LED	55–95	(b, c)
Broadened dichromatic white LED	10–60	(b, c)
Hg vapor light coated with phosphor	50	(b)
Hg vapor light	33	(b)
Low and high-pressure Na vapor light	10 and 22	(b)
Green monochromatic light	−50	(c)

An overview of the general color-rendering indices of common light sources is given in Table 19.1. The table includes several types of LED sources including dichromatic white LEDs, trichromatic white LEDs, and phosphor-based white LEDs. A CRI between 90 and 100 is suitable for virtually all illumination applications. A CRI between 70 and 90 is suitable for many standard illumination applications. Light sources with a CRI below 70 are considered to be of lower quality.

References

Berger-Schunn A. *Practical Color Measurement* (John Wiley and Sons, New York, 1994)

Billmeyer Jr. F. W. "Survey of color order systems" *Color Res. Appl.* **12**, 173 (1987)

CIE publication No. 15 (E.1.3.1) 1971: *Colorimetry* this publication was updated in 1986 to CIE Publication 15.2 *Colorimetry* (CIE, Vienna, Austria, 1986)

CIE publication No. 13.3 *Method of Measuring and Specifying Color-Rendering of Light Sources* (see also www.cie.co.at) (CIE, Vienna, Austria, 1995)

Duggal A. R. "Organic electroluminescent devices for solid-state lighting" in *Organic Electro-luminescence* edited by Z. H. Kafafi (Taylor and Francis Group, Boca Raton, Florida, 2005)

Kendall M. and Scholand M. *Energy Savings Potential of Solid State Lighting in General Lighting Applications* available to the public from National Technical Information Service (NTIS), US Department of Commerce, 5285 Port Royal Road, Springfield, Virginia 22161 (2001)

Long J. and Luke J. T. *The New Munsell Student Color Set* 2nd ring-bound edition (Fairchild Books and Visuals, New York, 2001)

MacAdam D. L. (Editor) *Colorimetry – Fundamentals* (SPIE Optical Engineering Press, Bellingham, Washington, 1993)

Munsell A. H. *A Color Notation – An Illustrated System Defining All Colors and Their Relations by Measured Scales of Hue, Value, and Chroma* (G. H. Ellis, Boston, 1905)

Munsell *Munsell Book of Color, Matte Edition* is available through GretagMacbeth Corporation, gretagmacbeth.com and munsell.com (Regensdorf, Switzerland, 2005)

Wyszecki G. and Stiles W. S. *Color Science – Concepts and Methods, Quantitative Data and Formulae* 2nd edition (John Wiley and Sons, New York, 1982)

Wyszecki G. and Stiles W. S. *Color Science – Concepts and Methods, Quantitative Data and Formulae* 2nd edition "Wiley Classics Library" (John Wiley and Sons, New York, 2000)

Appendix 19.1

Spectral reflectivity $R_i(\lambda)$ of the CIE 1974 Test-Color Samples (TCS) Nos. 1–8 to be used in calculating the General Color-Rendering Index (General CRI) (after CIE, 1995)

λ (nm)	R_1 (-)	R_2 (-)	R_3 (-)	R_4 (-)	R_5 (-)	R_6 (-)	R_7 (-)	R_8 (-)
360	0.116	0.053	0.058	0.057	0.143	0.079	0.150	0.075
365	0.136	0.055	0.059	0.059	0.187	0.081	0.177	0.078
370	0.159	0.059	0.061	0.062	0.233	0.089	0.218	0.084
375	0.190	0.064	0.063	0.067	0.269	0.113	0.293	0.090
380	0.219	0.070	0.065	0.074	0.295	0.151	0.378	0.104
385	0.239	0.079	0.068	0.083	0.306	0.203	0.459	0.129
390	0.252	0.089	0.070	0.093	0.310	0.265	0.524	0.170
395	0.256	0.101	0.072	0.105	0.312	0.339	0.546	0.240
400	0.256	0.111	0.073	0.116	0.313	0.410	0.551	0.319
405	0.254	0.116	0.073	0.121	0.315	0.464	0.555	0.416
410	0.252	0.118	0.074	0.124	0.319	0.492	0.559	0.462
415	0.248	0.120	0.074	0.126	0.322	0.508	0.560	0.482
420	0.244	0.121	0.074	0.128	0.326	0.517	0.561	0.490
425	0.240	0.122	0.073	0.131	0.330	0.524	0.558	0.488
430	0.237	0.122	0.073	0.135	0.334	0.531	0.556	0.482
435	0.232	0.122	0.073	0.139	0.339	0.538	0.551	0.473
440	0.230	0.123	0.073	0.144	0.346	0.544	0.544	0.462
445	0.226	0.124	0.073	0.151	0.352	0.551	0.535	0.450
450	0.225	0.127	0.074	0.161	0.360	0.556	0.522	0.439
455	0.222	0.128	0.075	0.172	0.369	0.556	0.506	0.426
460	0.220	0.131	0.077	0.186	0.381	0.554	0.488	0.413
465	0.218	0.134	0.080	0.205	0.394	0.549	0.469	0.397
470	0.216	0.138	0.085	0.229	0.403	0.541	0.448	0.382
475	0.214	0.143	0.094	0.254	0.410	0.531	0.429	0.366
480	0.214	0.150	0.109	0.281	0.415	0.519	0.408	0.352
485	0.214	0.159	0.126	0.308	0.418	0.504	0.385	0.337
490	0.216	0.174	0.148	0.332	0.419	0.488	0.363	0.325
495	0.218	0.190	0.172	0.352	0.417	0.469	0.341	0.310
500	0.223	0.207	0.198	0.370	0.413	0.450	0.324	0.299
505	0.225	0.225	0.221	0.383	0.409	0.431	0.311	0.289
510	0.226	0.242	0.241	0.390	0.403	0.414	0.301	0.283
515	0.226	0.253	0.260	0.394	0.396	0.395	0.291	0.276
520	0.225	0.260	0.278	0.395	0.389	0.377	0.283	0.270
525	0.225	0.264	0.302	0.392	0.381	0.358	0.273	0.262
530	0.227	0.267	0.339	0.385	0.372	0.341	0.265	0.256
535	0.230	0.269	0.370	0.377	0.363	0.325	0.260	0.251
540	0.236	0.272	0.392	0.367	0.353	0.309	0.257	0.250
545	0.245	0.276	0.399	0.354	0.342	0.293	0.257	0.251
550	0.253	0.282	0.400	0.341	0.331	0.279	0.259	0.254
555	0.262	0.289	0.393	0.327	0.320	0.265	0.260	0.258
560	0.272	0.299	0.380	0.312	0.308	0.253	0.260	0.264
565	0.283	0.309	0.365	0.296	0.296	0.241	0.258	0.269
570	0.298	0.322	0.349	0.280	0.284	0.234	0.256	0.272
575	0.318	0.329	0.332	0.263	0.271	0.227	0.254	0.274
580	0.341	0.335	0.315	0.247	0.260	0.225	0.254	0.278
585	0.367	0.339	0.299	0.229	0.247	0.222	0.259	0.284
590	0.390	0.341	0.285	0.214	0.232	0.221	0.270	0.295
595	0.409	0.341	0.272	0.198	0.220	0.220	0.284	0.316

600	0.424	0.342	0.264	0.185	0.210	0.220	0.302	0.348
605	0.435	0.342	0.257	0.175	0.200	0.220	0.324	0.384
610	0.442	0.342	0.252	0.169	0.194	0.220	0.344	0.434
615	0.448	0.341	0.247	0.164	0.189	0.220	0.362	0.482
620	0.450	0.341	0.241	0.160	0.185	0.223	0.377	0.528
625	0.451	0.339	0.235	0.156	0.183	0.227	0.389	0.568
630	0.451	0.339	0.229	0.154	0.180	0.233	0.400	0.604
635	0.451	0.338	0.224	0.152	0.177	0.239	0.410	0.629
640	0.451	0.338	0.220	0.151	0.176	0.244	0.420	0.648
645	0.451	0.337	0.217	0.149	0.175	0.251	0.429	0.663
650	0.450	0.336	0.216	0.148	0.175	0.258	0.438	0.676
655	0.450	0.335	0.216	0.148	0.175	0.263	0.445	0.685
660	0.451	0.334	0.219	0.148	0.175	0.268	0.452	0.693
665	0.451	0.332	0.224	0.149	0.177	0.273	0.457	0.700
670	0.453	0.332	0.230	0.151	0.180	0.278	0.462	0.705
675	0.454	0.331	0.238	0.154	0.183	0.281	0.466	0.709
680	0.455	0.331	0.251	0.158	0.186	0.283	0.468	0.712
685	0.457	0.330	0.269	0.162	0.189	0.286	0.470	0.715
690	0.458	0.329	0.288	0.165	0.192	0.291	0.473	0.717
695	0.460	0.328	0.312	0.168	0.195	0.296	0.477	0.719
700	0.462	0.328	0.340	0.170	0.199	0.302	0.483	0.721
705	0.463	0.327	0.366	0.171	0.200	0.313	0.489	0.720
710	0.464	0.326	0.390	0.170	0.199	0.325	0.496	0.719
715	0.465	0.325	0.412	0.168	0.198	0.338	0.503	0.722
720	0.466	0.324	0.431	0.166	0.196	0.351	0.511	0.725
725	0.466	0.324	0.447	0.164	0.195	0.364	0.518	0.727
730	0.466	0.324	0.460	0.164	0.195	0.376	0.525	0.729
735	0.466	0.323	0.472	0.165	0.196	0.389	0.532	0.730
740	0.467	0.322	0.481	0.168	0.197	0.401	0.539	0.730
745	0.467	0.321	0.488	0.172	0.200	0.413	0.546	0.730
750	0.467	0.320	0.493	0.177	0.203	0.425	0.553	0.730
755	0.467	0.318	0.497	0.181	0.205	0.436	0.559	0.730
760	0.467	0.316	0.500	0.185	0.208	0.447	0.565	0.730
765	0.467	0.315	0.502	0.189	0.212	0.458	0.570	0.730
770	0.467	0.315	0.505	0.192	0.215	0.469	0.575	0.730
775	0.467	0.314	0.510	0.194	0.217	0.477	0.578	0.730
780	0.467	0.314	0.516	0.197	0.219	0.485	0.581	0.730
785	0.467	0.313	0.520	0.200	0.222	0.493	0.583	0.730
790	0.467	0.313	0.524	0.204	0.226	0.500	0.585	0.731
795	0.466	0.312	0.527	0.210	0.231	0.506	0.587	0.731
800	0.466	0.312	0.531	0.218	0.237	0.512	0.588	0.731
805	0.466	0.311	0.535	0.225	0.243	0.517	0.589	0.731
810	0.466	0.311	0.539	0.233	0.249	0.521	0.590	0.731
815	0.466	0.311	0.544	0.243	0.257	0.525	0.590	0.731
820	0.465	0.311	0.548	0.254	0.265	0.529	0.590	0.731
825	0.464	0.311	0.552	0.264	0.273	0.532	0.591	0.731
830	0.464	0.310	0.555	0.274	0.280	0.535	0.592	0.731

Appendix 19.2

Spectral reflectivity $R_i(\lambda)$ of the CIE 1974 Test-Color Samples (TCS) Nos. 9–14 (after CIE, 1995)

λ (nm)	R_9 (-)	R_{10} (-)	R_{11} (-)	R_{12} (-)	R_{13} (-)	R_{14} (-)
360	0.069	0.042	0.074	0.189	0.071	0.036
365	0.072	0.043	0.079	0.175	0.076	0.036
370	0.073	0.045	0.086	0.158	0.082	0.036
375	0.070	0.047	0.098	0.139	0.090	0.036
380	0.066	0.050	0.111	0.120	0.104	0.036
385	0.062	0.054	0.121	0.103	0.127	0.036
390	0.058	0.059	0.127	0.090	0.161	0.037
395	0.055	0.063	0.129	0.082	0.211	0.038
400	0.052	0.066	0.127	0.076	0.264	0.039
405	0.052	0.067	0.121	0.068	0.313	0.039
410	0.051	0.068	0.116	0.064	0.341	0.040
415	0.050	0.069	0.112	0.065	0.352	0.041
420	0.050	0.069	0.108	0.075	0.359	0.042
425	0.049	0.070	0.105	0.093	0.361	0.042
430	0.048	0.072	0.104	0.123	0.364	0.043
435	0.047	0.073	0.104	0.160	0.365	0.044
440	0.046	0.076	0.105	0.207	0.367	0.044
445	0.044	0.078	0.106	0.256	0.369	0.045
450	0.042	0.083	0.110	0.300	0.372	0.045
455	0.041	0.088	0.115	0.331	0.374	0.046
460	0.038	0.095	0.123	0.346	0.376	0.047
465	0.035	0.103	0.134	0.347	0.379	0.048
470	0.033	0.113	0.148	0.341	0.384	0.050
475	0.031	0.125	0.167	0.328	0.389	0.052
480	0.030	0.142	0.192	0.307	0.397	0.055
485	0.029	0.162	0.219	0.282	0.405	0.057
490	0.028	0.189	0.252	0.257	0.416	0.062
495	0.028	0.219	0.291	0.230	0.429	0.067
500	0.028	0.262	0.325	0.204	0.443	0.075
505	0.029	0.305	0.347	0.178	0.454	0.083
510	0.030	0.365	0.356	0.154	0.461	0.092
515	0.030	0.416	0.353	0.129	0.466	0.100
520	0.031	0.465	0.346	0.109	0.469	0.108
525	0.031	0.509	0.333	0.090	0.471	0.121
530	0.032	0.546	0.314	0.075	0.474	0.133
535	0.032	0.581	0.294	0.062	0.476	0.142
540	0.033	0.610	0.271	0.051	0.483	0.150
545	0.034	0.634	0.248	0.041	0.490	0.154
550	0.035	0.653	0.227	0.035	0.506	0.155
555	0.037	0.666	0.206	0.029	0.526	0.152
560	0.041	0.678	0.188	0.025	0.553	0.147
565	0.044	0.687	0.170	0.022	0.582	0.140
570	0.048	0.693	0.153	0.019	0.618	0.133
575	0.052	0.698	0.138	0.017	0.651	0.125
580	0.060	0.701	0.125	0.017	0.680	0.118
585	0.076	0.704	0.114	0.017	0.701	0.112
590	0.102	0.705	0.106	0.016	0.717	0.106
595	0.136	0.705	0.100	0.016	0.729	0.101
600	0.190	0.706	0.096	0.016	0.736	0.098

605	0.256	0.707	0.092	0.016	0.742	0.095
610	0.336	0.707	0.090	0.016	0.745	0.093
615	0.418	0.707	0.087	0.016	0.747	0.090
620	0.505	0.708	0.085	0.016	0.748	0.089
625	0.581	0.708	0.082	0.016	0.748	0.087
630	0.641	0.710	0.080	0.018	0.748	0.086
635	0.682	0.711	0.079	0.018	0.748	0.085
640	0.717	0.712	0.078	0.018	0.748	0.084
645	0.740	0.714	0.078	0.018	0.748	0.084
650	0.758	0.716	0.078	0.019	0.748	0.084
655	0.770	0.718	0.078	0.020	0.748	0.084
660	0.781	0.720	0.081	0.023	0.747	0.085
665	0.790	0.722	0.083	0.024	0.747	0.087
670	0.797	0.725	0.088	0.026	0.747	0.092
675	0.803	0.729	0.093	0.030	0.747	0.096
680	0.809	0.731	0.102	0.035	0.747	0.102
685	0.814	0.735	0.112	0.043	0.747	0.110
690	0.819	0.739	0.125	0.056	0.747	0.123
695	0.824	0.742	0.141	0.074	0.746	0.137
700	0.828	0.746	0.161	0.097	0.746	0.152
705	0.830	0.748	0.182	0.128	0.746	0.169
710	0.831	0.749	0.203	0.166	0.745	0.188
715	0.833	0.751	0.223	0.210	0.744	0.207
720	0.835	0.753	0.242	0.257	0.743	0.226
725	0.836	0.754	0.257	0.305	0.744	0.243
730	0.836	0.755	0.270	0.354	0.745	0.260
735	0.837	0.755	0.282	0.401	0.748	0.277
740	0.838	0.755	0.292	0.446	0.750	0.294
745	0.839	0.755	0.302	0.485	0.750	0.310
750	0.839	0.756	0.310	0.520	0.749	0.325
755	0.839	0.757	0.314	0.551	0.748	0.339
760	0.839	0.758	0.317	0.577	0.748	0.353
765	0.839	0.759	0.323	0.599	0.747	0.366
770	0.839	0.759	0.330	0.618	0.747	0.379
775	0.839	0.759	0.334	0.633	0.747	0.390
780	0.839	0.759	0.338	0.645	0.747	0.399
785	0.839	0.759	0.343	0.656	0.746	0.408
790	0.839	0.759	0.348	0.666	0.746	0.416
795	0.839	0.759	0.353	0.674	0.746	0.422
800	0.839	0.759	0.359	0.680	0.746	0.428
805	0.839	0.759	0.365	0.686	0.745	0.434
810	0.838	0.758	0.372	0.691	0.745	0.439
815	0.837	0.757	0.380	0.694	0.745	0.444
820	0.837	0.757	0.388	0.697	0.745	0.448
825	0.836	0.756	0.396	0.700	0.745	0.451
830	0.836	0.756	0.403	0.702	0.745	0.454

20

White-light sources based on LEDs

As the trend of higher efficiencies in LEDs continues, the number of possible applications increases as well. A highly interesting application with a very large potential market size is *general daylight illumination* in homes and offices. The field of ***solid-state lighting*** (SSL) is concerned with the development of solid-state sources for illumination applications. LEDs are inherently monochromatic emitters. However, there are several ways to generate white light using LEDs. Approaches to white-light generation based on LEDs will be covered in the current chapter, whereas approaches based on LEDs and wavelength-converting materials will be discussed in the following chapter. A pivotal discussion of the promise of solid-state lighting was given by Bergh *et al*. (2001). A comprehensive introduction to lighting technology using solid-state sources was given by Zukauskas *et al*. (2002a).

In the field of general daylight illumination, devices should have the following properties (*i*) high efficiency, (*ii*) high power capability, (*iii*) good color-rendering capabilities (*iv*) high reliability, (*v*) low-cost manufacturability, and (*vi*) environmental benignity. Such properties would allow LEDs to compete with conventional illumination sources, in particular incandescent and fluorescent lamps.

20.1 Generation of white light with LEDs

Light is perceived as *white* light if the three types of cones located on the retina of the human eye are excited in a certain ratio, namely with similar intensity. For the case of white light, the tristimulus values are such that the location of the chromaticity point is near the center of the chromaticity diagram.

The generation of white light can be accomplished with a huge number of possible spectra. The creation of white light out of monochromatic visible-spectrum emitters can be based on dichromatic, trichromatic, or tetrachromatic approaches, as shown in Fig. 20.1, or on approaches of higher chromaticity. The optical sources can be classified in terms of their luminous efficacy

of radiation, luminous source efficiency, and color-rendering properties.

Whereas high luminous efficacy and high luminous efficiency are always desirable properties of high-power light sources, color rendering depends strongly on the application. Generally, high-quality daylight illumination applications, e.g. illumination in museums, homes, offices, and stores, require a high color-rendering capability.

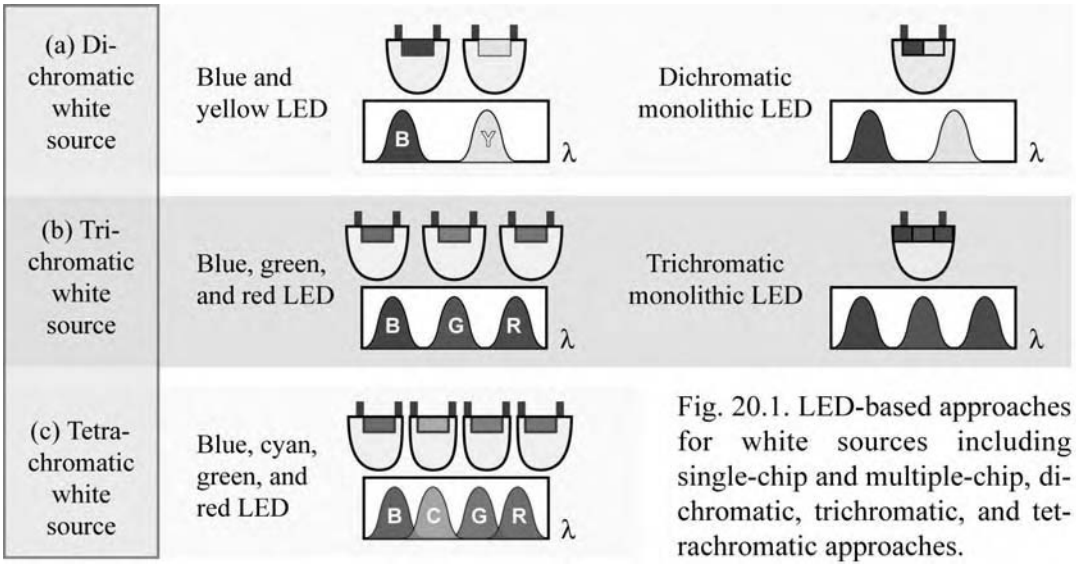

Fig. 20.1. LED-based approaches for white sources including single-chip and multiple-chip, dichromatic, trichromatic, and tetrachromatic approaches.

However, there are numerous applications where the color rendering capability is of lower priority, for example in the illumination of streets, parking garages, and stairwells. Finally, in signage applications, color rendering is irrelevant. Such signage applications include white pedestrian traffic lights, displays, and indicator lights.

There is a fundamental trade-off between the luminous efficacy of radiation and color rendering capability of a light source. Generally, dichromatic white light has the highest luminous efficacy and the poorest color-rendering capabilities. A trichromatic white source can have very acceptable color-rendering properties (CRI > 80) and luminous efficacies greater than 300 lm/W. Tetrachromatic sources can have color-rendering indices greater than 90.

20.2 Generation of white light by dichromatic sources

White light can be generated in several different ways. One way of generating white light is the use of two narrow emission bands, called ***complementary wavelengths*** or ***complementary colors***. Two complementary colors, at a certain power ratio, result in tristimulus values that are perceived as white light. The wavelengths of complementary colors are shown in Fig. 20.2.

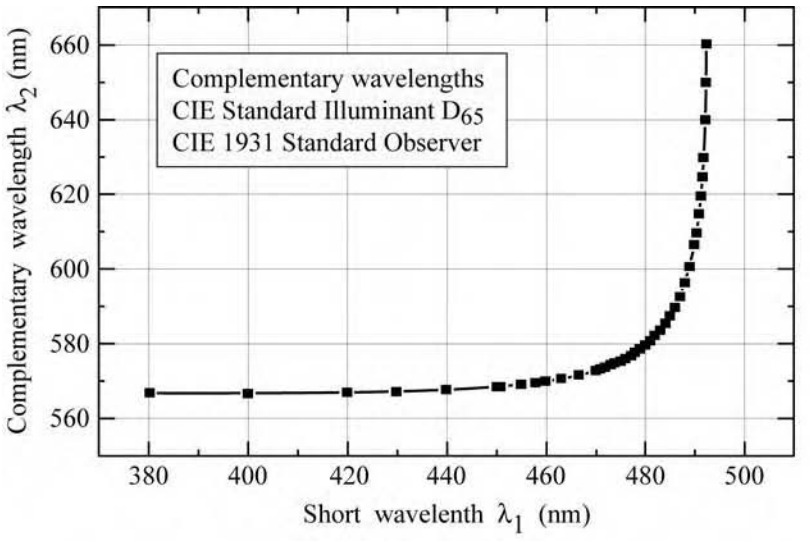

Fig. 20.2. Monochromatic complementary wavelengths resulting in the perception of white light at a certain power ratio (after Wyszecki and Stiles, 1982).

The numerical values for monochromatic complementary wavelengths are given in Table 20.1. The table also gives the power ratio required to attain the same chromaticity coordinate as Illuminant D_{65}.

Table 20.1. Wavelengths λ_1 and λ_2 of monochromatic complementary colors with respect to CIE Illuminant D_{65} and the CIE 1964 Standard Observer. Also given is the required power ratio. Illuminant D_{65} has chromaticity coordinates $x_{D65} = 0.3138$ and $y_{D65} = 0.3310$ (after Wyszecki and Stiles, 1982).

Complementary wavelengths		**Power ratio**	**Complementary wavelengths**		**Power ratio**
λ_1 (nm)	λ_2 (nm)	$P(\lambda_2) / P(\lambda_1)$	λ_1 (nm)	λ_2 (nm)	$P(\lambda_2) / P(\lambda_1)$
380	560.9	0.000642	460	565.9	1.53
390	560.9	0.00955	470	570.4	1.09
400	561.1	0.0785	475	575.5	0.812
410	561.3	0.356	480	584.6	0.562
420	561.7	0.891	482	591.1	0.482
430	562.2	1.42	484	602.1	0.440
440	562.9	1.79	485	611.3	0.457
450	564.0	1.79	486	629.6	0.668

Next we analyze the luminous efficacy of radiation of a source with two complementary emission lines. It is assumed that the two lines are thermally broadened to a full-width at half-maximum of ΔE. Emission lines of $\Delta E = 2\,kT$ to $10\,kT$ have been found experimentally for the GaInN system at room temperature (kT = 25.9 meV at 300 K). A ***gaussian distribution*** is assumed for the two emission lines, so that the spectral power density is given by

$$P(\lambda) = P_1 \frac{1}{\sigma_1\sqrt{2\pi}} e^{-\frac{1}{2}\left(\frac{\lambda-\lambda_1}{\sigma_1}\right)^2} + P_2 \frac{1}{\sigma_2\sqrt{2\pi}} e^{-\frac{1}{2}\left(\frac{\lambda-\lambda_2}{\sigma_2}\right)^2} \quad (20.1)$$

where P_1 and P_2 are the optical powers of the two emission lines, and λ_1 and λ_2 are the peak wavelengths of the source. The gaussian standard deviation σ is related to the full-width at half-maximum of an emission spectrum, $\Delta\lambda$, by

$$\sigma = \Delta\lambda \Big/ \left[2\sqrt{2\ln 2} \right] = \Delta\lambda / 2.355 \; . \quad (20.2)$$

The peak emission wavelengths λ_1 and λ_2 are chosen from Table 20.1. The table also gives the required power ratio of the two light sources. Although the table applies to strictly monochromatic sources ($\Delta\lambda \to 0$), the data can be used, as an excellent approximation, for sources exhibiting moderate spectral broadening such as LEDs.

The luminous efficacy of radiation of a dichromatic source is shown in Fig. 20.3. The figure reveals that the highest luminous efficacy of 440 lm/W occurs at a primary wavelength of $\lambda_1 = 445\,\text{nm}$ for $\Delta E = 2kT$. The very high value of the efficacy shows the great potential of dichromatic sources.

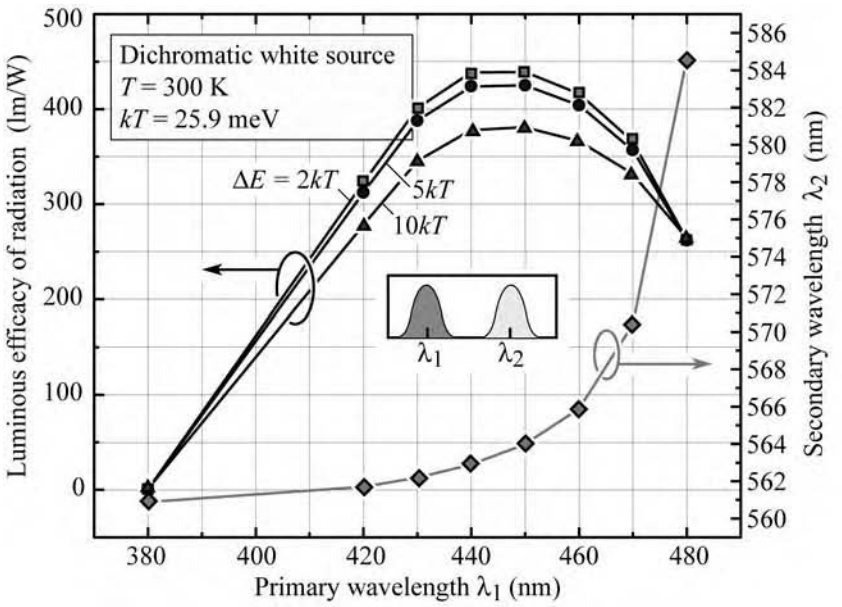

Fig. 20.3. Calculated luminous efficacy of dichromatic white-light source (with chromaticity point at D_{65} standard illuminant) for different linewidths ΔE as a function of the primary wavelength. Also shown is the complementary secondary wavelength (after Li *et al.*, 2003).

Several approaches for the generation of white light by mixing two complementary colors have been demonstrated (Guo *et al.*, 1999; Sheu *et al.*, 2002; Dalmasso *et al.*, 2002; Li *et al.*,

2003). One possibility uses the mixing of light emitted by two LEDs, one emitting in the blue and the other one in the yellow spectral region. Another possibility, demonstrated by Guo *et al.* (1999), generates white light by using a GaN-based blue LED and a second semiconductor, AlGaInP, as a wavelength converter. Sheu *et al*. (2002) demonstrated a codoped single active region quantum well white LED. The active region is doped with both Si and Zn. Blue light emission originates from quantum well band-to-band transitions, whereas a wide yellowish emission originates from donor-acceptor-pair (D-A) transitions. Because the D-A transition is spectrally wide, the codoped approach has the advantage of good color rendering. A dichromatic monolithic LED has also been reported by Dalmasso *et al*. (2002), who employed two closely spaced GaInN active regions within the pn-junction region. A strong dependence of the emission spectrum on the injection current was found.

Li *et al*. (2003) reported a monolithic GaInN based LED with two active regions separated by a thin GaN layer. The device was designed for emission at 465 nm and 525 nm. The device structure is shown in Fig. 20.4.

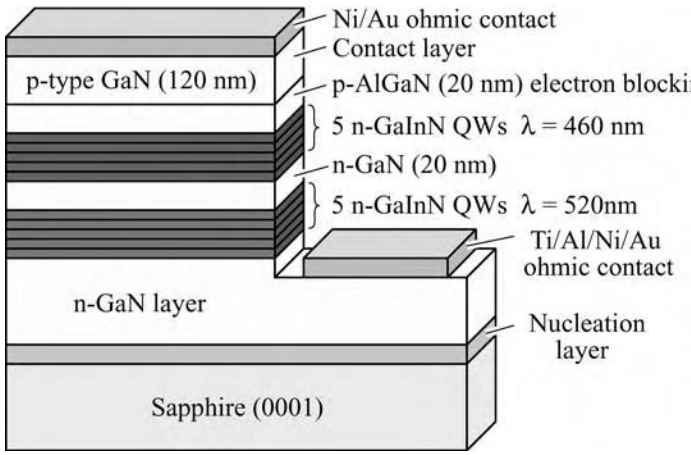

Fig. 20.4. Structure of a monolithic dichromatic LED with two active regions (after Li *et al.*, 2003).

Photoluminescence results are shown in Fig. 20.5 (a). The spectra exhibit two emission bands one centered at about 465 nm and one at 525 nm. As the excitation density is varied, the two peak positions do not change. However, the ratio of the two peak intensities changes with the excitation power density of the laser. The excitation-density-dependent emission ratio can be explained by the competition of different recombination paths (Li *et al*., 2003). Neglecting non-radiative recombination, possible recombination paths of an electron in the blue quantum well (QW) are either direct radiative recombination in the blue QW or tunneling to the green QW with subsequent radiative recombination. Electrons and holes can tunnel from the blue QW to

the green QW and recombine there radiatively. However, once in the green QW, carriers cannot tunnel back to the blue QW due to the higher energy of this QW.

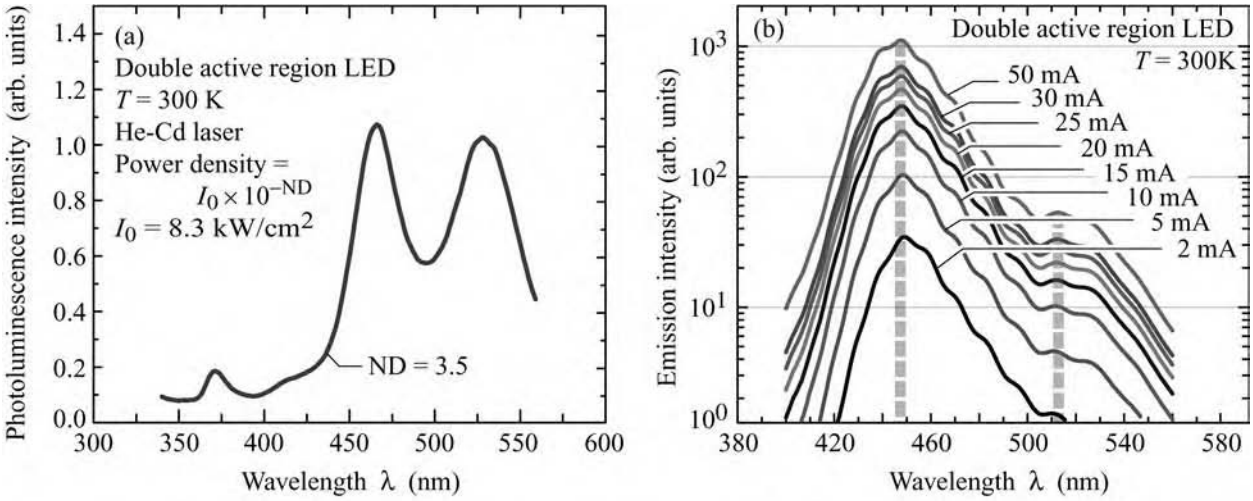

Fig. 20.5. Room temperature (a) photoluminescence and (b) electroluminescence spectra of monolithic dichromatic LED with two active regions (after Li *et al*., 2003).

Electroluminescence (EL) spectra of the device are shown in Fig. 20.5 (b). Two emission peaks are clearly observed with center wavelengths at about 450 nm and 520 nm. The blue peak is more intense than the green peak which can be attributed to the higher quantum efficiency of blue QWs compared with green QWs. In addition, holes are injected from the blue side (i.e. the side of the high-energy, blue-emitting QWs), whereas electrons are injected from the green side. As holes have a lower mobility and a higher effective mass, they are less likely to reach the green QWs, which can explain the higher intensity of the blue emission.

For current injection, holes are injected into the blue QWs, whereas electrons are injected into the green QWs. This is very different from optical excitation, where both types of carriers are injected from both sides of the active region. For the structure discussed here, the optical absorption length is longer than the distance between the active regions and the surface. This can explain the marked difference between the results for photoluminescence and electroluminescence (Li *et al*., 2003).

Room temperature *I–V* curves of the double-active region LED exhibit excellent forward voltages < 3.0 V at small contact diameters of 100 μm indicating high-quality ohmic contacts. The increase in forward voltage for contacts with larger diameters was attributed to an increased voltage drop in the n-type buffer layer, because, at a given current density, the current in the buffer layer scales with the area of the contact *A*, but the access resistance through the n-type

buffer layer scales with the circumference $A^{-1/2}$. In addition, the current crowding effect leads to non-uniform current injection particularly in large-diameter contacts and thus to an increased forward voltage.

20.3 Generation of white light by trichromatic sources

Whereas high-quality white light suitable for illumination applications cannot be generated by additive mixing of *two* complementary colors, such high-quality white light can be generated by mixing of *three* primary colors or more than three colors. In a detailed analysis, Thornton (1971) showed that mixing of discrete emission bands with peak wavelengths near 450 nm, 540 nm, and 610 nm resulted in a high-quality source. Thornton (1971) reported experiments with 60 human subjects who judged the quality of a trichromatic source in terms of its color rendition capability of meat, vegetables, flowers, and complexion, to be "very good, if not excellent". Thornton (1971) also reported that, for high-quality color rendition of trichromatic sources, the use of emitters near 500 nm and 580 nm should be avoided.

Although Thornton (1971) established that trichromatic sources can have high quality, the individual emission bands used in the experiments had a broad spectral width: The full-widths at half-maximum of the phosphor emitters employed in the study exceeded 50 nm. Semiconductors, with typical spectral widths < 50 nm, have much narrower emission lines than phosphors.

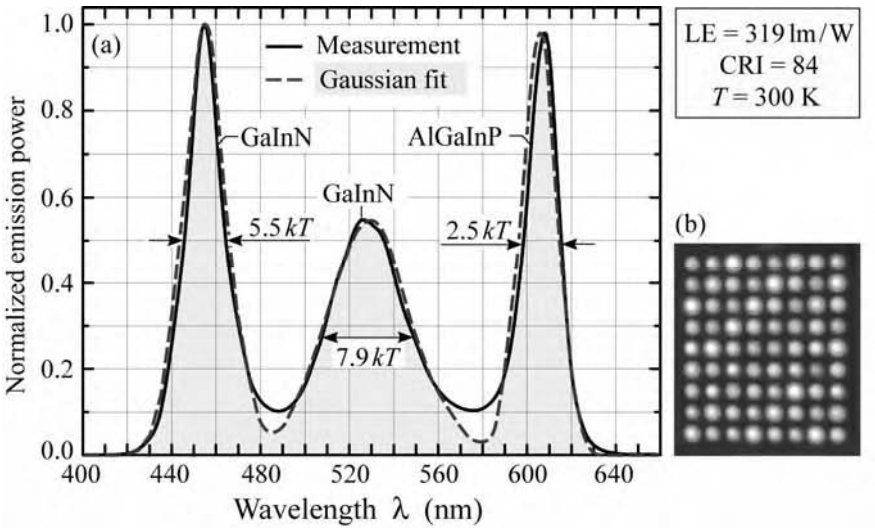

Fig. 20.6. (a) Emission spectrum of trichromatic white multi-LED source with color temperature of 6500 K (solid line) and gaussian fit (dashed line). The source has a luminous efficacy of radiation of 319 lm/W and a color rendering index of 84. (b) Photograph of source assembled from standard commercial devices (after Chhajed *et al.*, 2005).

The trichromatic emission spectrum of a white-light source made out of three types of LEDs emitting at 455 nm, 525 nm, and 605 nm is shown in Fig. 20.6 (a). The experimentally determined full-width at half-maximum of the spectra at room temperature (20 °C) is 5.5 kT,

7.9 kT, and 2.5 kT for the GaInN blue, GaInN green, and AlGaInP orange emitter, respectively, where kT = 25.25 meV. The expression of the full-width at half-maximum in terms of kT is very useful, as it can be easily related to the theoretical full-width at half-maximum of a thermally broadened emission band of a semiconductor, which is 1.8 kT. Using the full-width at half-maximum given in the figure and

$$\Delta\lambda \quad = \quad \frac{\lambda^2}{hc}\ \Delta E \quad = \quad \frac{(\lambda / \mathrm{nm})^2}{1239.8}\ (\Delta E / \mathrm{eV})\ , \tag{20.3}$$

the full-widths at half-maximum of the blue, green, and orange sources are 23.2 nm, 44.3 nm, and 18.6 nm, respectively. Note that the green emission line is particularly broad, which can be attributed to alloy broadening and the formation of quantum-dot-like InN-rich regions within the high-In-content GaInN.

Also shown in the figure are gaussian fits to the experimental spectra. The gaussian fits match the experimental spectra well. Note that the gaussian curves (equations were given earlier in this chapter) are symmetric in terms of wavelength. *Asymmetric gaussian distributions*, which have a more pronounced long-wavelength tail, have been employed for phosphors (Ivey, 1963). The use of such asymmetric gaussian distributions does not appear to be warranted for semiconductors as their spectral power distribution is quite symmetric when plotted versus wavelength.

A photograph of the light source assembled from a large number of LEDs is shown in Fig. 20.6 (b). The power ratio of the orange, green, and blue emitters is adjusted to match the chromaticity of a planckian radiator with color temperature 6500 K. The LED source, assembled from standard commercial devices, has a luminous efficacy of radiation of 319 lm/W, a luminous source efficiency of 32 lm/W, and a color-rendering index of 84 (Chhajed *et al*., 2005).

There are a large number of possible wavelength combinations for trichromatic sources. To attain a high efficacy of radiation, sources near the fringes of the visible spectrum (deep red and deep violet) should be avoided. Contour plots of the luminous efficacy of radiation and of the color rendering index of a trichromatic source with color temperature of 6500 K are shown in Fig. 20.7 for a full-width at half-maximum for each emission line of 5 kT. Inspection of the figure reveals that λ_1 = 455 nm, λ_2 = 530 nm, and λ_3 = 605 nm are particularly favorable in terms of the color-rendering index. The CIE general CRI is about 85 for this wavelength combination with the luminous efficacy of radiation being 320 lm/W.

The figure also reveals that the CRI depends very sensitively on the exact peak positions. For

example, changing the red peak wavelength from 605 nm to 620 nm decreases the CRI from 85 to 65. Similarly, changing the green wavelength from 530 nm to 550 nm decreases the CRI to values less than 60.

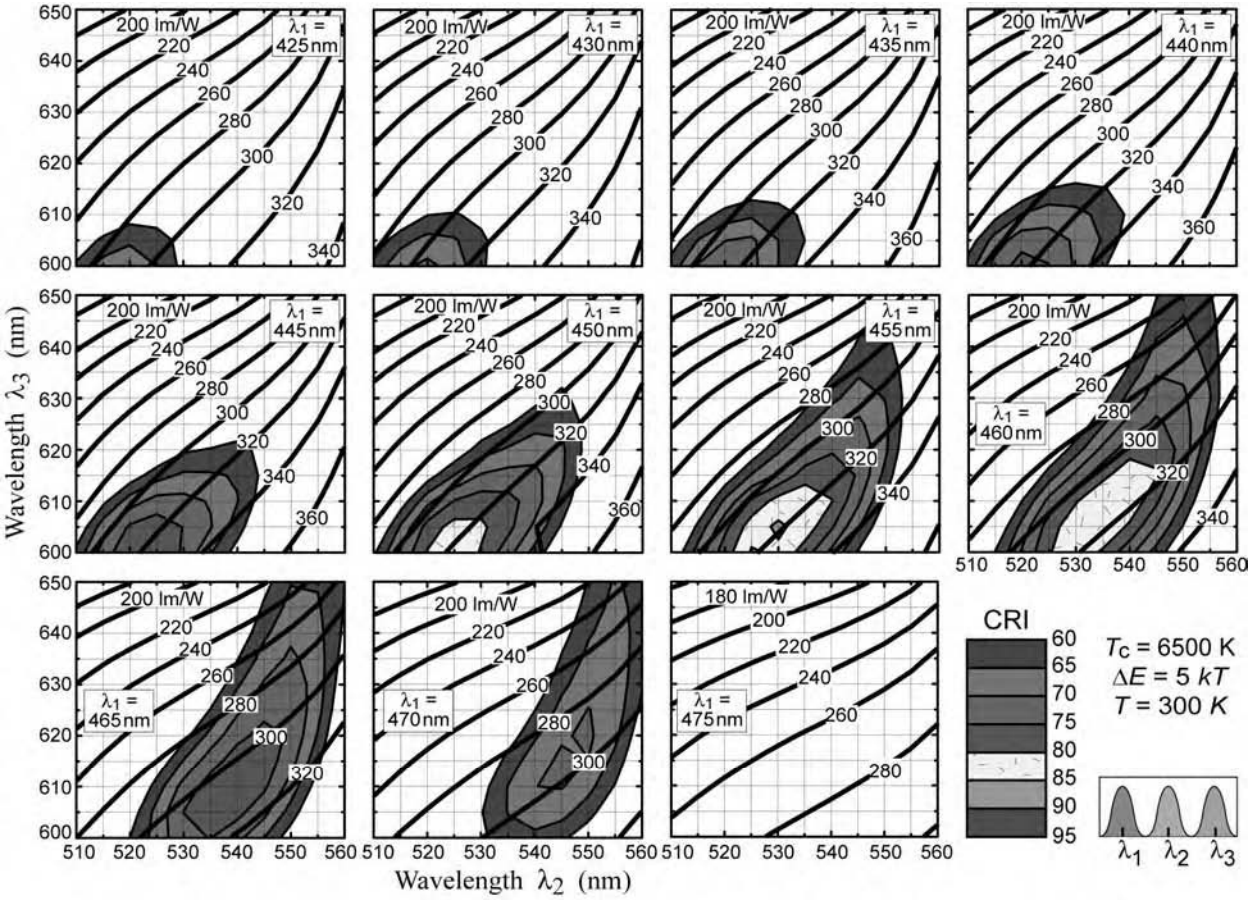

Fig. 20.7. Contour plot of luminous efficacy of radiation and CIE color-rendering index of white trichromatic LED source with color temperature 6500 K as a function of the three wavelengths for a linewidth (FWHM) of $5kT$ (after Chhajed *et al.*, 2005).

Contour plots of the luminous efficacy of radiation and of the color-rendering index of a trichromatic source with color temperature of 6500 K are shown in Fig. 20.8 for a full-width at half-maximum for each emission line of $8kT$. A higher CRI results from the broader emission lines. A very favorable combination in terms of a high CRI is obtained for λ_1 = 450–455 nm, λ_2 = 525–535 nm, and λ_3 = 600–615 nm, where a CRI in the range 90–95 is obtained.

20.4 Temperature dependence of trichromatic LED-based white-light source

The relatively small range of wavelengths that enables a high color-rendering capability raises the question as to the stability of trichromatic sources with respect to junction and ambient

temperature. It is known that emission power (P), peak wavelength (λ_{peak}), and spectral width ($\Delta\lambda$) depend on temperature, each of these quantities having a different temperature coefficient.

The optical output power of LEDs is temperature dependent in a manner that can be described by an exponential function and a characteristic temperature, T_1. The light output power of an LED is then given by

$$P = P\big|_{300\,\mathrm{K}} \exp \frac{T - 300\,\mathrm{K}}{T_1} . \tag{20.4}$$

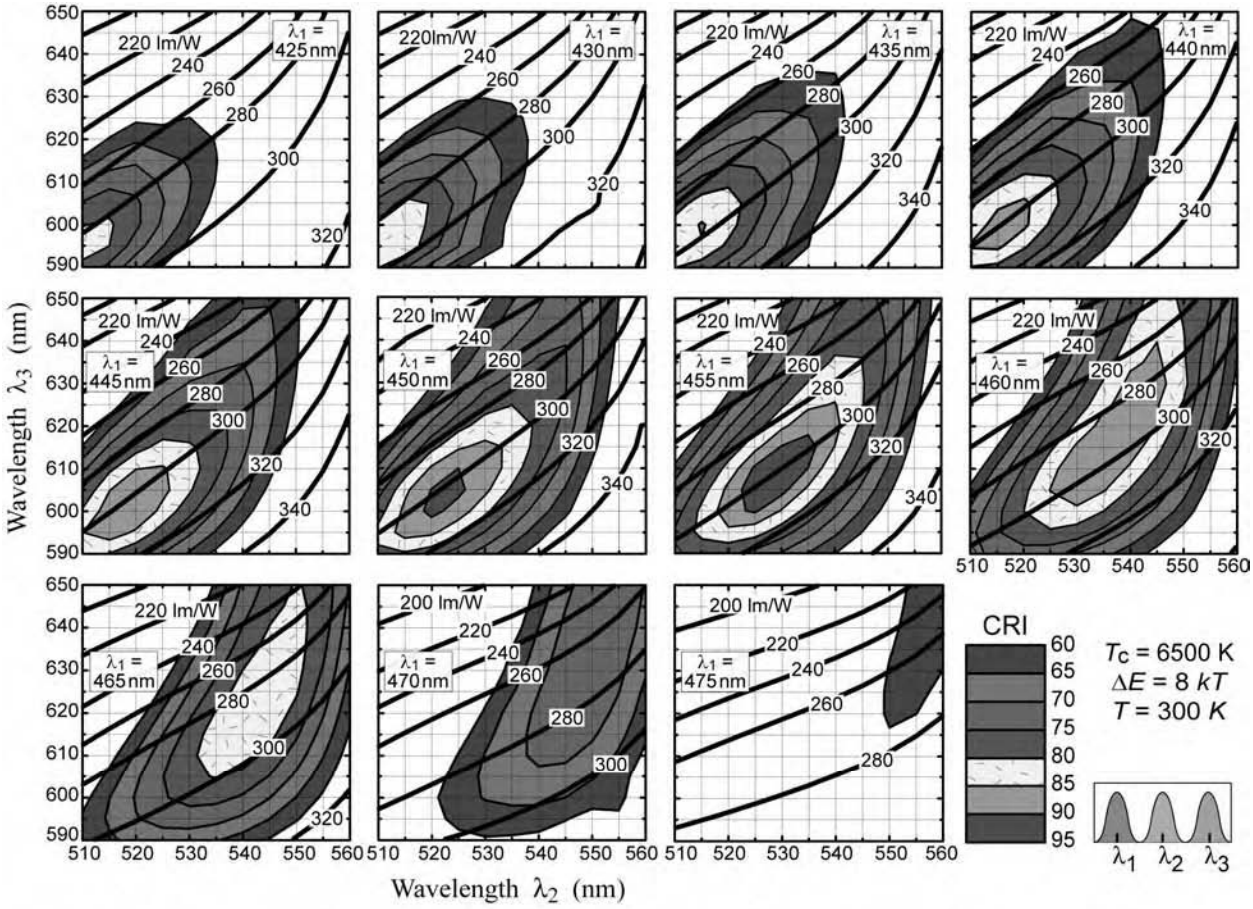

Fig. 20.8. Contour plot of luminous efficacy of radiation and CIE color-rendering index of white trichromatic LED source with color temperature 6500 K as a function of the three wavelengths for a linewidth (FWHM) of $8kT$ (after Chhajed *et al*., 2005).

As a result of these temperature dependences, the chromaticity point of a multi-LED white-light source changes with temperature. Consider a white-light source consisting of three types of emitters emitting in the red, green, and blue. For such LEDs, the temperature coefficients of the peak emission wavelength, spectral width, and emission power have been measured and are

given in Table 20.2 (Chhajed *et al*., 2005).

Table 20.2. Experimentally determined temperature coefficients for peak wavelength, spectral width, and emission power for blue, green, and red LEDs.

	Blue	**Green**	**Red**
$d\lambda_{peak}/dT$	0.0389 nm / °C	0.0308 nm / °C	0.156 nm / °C
$d\Delta\lambda/dT$	0.0466 nm / °C	0.0625 nm / °C	0.181 nm / °C
$T_{characteristic}$	493 K	379 K	209 K

Consider further that the three currents feeding the red, green, and blue LEDs are adjusted in such a way that the resulting chromaticity point equals that of Illuminant D_{65} when the device temperature is 20 °C. The optical spectrum of such a trichromatic white source is shown in Fig. 20.9.

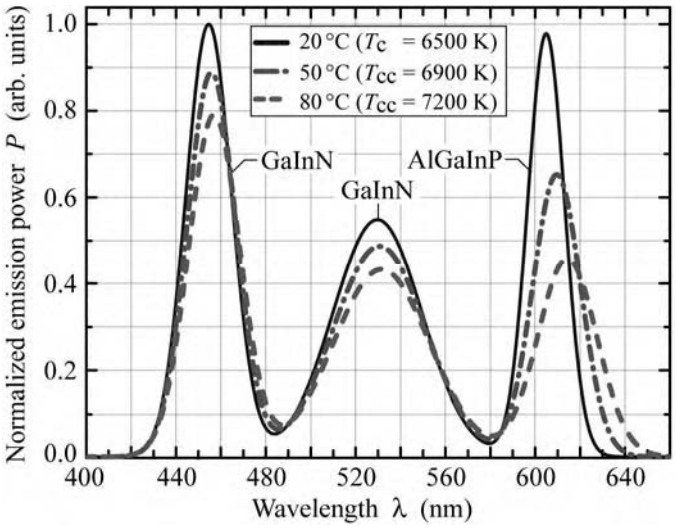

Fig. 20.9. Emission spectrum of trichromatic white LED source for different ambient temperatures (junction heating neglected). Optical power, linewidth, and peak wavelength change with temperature. As a result of these changes, the color temperature of the source increases (after Chhajed *et al*., 2005).

However, as the device temperature increases, the chromaticity point of the trichromatic source changes due to the temperature dependences of the emission power, peak wavelength, and spectral width. This shift of the chromaticity point is shown in Fig. 20.10. Inspection of the figure reveals that the chromaticity point shifts towards higher color temperatures. This can be explained by the stronger temperature dependence of the red LED emission power. At high temperatures, the red component of the light source decreases more strongly (due to low T_1 value) than the green component, and the blue component, which is particularly stable.

Figure 20.11 shows the chromaticity shift of the trichromatic source on a magnified scale in the CIE 1931 (x, y) chromaticity coordinate system as well as in the CIE 1976 (u', v') uniform

chromaticity coordinate system along with the planckian locus. At T_j = 50 °C, the chromaticity point is 0.009 units away from the original point, and at 80 °C, it is shifted 0.02 units from the original point. This shift causes a clearly noticeable change in color appearance and exceeds the deviation limit of 0.01 units (“***0.01 rule***”) commonly used in the lighting industry (Duggal, 2005).

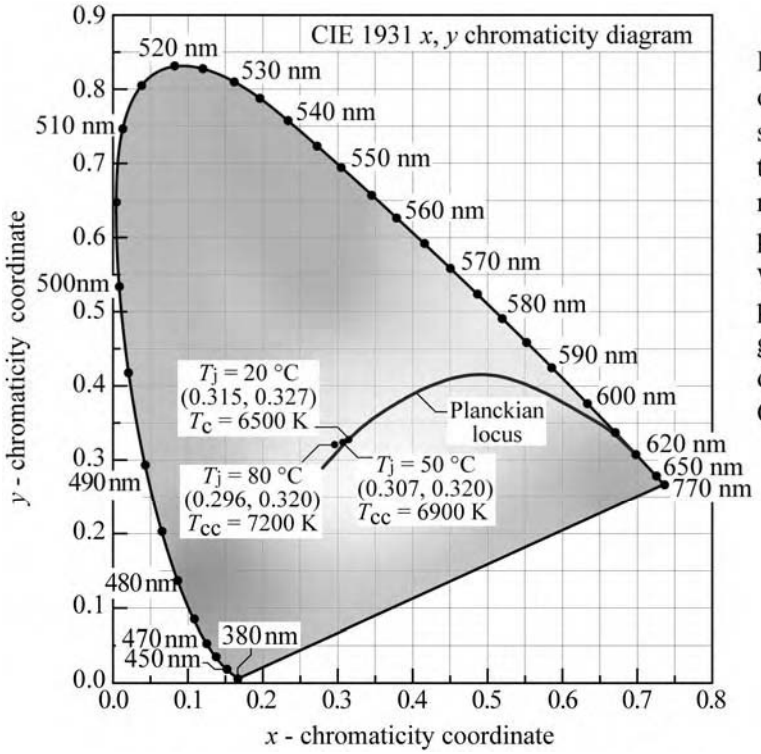

Fig. 20.10. Change in chromaticity of trichromatic white LED-based source. The source color temperature is 6500 K when devices are at room temperature. Due to the dependence of emission power, peak wavelength, and linewidth on temperature, the chromaticity point migrates off the planckian locus as the device temperature increases (after Chhajed *et al*., 2005).

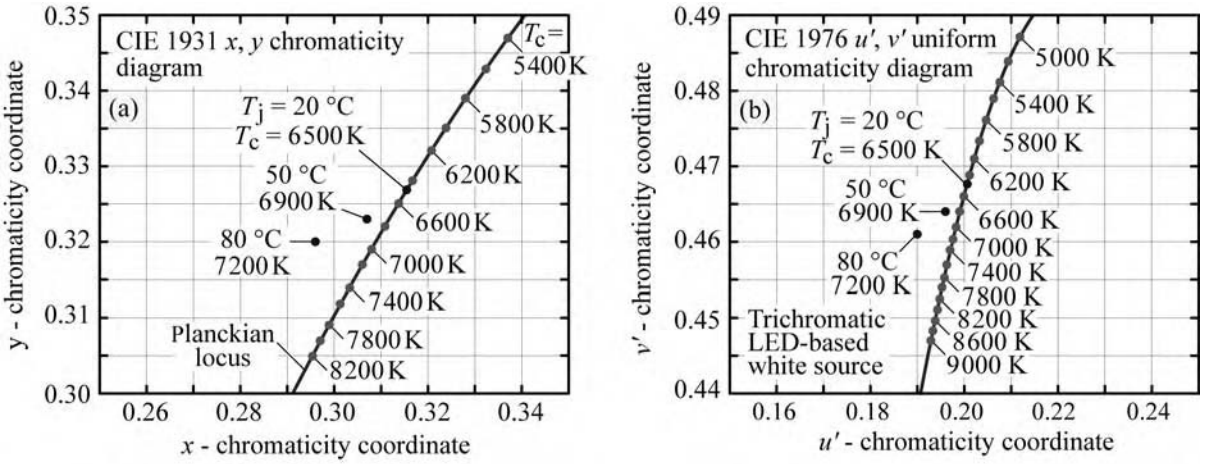

Fig. 20.11. Change in (a) x, y and (b) u', v' chromaticity of trichromatic white LED source. T_c = 6500 K when p-n junctions are at room temperature (after Chhajed *et al*., 2005).

The shift in chromaticity can be eliminated by adjusting the relative power ratio of the three LED sources. There are two possible implementations for adjusting the power ratio. In one implementation, the spectrum of the light source is constantly measured and a feedback control is used to adjust the optical power of the three components. In an alternative implementation, the device temperature is monitored and the optical power of the three components is adjusted using the known temperature dependence of the different types of emitters. The second method is easier due to the simplicity of a temperature measurement. However, the second method does not enable a compensation for device-aging effects.

20.5 Generation of white light by tetrachromatic and pentachromatic sources

Tetrachromatic and pentachromatic white sources use four and five types of LEDs, respectively (Zukauskas *et al*., 2002a; Schubert and Kim, 2005). The color-rendering index of polychromatic sources generally increases with the number of sources. However, the luminous efficacy generally decreases with increasing number of sources. Thus, the color-rendering index and the luminous efficacy of tetrachromatic sources are generally higher and lower than those of trichromatic sources, respectively. However, the specifics depend on the exact choice of the emission wavelengths. Due to the greater number of wavelength choices, the color temperatures of such sources can be adjusted more liberally without compromising the color-rendering capability of the source.

References

Bergh A., Craford G., Duggal A., and Haitz R. “The promise and challenges of solid-state lighting” *Physics Today* p. 42 (December 2001)

Chhajed S., Xi Y., Li Y.-L., Gessmann Th., and Schubert E. F. “Influence of junction temperature on chromaticity and color rendering properties of trichromatic white light sources based on light-emitting diodes” *J. Appl. Phys*. **97**, 054506 (2005)

Duggal A. R. “Organic electroluminescent devices for solid-state lighting” in *Organic Electroluminescence* edited by Z. H. Kafafi (Taylor & Francis Group, Boca Raton, Florida, 2005)

Dalmasso S., Damilano B., Pernot C., Dussaigne A., Byrne D., Grandjean N., Leroux M., and Massies J. “Injection dependence of the electroluminescence spectra of phosphor free GaN-based white light emitting diodes” *Phys. Stat. Sol. (a)* **192,** 139 (2002)

Guo X., Graff J. W., and Schubert E. F. “Photon-recycling semiconductor light-emitting diodes” *IEDM Technol. Dig.*, **IEDM-99**, 600 (1999)

Ivey H. F. “Color and efficiency of luminescent light sources” *J. Opt. Soc. Am.* **53**, 1185 (1963)

Li Y.-L., Gessmann Th., Schubert E. F., and Sheu J. K. “Carrier dynamics in nitride-based light-emitting p-n junction diodes with two active regions emitting at different wavelengths” *J. Appl. Phys.* **94**, 2167 (2003)

Schubert E. F. and Kim J. K. “Solid-state light sources becoming smart” *Science* **308**, 1274 (2005)

Sheu J. K., Pan C. J., Chi G. C., Kuo C. H., Wu L. W., Chen C. Chang H., S. J., and Su Y. K. "White-light emission from InGaN-GaN multiquantum-well light-emitting diodes with Si and Zn co-doped active well layer" *IEEE Photonics Technol. Lett.*, **14**, 450 (2002)

Thornton W. A. "Luminosity and color rendering capability of white light" *J. Opt. Soc. Am.* **61**, 1155 (1971)

Wyszecki G. and Stiles W. S. *Color Science – Concepts and Methods, Quantitative Data and Formulae* 2nd edition (John Wiley and Sons, New York, 1982)

Zukauskas A., Shur M. S., and Gaska R. *Introduction to Solid-State Lighting* (John Wiley and Sons, New York, 2002a)

Zukauskas A., Vaicekauskas R., Ivanauskas F., Gaska R., and Shur M. S. "Optimization of white polychromatic semiconductor lamps" *Appl. Phys. Lett*. **80**, 234 (2002b)

21

White-light sources based on wavelength converters

The generation of white light by a semiconductor LED whose light is partially or fully used to optically excite one or several phosphors, is a viable and common method to generate white light for general illumination applications. There are several different approaches to generate white light based on phosphors excited by semiconductor LEDs, which are shown in Fig. 21.1. They can be classified in dichromatic, trichromatic, and tetrachromatic approaches. These approaches use either UV-excitation sources or visible-spectrum-excitation sources (mostly blue semiconductor LEDs).

Generally, the luminous source efficiency decreases with increasing multi-chromaticity of the source. Thus, dichromatic sources have the highest luminous efficacy of radiation and also the highest potential luminous source efficiency. On the other hand, the color-rendering capability is lowest for dichromatic sources and it increases with the multi-chromaticity of the source. The color-rendering index can reach values very close to CRI = 100 for tetrachromatic sources.

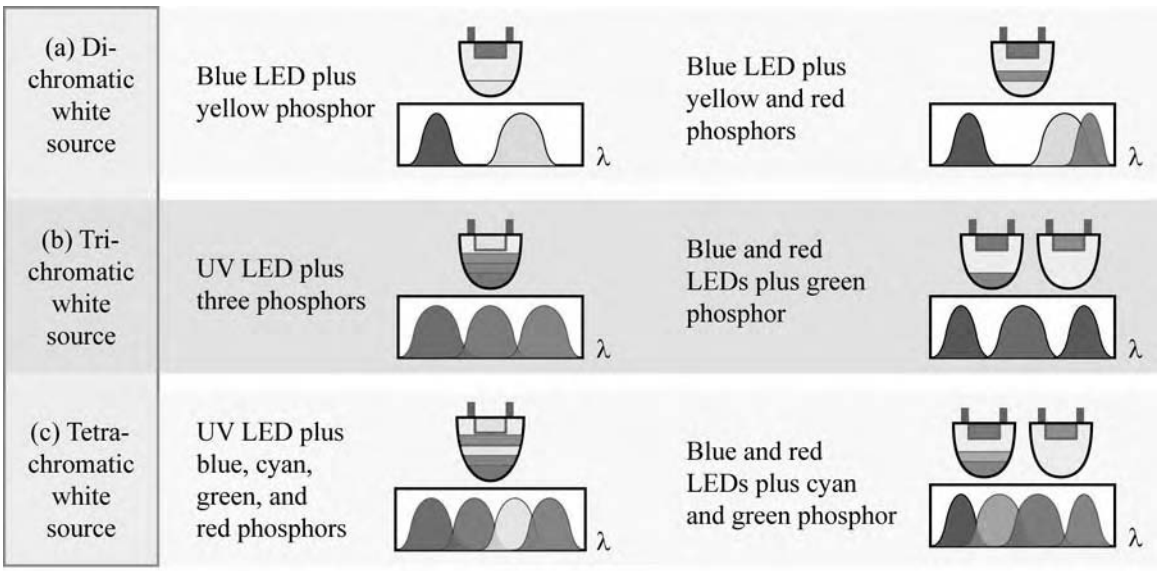

Fig. 21.1. White sources using phosphors that are optically excited by UV or blue LEDs.

21.1 Efficiency of wavelength-converter materials

The conversion efficiency of short-wavelength light to long-wavelength light by a ***wavelength-converter*** (λ-converter) material is determined by two distinct factors, namely (*i*) the external quantum efficiency of the λ-converter and (*ii*) the inherent quantum-mechanical-energy loss incurred in wavelength conversion.

The ***external quantum efficiency*** of the converter material, η_{ext}, is given by

$$\eta_{ext} = \frac{\text{number of photons emitted into free space by } \lambda\text{-converter per second}}{\text{number of photons absorbed by } \lambda\text{-converter per second}} . \qquad (21.1)$$

The external efficiency originates in the *internal efficiency* and the *extraction efficiency* of the converter material according to $\eta_{ext} = \eta_{internal}\, \eta_{extraction}$. Note that the internal quantum efficiency depends on the inherent efficiency of the material whereas the extraction efficiency depends on the spatial distribution of the λ-converter material. Generally, thin films have high extraction efficiencies whereas lumpy aggregations of converter materials have lower extraction efficiency due to reabsorption. It is therefore desirable to employ λ-converter materials in the form of thin layers.

The inherent ***wavelength-conversion loss*** (sometimes called ***quantum deficit*** or ***Stokes shift***) incurred when converting a photon with wavelength λ_1 to a photon with wavelength λ_2 ($\lambda_1 < \lambda_2$) is given by

$$\Delta E = h\nu_1 - h\nu_2 = \frac{hc}{\lambda_1} - \frac{hc}{\lambda_2} . \qquad (21.2)$$

Thus the wavelength-conversion efficiency is given by

$$\eta_{\lambda\text{-conversion}} = \frac{h\nu_2}{h\nu_1} = \frac{\lambda_1}{\lambda_2} \qquad (21.3)$$

where λ_1 is the wavelength of the photon absorbed by the phosphor and λ_2 is the wavelength of the photon emitted by the phosphor. Note that wavelength-conversion loss is fundamental in nature. The loss cannot be overcome with conventional λ-converter materials.

However, ***quantum-splitting phosphors*** allow one to convert one short-wavelength photon into two longer-wavelength photons so that $h\nu_1 = h\nu_2 + h\nu_3$, where $h\nu_1$ is the energy of the photon absorbed by the phosphor and $h\nu_2$ and $h\nu_3$ are the energies of the photons emitted by the

phosphors. Several quantum-splitting phosphors have been reported (Justel *et al.*, 1998; Wegh *et al.*, 1999; Srivastava and Ronda, 2003; Srivastava, 2004). The possibility of quantum efficiencies approaching 200% for Eu^{3+}-doped $LiGdF_4$ has been proposed (Wegh *et al.*, 1999). The quantum-splitting phosphor $YF_3:Pr^{3+}$ at room temperature has a quantum efficiency of about 140% for 185 nm excitation (Justel *et al.*, 1998). However, viable quantum phosphors suitable for commercial applications have not yet been demonstrated.

The power-conversion efficiency of a wavelength converter is the product of Eqs. (21.1) and (21.3)

$$\eta_{\lambda\text{-converter}} = \eta_{\lambda\text{-conversion}}\, \eta_{\text{ext}} \ . \tag{21.4}$$

The inherent wavelength-conversion loss is the reason that λ-converter-based white LEDs such as phosphor-based white LEDs have a fundamentally lower efficiency limit than white-light sources based on multiple LEDs.

The wavelength-conversion loss is highest for wavelength conversion from the UV to the red. For example, the conversion from UV (405 nm) to red (625 nm) can have a λ-conversion efficiency of at most 65%. The low λ-conversion efficiency represents a strong driving force to employ red LEDs (rather than red phosphors) in highly efficient lighting systems.

Most white-light emitters use an LED emitting at short wavelength (e.g. blue) and a ***wavelength converter***. Some of the light emitted by the blue LED is absorbed in the converter material and then re-emitted as light with a longer wavelength. As a result, the lamp emits at least two different wavelengths. The types and characteristics of wavelength-converter materials will be discussed below.

The possibility that white light can be generated in different ways raises the question as to which is the optimum way to generate white light? There are two parameters that need to be considered: Firstly, the luminous efficiency and, secondly, the color-rendering index. For *signage applications*, the luminous efficiency is of primary importance and the color-rendering index is irrelevant. For *illumination applications*, both the luminous efficiency and the color-rendering index are important.

White-light sources employing two monochromatic complementary colors result in the highest possible luminous efficacy. However, the color-rendering index of such a dichromatic light source is lower than that of broad-band emitters.

The maximum luminous efficacy of radiation, attainable for white light created by two complementary monochromatic colors was calculated by MacAdam (1950). MacAdam showed

that luminous efficacies exceeding 400 lm/W can be attained using a dichromatic source for white-light generation. The work of MacAdam (1950) was further refined by Ivey (1963) and Thornton (1971). These authors showed that dichromatic white-light sources have high luminous efficacy but low color-rendering properties, making them perfectly suitable for display applications but unsuitable for daylight illumination applications. In addition, Thornton (1971) showed that trichromatic white-light sources, i.e. sources creating white light by additive mixing of three discrete colors, have a color-rendering index suited for most applications. Thornton reported on an experiment in which 60 observers judged the color rendition of meat, vegetables, flowers, complexions, etc., when illuminated with a trichromatic light source with peak wavelengths at 450, 540, and 610 nm. The color rendition in this experiment was found to be "very good, if not excellent" illustrating the suitability of trichromatic white-light sources as potent daylight illumination sources.

A white-light source duplicating the sun's spectrum would have good color-rendering capability. However, the radiation efficacy of such a light source would be lower than what is possible with other spectral distributions, e.g. a trichromatic distribution. The sun's spectrum has strong emission near the boundaries of the visible spectrum (390 and 720 nm) where the eye sensitivity is very low. Thus exact duplication of the sun's spectrum is not a viable strategy for high-efficiency light sources.

21.2 Wavelength-converter materials

There are several types of converter materials including ***phosphors***, ***semiconductors***, and ***dyes***. Converter materials have several parameters of interest, including the absorption wavelength, the emission wavelength, and the quantum efficiency. A good converter has near 100% quantum efficiency. The overall power-conversion efficiency of a wavelength converter is given by

$$\eta = \eta_{ext}\,(\lambda_1/\lambda_2) \tag{21.5}$$

where η_{ext} is the external quantum efficiency of the converter, λ_1 is the wavelength of photons absorbed by the phosphor, and λ_2 is the wavelength of photons emitted by the phosphor. Even if the external quantum efficiency is unity, there is always energy loss associated with the wavelength-conversion process, so that the power-conversion efficiency of a wavelength converter is always less than unity.

The most common wavelength-converter materials are ***phosphors*** and they will be discussed in greater detail in the following section. The optical absorption and emission spectrum of a

commercial phosphor is shown in Fig. 21.2. The phosphor displays an absorption band and a lower-energy emission band. The emission band is rather broad, making this particular phosphor suitable for white-light emission. Phosphors are very stable materials and can have quantum efficiencies close to 100%. A common phosphor used for white LEDs is cerium-doped (Ce-doped) YAG phosphor (Nakamura and Fasol, 1997). For Ce-doped phosphors, quantum efficiencies of 75% have been reported (Schlotter *et al.*, 1999).

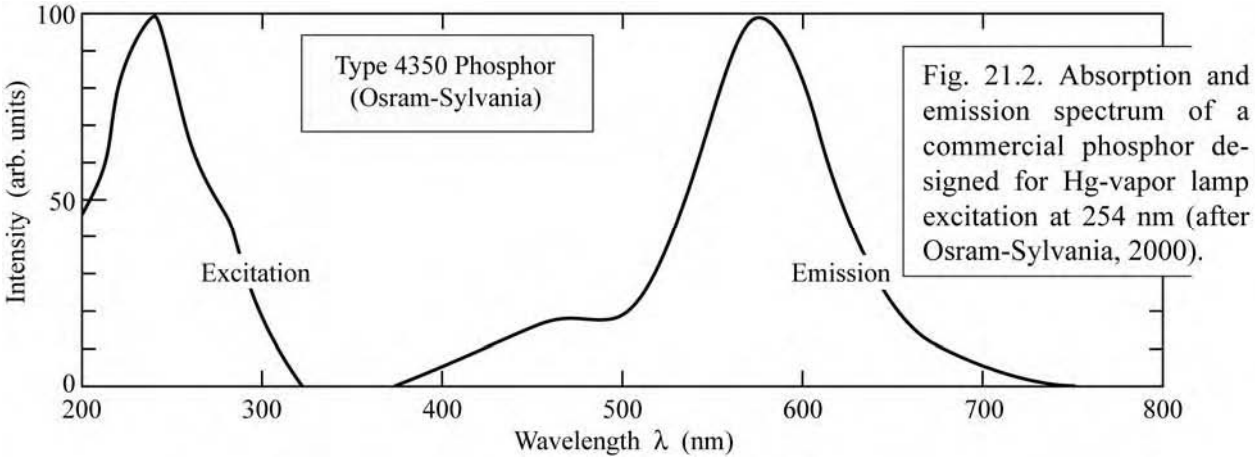

Fig. 21.2. Absorption and emission spectrum of a commercial phosphor designed for Hg-vapor lamp excitation at 254 nm (after Osram-Sylvania, 2000).

Dyes are another type of wavelength converter. Many different dyes are commercially available. An example of a dye optical absorption and emission spectrum is shown in Fig. 21.3. Dyes can have quantum efficiencies close to 100%. However, dyes, as organic molecules, lack the long-term stability afforded by phosphors and semiconductors.

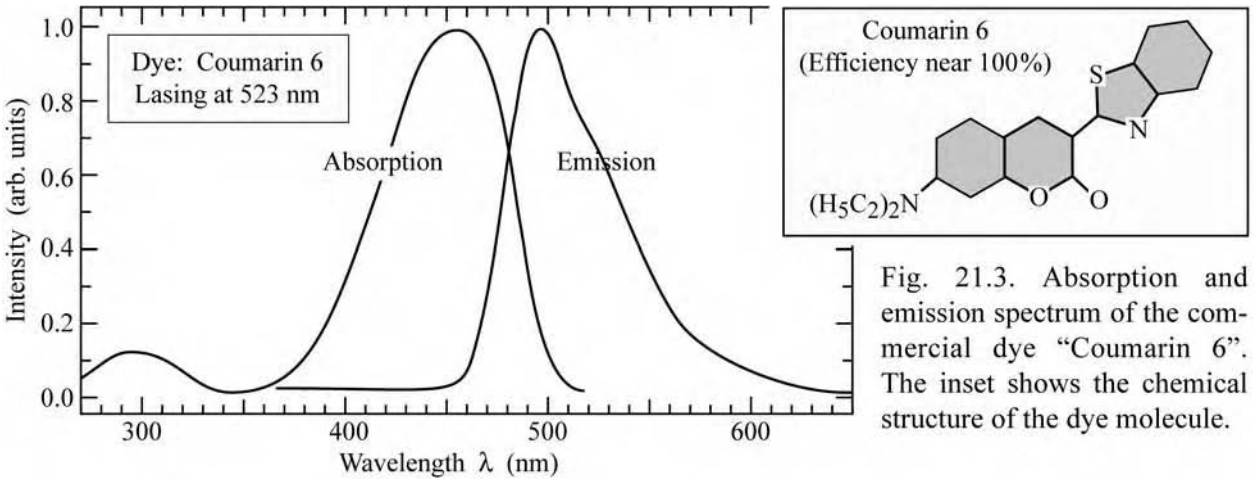

Fig. 21.3. Absorption and emission spectrum of the commercial dye "Coumarin 6". The inset shows the chemical structure of the dye molecule.

Finally, ***semiconductors*** are another type of wavelength converter. Semiconductors are

characterized by narrow emission lines with linewidths of the order of $2kT$. The spectral emission linewidth of semiconductors is narrower than the linewidth of many phosphors and dyes. Thus, semiconductors allow one to tailor the emission spectrum of a semiconductor wavelength converter with good precision.

As for phosphors and dyes, semiconductors can have internal quantum efficiencies near 100%. The light escape problem in semiconductor converters is less severe than it is in LEDs due to the fact that semiconductor converters do not need electrical contacts that could block the light.

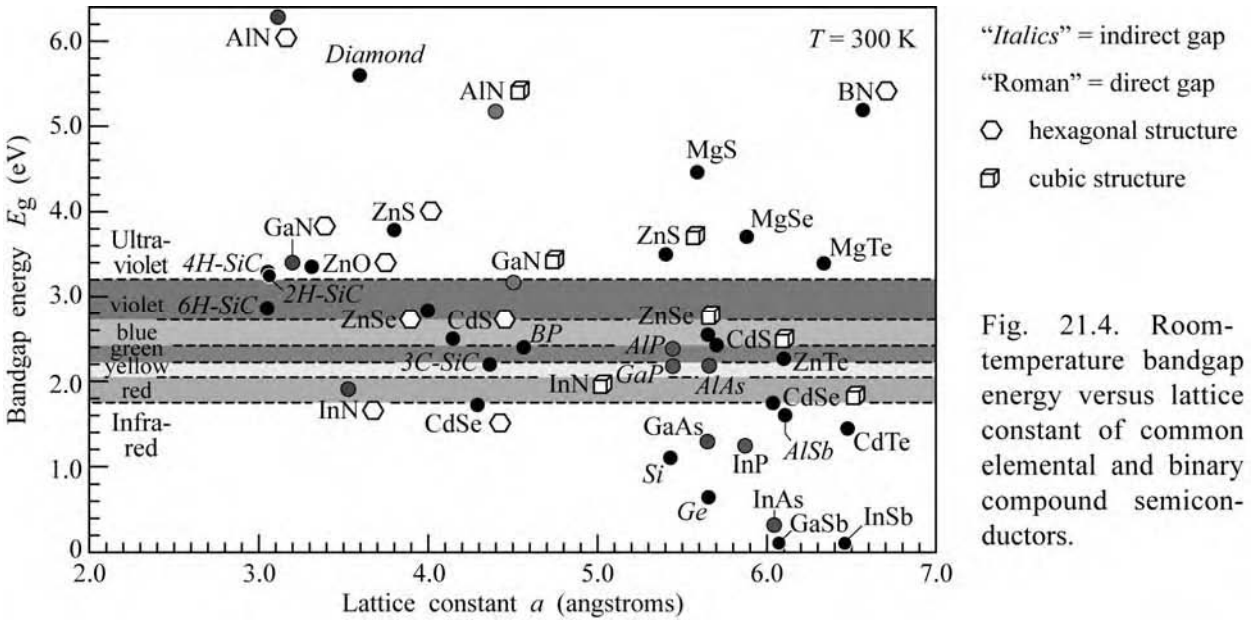

Fig. 21.4. Room-temperature bandgap energy versus lattice constant of common elemental and binary compound semiconductors.

Similar to phosphors and dyes, a great variety of semiconductors is available. Figure 21.4 shows elemental and binary compound semiconductors versus the semiconductor lattice constant. Using ternary or quaternary alloys, wavelength converters operating at virtually any visible wavelength can be fabricated.

21.3 Phosphors

Phosphors consist of an inorganic host material doped with an optically active element. Common hosts are ***garnets***, which have the chemical formula $A_3B_5O_{12}$ where A and B are chemical elements and O is oxygen. Among the large group of garnets, yttrium aluminum garnet (YAG), $Y_3Al_5O_{12}$, is a particularly common host material. Phosphors having YAG as a host material are called ***YAG phosphors***. The optically active dopant is a rare-earth element, a rare-earth oxide, or

another rare-earth compound. Most rare-earth elements are optically active. Rare-earth light-emitting elements include cerium (Ce) used in white-light YAG phosphors, neodymium (Nd) used in lasers (Nd-doped YAG lasers), erbium (Er) used in optical amplifiers, and thorium (Th) oxide used in the mantle of gas lights.

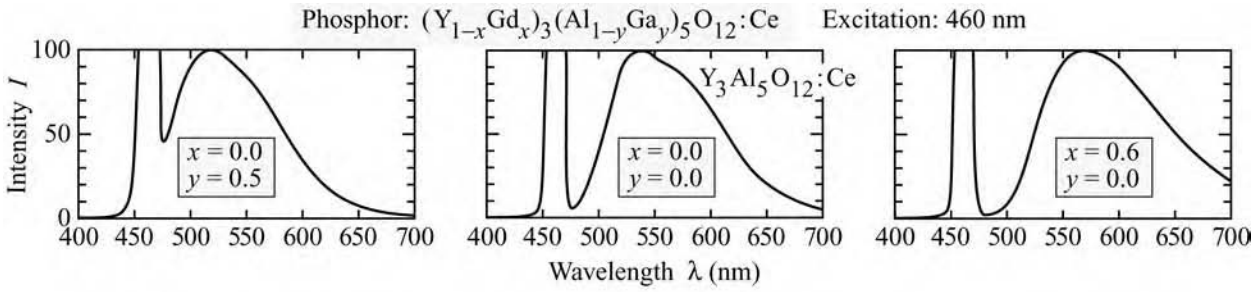

Fig. 21.5. Emssion spectrum of Ce-doped yttrium aluminum garnet (YAG:Ce) phosphor for different chemical compositions. The excitation wavelength is 460 nm (after Nakamura and Fasol, 1997).

The optical characteristics of YAG phosphors can be modified by partially substituting Gd for Y and Ga for Al so that the phosphor host has the composition $(Y_{1-x}Gd_x)_3(Al_{1-y}Ga_y)_5O_{12}$. The emission spectra for a Ce-doped $(Y_{1-x}Gd_x)_3(Al_{1-y}Ga_y)_5O_{12}$ phosphor with different compositions are shown in Fig. 21.5 (Nakamura and Fasol, 1997). The figure reveals that the addition of Gd shifts the emission spectrum to longer wavelengths whereas the addition of Ga shifts the emission spectrum to shorter wavelengths.

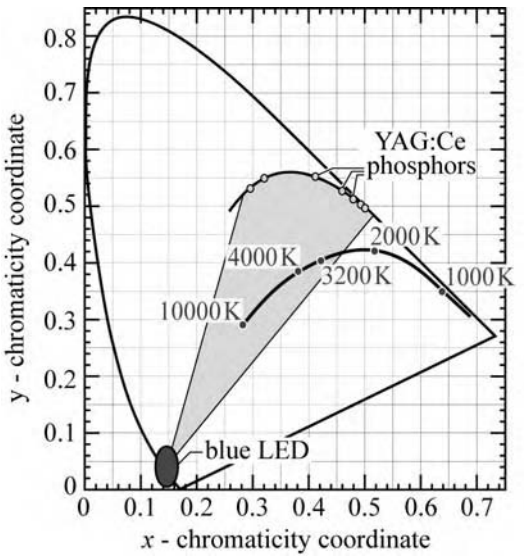

Fig. 21.6. Chromaticity points of YAG:Ce phosphor, and the general area (shaded) accessible to white emitters consisting of a blue LED and YAG:Ce phosphor (adapted from Nakamura and Fasol, 1997). Also shown is the planckian locus with color temperatures.

The chromaticity points of the YAG:Ce phosphors are shown in Fig. 21.6. The shaded region

reveals the chromaticities that can be attained by mixing light from a blue LED source with the light of YAG:Ce. The figure reveals that such white emitters can have a very high color temperature.

An alternative to YAG phosphor is ***TAG phosphor***, which is based on terbium aluminum garnet, $Tb_3Al_5O_{12}$. Both YAG and TAG crystallize with the garnet structure. Additionally, the Y^{3+} and Tb^{3+} ionic radii are very close (r_{Y3+} = 1.02 Å and r_{Tb3+} = 1.04 Å). Consequently, the X-ray diffraction pattern of YAG does not strongly change as Y in YAG is substituted with Tb, even for Tb mol fractions of 30% (Potdevin *et al.*, 2005). Although TAG phosphors may have slightly lower radiative efficiency than YAG phosphors, TAG phosphors represent a viable alternative to YAG phosphors (Kim, 2005).

21.4 White LEDs based on phosphor converters

A white LED lamp using a phosphor wavelength converter and a blue GaInN/GaN optical excitation LED was first reported by Bando *et al.* (1996) and reviewed by Nakamura and Fasol (1997). The GaInN/GaN LED used for optical excitation ("optical pumping") was a device reported by Nakamura *et al.* (1995). The phosphor used as a wavelength converter was Ce-doped YAG with chemical formula $(Y_{1-a}Gd_a)_3(Al_{1-b}Ga_b)_5O_{12}$: Ce. The exact chemical composition of the host (YAG) and the dopants (e.g. Ce) is usually proprietary and not publicly available.

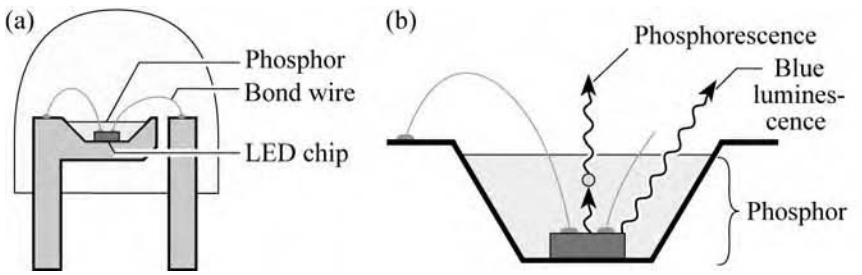

Fig. 21.7. (a) Structure of white LED lamp consisting of a GaInN blue LED chip and a phosphor. (b) Wavelength-converting phosphorescence and blue luminescence (after Nakamura and Fasol, 1997).

The cross-sectional structure of a white LED lamp is shown in Fig. 21.7 (a). The figure shows the LED die emitting in the blue and the YAG phosphor surrounding the die. The YAG phosphor can be made as a powder and suspended in epoxy resin. During the manufacturing process, a droplet of the YAG phosphor suspended in the epoxy is deposited on the LED die, so that the resin fills the cup-shaped depression in which the LED die is located, as shown in Fig. 21.7 (b). As indicated in the figure, a fraction of the blue light is absorbed by the phosphor and re-emitted as longer-wavelength light.

The emission spectrum of the phosphor-based white lamp thus consists of the blue emission

band originating from the semiconductor LED and longer-wavelength phosphorescence, as shown in Fig. 21.8. The thickness of the phosphor-containing epoxy and the concentration of the phosphor suspended in the epoxy determine the relative strengths of the two emission bands. The two bands can thus be adjusted to optimize the luminous efficiency and the color-rendering characteristics of the LED.

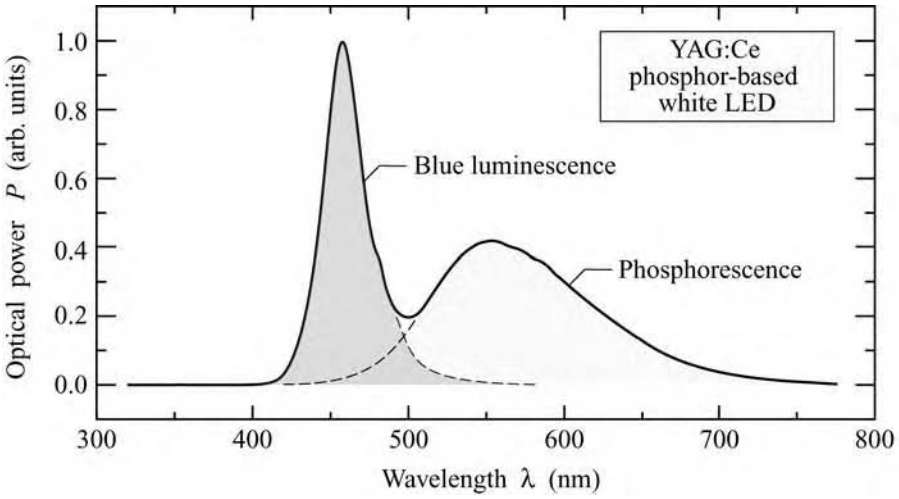

Fig. 21.8. Emission spectrum of a phophor-based white LED manufactured by Nichia Corporation (Anan, Tokushima, Japan).

The location of the white lamp in the chromaticity diagram is shown in Fig. 21.9. The location suggests that the emission color is white with a bluish tint. A bluish white is indeed confirmed when looking at the lamp.

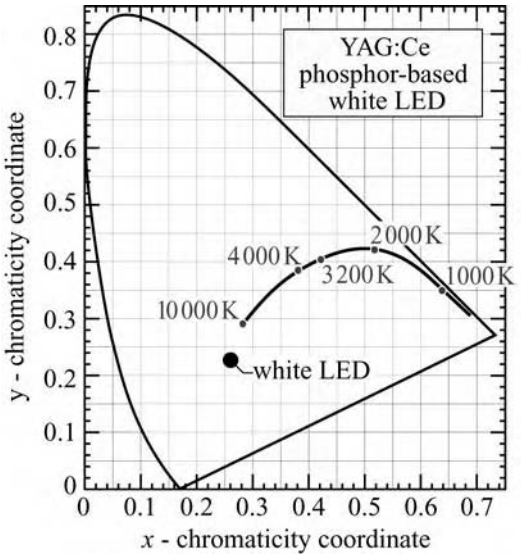

Fig. 21.9. Chromaticity coordinates of a commercial phophor-based white LED manufactured in 2001 by Nichia Corporation (Anan, Tokushima, Japan). Also shown is the planckian locus and associated color temperatures.

First-generation white LEDs from Nichia Corporation were improved in terms of their color

rendering capability by adding an additional phosphor that, when excited by 460 nm blue light, has a peak emission wavelength of 655 nm and a full-width at half-maximum of 110 nm (Narukawa, 2004). As a result, the emission can be enhanced in the red range, as shown in Fig. 21.10. Furthermore, by using an optimized phosphor mix, the pronounced notch in the first-generation white LED is reduced. The second-generation white LED lamps from Nichia Corporation (Narukawa, 2004) render red colors better than the first-generation and have a lower color temperature that can range between 2800 K (warm white) and 4700 K depending on the phosphor mix.

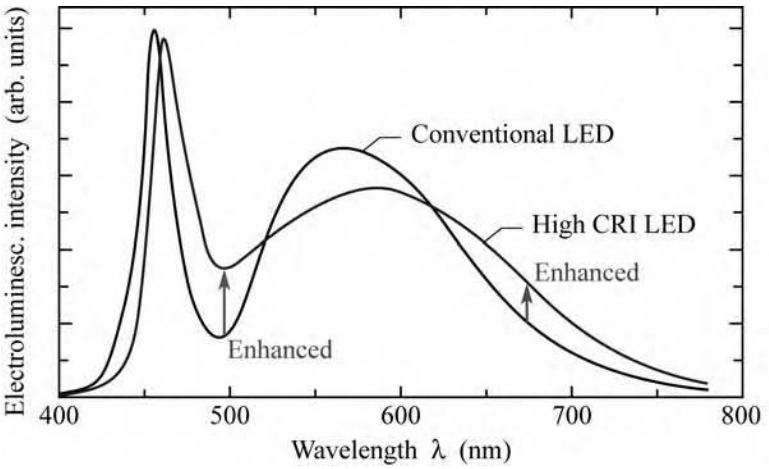

Fig. 21.10. Electroluminescence spectrum of conventional white LED and of high-color-rendering-index white LED. The high CRI results from the broader emission spectrum and the reduction of the notch in the spectrum (after Narukawa, 2004).

Note that the downside of adding red phosphors is a reduced luminous efficiency: The large Stokes shift of red phosphors reduces the efficiency (excitation 460 nm; emission 655 nm) Furthermore, it is well known that red phosphors excitable at 460 nm are comparatively inefficient. Thus, although color rendering capabilities are improved, they are improved at the expense of luminous efficiency.

A concern with white sources is spatial ***color uniformity***. The chromaticity of the white source should not depend on the emission direction. Color uniformity can be attained by a phosphor distribution that provides an ***equal optical path length*** in the phosphor material independent of the emission direction (Reeh *et al*., 2003).

Spatial uniformity can also be attained by adding ***mineral diffusers*** to the encapsulant (Reeh *et al*., 2003). Such mineral diffusers are optically transparent substances, such as TiO_2, CaF_2, SiO_2, $CaCO_3$, and $BaSO_4$, with a refractive index different from the encapsulant. The diffuser will cause light to reflect, refract, and scatter, thereby randomizing the propagation direction and uniformizing the far-field distribution in terms of chromaticity (i.e. spectral composition).

21.5 Spatial phosphor distributions

The ***spatial phosphor distribution*** in white LED lamps strongly influences the color uniformity and efficiency of the lamp. One can distinguish between ***proximate*** and ***remote phosphor distributions*** (Goetz, 2003; Holcomb *et al*., 2003; Kim *et al*., 2005; Luo *et al*., 2005; Narendran *et al*., 2005). In proximate phosphor distributions, the phosphor is located in close proximity to the semiconductor chip. Proximate phosphor distributions are shown in Fig. 21.11(a) and (b). In remote phosphor distributions, the phosphor is spatially removed from the semiconductor chip. A remote phosphor distribution is shown in Fig. 21.11(c).

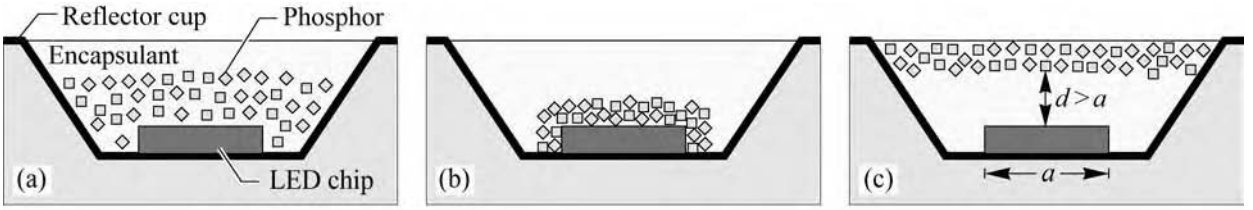

Fig. 21.11. (a) Proximate phosphor distribution, (b) proximate conformal phosphor distribution, and (c) remote phosphor distribution in which phosphor and chip are separated by at least one times the lateral dimension of the chip (after Kim *et al*., 2005).

Photographs of the different phosphor distributions are shown in Fig. 21.12. The proximate phosphor distribution shown in Fig. 21.12(a) was introduced by Nichia Corporation during the 1990s. The phosphor particles are dissolved in the encapsulation material that is dispensed into the reflector cup. Gravity, buoyancy, and friction generally lead to a distribution of phosphor particles that favors larger phosphor particles to move downward, thereby bringing them closer to the chip surface.

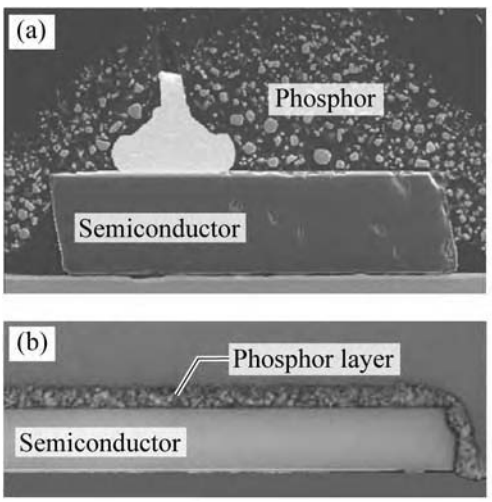

Fig. 21.12. Phosphor distributions in white LEDs: (a) Proximate phosphor distribution. (b) Proximate conformal phosphor distribution. (c) Remote phosphor distribution ((a) and (b) adopted from Goetz, 2003; (c) after Kim *et al*., 2005).

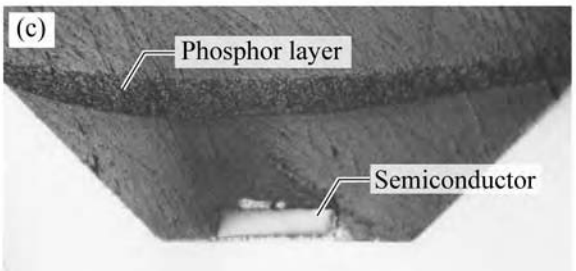

Another proximate phosphor distribution, called the ***conformal phosphor distribution***, is shown in Fig. 21.12 (b). Conformal phosphor distributions are accomplished by wafer-level phosphor dispensation thereby lowering the manufacturing cost as compared with a lamp-level phosphor dispensation. Conformal phosphor distributions provide a small emission area and high luminance, which is particularly relevant for imaging-optics applications. Imaging-optics applications (e.g. automotive headlights) frequently require the use of lenses. Optical design considerations show that point-like sources, i.e. sources with a small emission area, are desirable for these applications.

A general drawback of proximate phosphor distributions is the absorption of phosphorescence by the semiconductor chip. Phosphorescence emitted toward the semiconductor chip can be absorbed by the chip, e.g. by the metal contacts covering the chip. The reflectivity of the semiconductor chip and metal contacts is generally not very high.

This drawback can be avoided by remote phosphor distributions in which the phosphor is spatially distanced from the semiconductor chip (Kim *et al*., 2005; Luo *et al*., 2005; Narendran *et al*., 2005). In such remote phosphor structures, it is less likely that phosphorescence impinges on the low-reflectance semiconductor chip due to the spatial separation between the primary emitter (semiconductor chip) and the secondary emitter (phosphor). The probability that phosphorescence impinges on the semiconductor chip is greatly diminished if the distance between chip and phosphor is equal to or greater than the chip's lateral dimension, i.e. $d > a$, as shown in Fig. 21.11(c). As a result, higher phosphorescence efficiency is enabled. Ray-tracing simulations and experiments using a remote blue phosphor pumped by a GaInN emitter have indeed demonstrated phosphorescence efficiency improvements of 75% and 27%, respectively (Kim *et al*., 2005; Luo *et al*., 2005). Narendran *et al*. (2005) reported an average of 61% improvement in light output by using the "scattered photon extraction" (SPE) method. At low currents, the SPE packages exceeded 80 lm/W, compared to 54 lm/W for a typical conventional package.

21.6 UV-pumped phosphor-based white LEDs

White LEDs can also be fabricated with optical excitation of phosphor in the ultraviolet (UV) wavelength range (Karlicek, 1999). Semiconductor sources emitting in the near-UV (320–390 nm) and in the violet, close the edge of the visible spectrum (390–410 nm) are frequently used for such white sources. Semiconductor diodes emitting near 400 nm with remarkably high efficiencies have been reported (Morita *et al*., 2004).

For deep-UV semiconductor sources (200–320 nm), conventional phosphors, as used in fluorescent lighting, can be used for wavelength conversion. However, the large Stokes shift associated with deep-UV sources is a significant drawback for such sources. Furthermore the development of deep-UV LEDs is challenging due to the low p-type and n-type doping efficiency in AlGaN with high Al content and the difficulties encountered in epitaxially growing high-quality AlGaN with low dislocation and defect densities.

In UV-pumped white LEDs, the entire visible emission originates in the phosphor. Phosphors excited in the deep UV have been used since the 1950s in fluorescent light tubes and since the 1980s in compact fluorescent lamps (CFLs). Phosphors in fluorescent light sources are pumped by the UV emission coming from the low-pressure mercury-vapor discharge occurring inside the tube. The dominant emission of low-pressure mercury-vapor discharge lamps (***Hg lamps***) occurs in the UV at 254 nm. Phosphors with strong absorption in this wavelength range are readily available. The color rendering properties of such phosphors are very suitable for most applications.

A white LED using a UV AlGaInN LED pump source and a tricolor phosphor blend was reported by Kaufmann *et al*. (2001). The LED pump source emitted at 380–400 nm, that is, near the boundary between the visible and UV spectrum. The phosphor blend consisted of three phosphors emitting in the red, green, and blue parts of the spectrum. A color-rendering index of 78 was reported for the lamp.

The color-rendering index (CRI) of UV-excited phosphor mixes ranges between 60 and 100. Excellent CRIs as high as 97 were reported by Radkov *et al*. (2003) for phosphor blends excited near 400 nm. Furthermore, such UV-LED based sources exhibit independence of the phosphor-emission spectrum on the exact UV-LED excitation wavelength, because the visible emission is solely due to the phosphor. Consequently, UV-pumped white lamps are expected to have a highly reproducible optical spectrum so that “binning” will likely not be required. Monte Carlo simulations reported by Radkov *et al*. (2004) indeed showed a very low chromaticity point variation (entirely within the first MacAdam ellipse) for phosphor sources excited with a variety of LEDs coming from chip bins with peak wavelengths ranging between 400 nm and 410 nm. The chromaticity variation was shown to be much lower for UV-LED/phosphor sources than for blue-LED/phosphor sources.

A fundamental drawback of UV-pumped white LEDs is the energy loss (Stokes shift) incurred when converting UV light to white light. The potential luminous efficiency of UV-pumped white LED lamps is therefore markedly lower than that of white sources based on a blue

LED exciting a yellow phosphor.

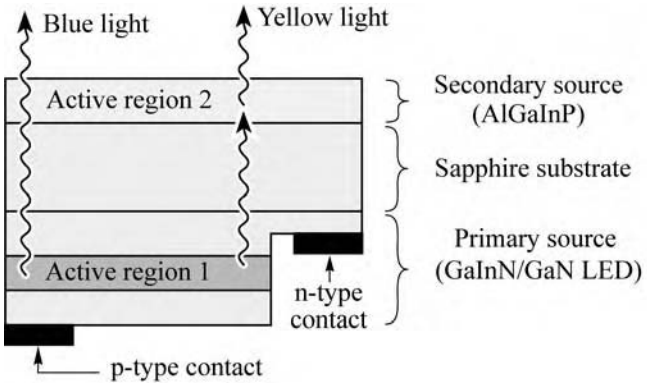

Fig. 21.13. Schematic structure of a photon-recycling semiconductor LED with one current-injected active region (Active region 1) and one optically excited active region (Active region 2) (after Guo *et al*., 1999).

21.7 White LEDs based on semiconductor converters (PRS-LED)

Light-emitting diodes using semiconductor wavelength converters have been demonstrated by Guo *et al*. (1999). The schematic structure of the photon-recycling semiconductor LED (PRS-LED) is shown in Fig. 21.13. The figure indicates that a fraction of the light emitted by the blue GaInN LED is absorbed by a AlGaInP secondary active region and re-emitted (or "recycled") as lower-energy photons. In order to obtain white light, the intensity of the two light sources must have a certain ratio that will be calculated below. The schematic power budget of the device is shown in Fig. 21.14. It is assumed that the electrical input power is P_0, and the output powers in the blue and amber spectral range are P_1 and P_2, respectively. The power-conversion efficiency of the blue LED and the photon-recycling semiconductor are assumed to be η_1 and η_2, respectively. The efficiency and luminous efficiency of the device are calculated below.

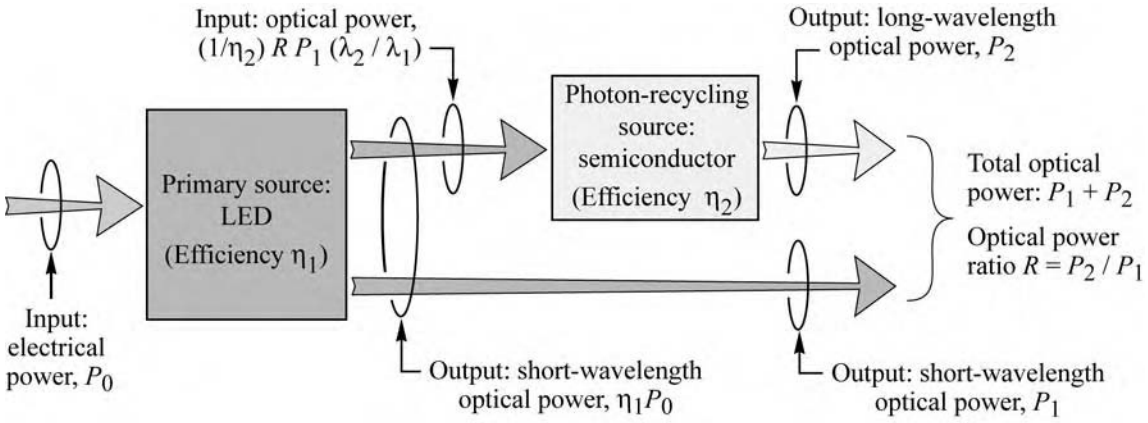

Fig. 21.14. Photon-recycling semiconductor LED power budget with electrical input power P_0 and optical output power P_1 and P_2.

The energy loss occurring in the photon-recycling process must be taken into account when determining the optimum choice of wavelengths for highest efficiency. Note that energy is lost even if the recycling process occurs with unit quantum efficiency. To calculate the optimum wavelength of operation, we represent white light by the Illuminant C standard, for which the chromaticity coordinates are $x_c = 0.3101$, $y_c = 0.3163$, $z_c = 0.3736$. Using these chromaticity coordinates, the pairs of complementary wavelengths can be determined.

21.8 Calculation of the power ratio of PRS-LED NO

Next, we calculate the light-power ratio between two sources required for the emission of white light and the luminous efficiency of the photon-recycling semiconductor LED. We refer to λ_1 and λ_2 as the primary (short) and secondary (long) wavelength, respectively. For white light, λ_1 and λ_2 are pairs of complementary wavelengths. We define the color masses of the two light sources as

$$m_1 = \bar{x}_1 + \bar{y}_1 + \bar{z}_1 \qquad \text{and} \qquad m_2 = \bar{x}_2 + \bar{y}_2 + \bar{z}_2 \tag{21.6}$$

where $\bar{x}_1$, $\bar{y}_1$, $\bar{z}_1$, $\bar{x}_2$, $\bar{y}_2$, and $\bar{z}_2$ are color-matching functions at the two emission wavelengths λ_1 and λ_2, respectively (Judd, 1951; Vos, 1978; MacAdam, 1950, 1985). We define the power ratio of the two light sources as

$$R = P_2 / P_1 \tag{21.7}$$

where P_1 and P_2 are the optical powers of the short-wavelength source (λ_1) and the long-wavelength source (λ_2), respectively. The chromaticity coordinates of the newly generated color are then given by

$$y_{\text{new}} = \frac{P_1 \bar{y}_1 + P_2 \bar{y}_2}{P_1 m_1 + P_2 m_2} = \frac{\bar{y}_1 + R \bar{y}_2}{m_1 + R m_2} \tag{21.8}$$

and

$$x_{\text{new}} = \frac{\bar{x}_1 + R \bar{x}_2}{m_1 + R m_2} . \tag{21.9}$$

For a white-light emitter, x_{new} and y_{new} can be chosen to coincide with the chromaticity coordinates of the Illuminant C standard ($x_c = 0.3101$, $y_c = 0.3162$; CIE, 1932; Judd, 1951), i.e. $x_{\text{new}} = x_c = 0.3101$ and $y_{\text{new}} = y_c = 0.3162$. Solving Eq. (21.9) for the power ratio R yields

$$R = \frac{\bar{y}_1 - y_c m_1}{y_c m_2 - \bar{y}_2} . \tag{21.10}$$

The power ratio as calculated from Eq. (21.10) is shown as a function of wavelength in Fig. 21.15.

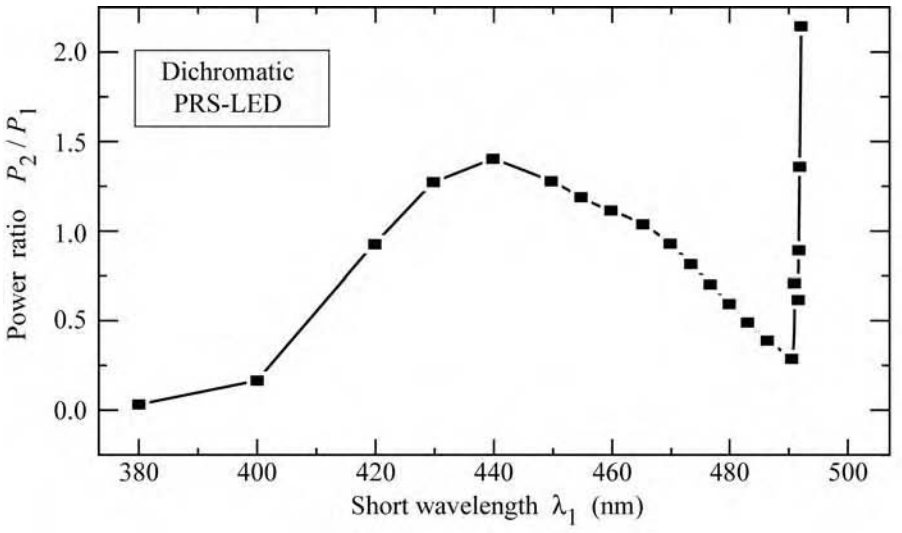

Fig. 21.15. Calculated power ratio between the two optical output powers P_1 and P_2 required to obtain white-light emission (after Guo *et al.*, 1999).

21.9 Calculation of the luminous efficiency of PRS-LED NO

To produce the optical power P_2 at the wavelength of λ_2 through the recycling of photons from the primary source with wavelength λ_1, the optical power required from the primary source is given by

$$\frac{P_2}{\eta_2}\,\frac{\lambda_2}{hc}\,\frac{hc}{\lambda_1} = \frac{P_2\lambda_2}{\eta_2\lambda_1} \tag{21.11}$$

where η_2 is the optical-to-optical conversion efficiency of the photon-recycling light source. If P_0 is the electrical input power, then the optical power emitted by the primary LED source is $\eta_1 P_0$, where η_1 is the electrical-to-optical power conversion efficiency of the primary LED. Thus, the optical power emitted by the primary LED is given by

$$P_1 + \frac{P_2\lambda_2}{\eta_2\lambda_1} = \eta_1 P_0 . \tag{21.12}$$

Solving the equation for the electrical input power and using $P_2 = RP_1$ yields

$$P_0 = P_1\left(\frac{1}{\eta_1} + \frac{R\lambda_2}{\eta_1\eta_2\lambda_1}\right). \tag{21.13}$$

The total optical output power of the PRS-LED is given by

$$P_{\text{out}} = P_1 + P_2 = (1 + R)P_1 \tag{21.14}$$

so that the overall electrical-to-optical power efficiency of the photon-recycling dichromatic light source is given by

$$\eta = \frac{P_{\text{out}}}{P_0} = \frac{P_1(1+R)}{P_1\left(\frac{1}{\eta_1} + \frac{R}{\eta_1\eta_2}\frac{\lambda_2}{\lambda_1}\right)} = \frac{1+R}{\frac{1}{\eta_1} + \frac{R}{\eta_1\eta_2}\frac{\lambda_2}{\lambda_1}}. \tag{21.15}$$

The luminous flux Φ_{lum} of the device is given by

$$\Phi_{\text{lum}} = 683\frac{\text{lm}}{\text{W}}\left(\bar{y}_1 P_1 + \bar{y}_2 P_2\right) = 683\frac{\text{lm}}{\text{W}}\left(\bar{y}_1 + \bar{y}_2 R\right)P_1. \tag{21.16}$$

Then the luminous efficacy of radiation (measured in lumens per optical watt) of the photon-recycling semiconductor LED is given by

$$\frac{\Phi_{\text{lum}}}{P_{\text{out}}} = 683\frac{\text{lm}}{\text{W}}\,\frac{\bar{y}_1 + \bar{y}_2 R}{1 + R}. \tag{21.17}$$

Thus, the luminous efficiency of the source (measured in lumens per electrical watt) of the PRS-LED is given by

$$\frac{\Phi_{\text{lum}}}{P_0} = 683\frac{\text{lm}}{\text{W}}\,\eta\,\frac{\bar{y}_1 + \bar{y}_2 R}{1 + R}. \tag{21.18}$$

Using this formula, we calculate the luminous efficiency as a function of the primary wavelength. The result of the calculation is shown in Fig. 21.16 for *ideal* sources, i.e. for $\eta_1 = \eta_2 = 100\%$.

The maximum luminous efficiency occurs if the primary source emits at the wavelength 440 nm. A theoretical luminous efficiency of 336 lm/W is obtained for this wavelength. Note that in the calculation we assume that both light sources emit monochromatic light. However, the spontaneous emission from semiconductors has a 1.8 *kT* spectral width. Taking into account a

finite linewidth, the expected luminous efficiency is slightly lower.

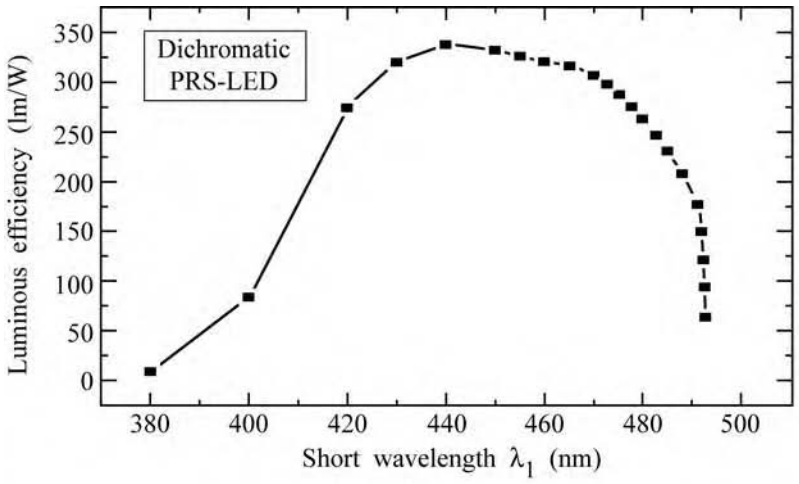

Fig. 21.16. Calculated luminous efficiency of a dichromatic PRS-LED versus its primary emission wavelength (after Guo *et al*., 1999).

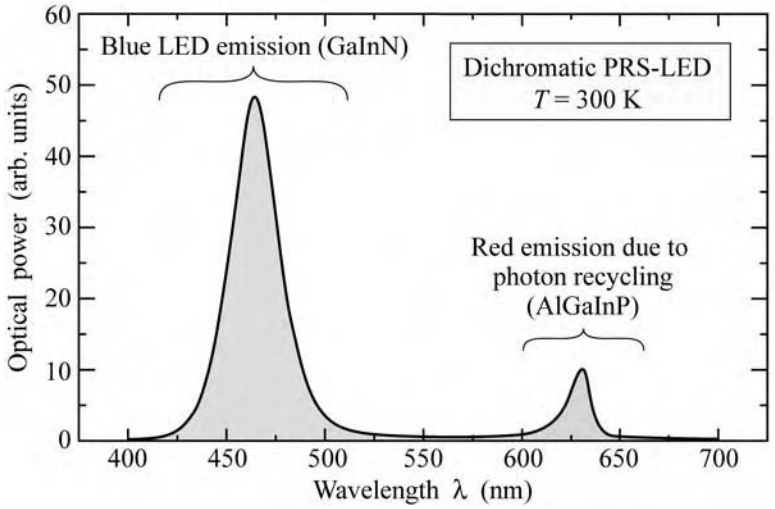

Fig. 21.17. Emission spectrum of dichromatic PRS-LED with current-injected GaInN blue LED primary source and AlGaInP photon recycling wafer (secondary source) emitting in the red (after Guo *et al*., 2000).

21.10 Spectrum of PRS-LED NO

PRS-LEDs have been demonstrated using a GaInN/GaN LED emitting in the blue and an electrically passive AlGaInP photon-recycling semiconductor emitting in the red part of the spectrum (Guo *et al*., 1999). The emission spectrum of the device, depicted in Fig. 21.17, shows the emission line of the primary LED at 470 nm and a second emission line at 630 nm due to absorption of the 470 nm light in the AlGaInP layer and re-emission of light at 630 nm. The recycling semiconductor used in this experiment is an AlGaInP/GaAs double heterostructure. The photon-recycling semiconductor is planar and no surface texturing was performed.

To avoid absorption of light in the GaAs substrate, the GaAs substrate of the AlGaInP

epitaxial layer was removed. Firstly, the AlGaInP/GaAs recycling semiconductor was mounted on a glass slide. Subsequently, the GaAs substrate was removed by polishing and selective wet chemical etching. Then the primary LED wafer and the photon-recycling wafer were bonded together.

The approximate theoretical luminous efficiency of several types of white LED lamps is given in Table 21.2. The data show that the dichromatic light source has the highest luminous efficiency as compared to spectrally broader emitters.

Type of LED	**Luminous efficiency** (lm/W)	**Chromaticity coordinates** (*x*, *y*)
Dichromatic PRS LED	300–360	(0.31, 0.32)
Broadened dichromatic PRS LED	280–350	(0.31, 0.32)
Trichromatic LED	240–340	(0.31, 0.32)
Phosphor-based LED	200–280	(0.31, 0.32)

Table 21.2. Approximate theoretical luminous efficiencies of different types of white LEDs assuming unit quantum efficiency and the absence of resistive power losses.

Generally, dichromatic white LEDs have a higher luminous efficacy but lower color-rendering index (CRI) compared with trichromatic white LEDs. It can be shown that there is a fundamental trade-off between color rendering and the luminous efficacy of light-emitting devices (Walter, 1971). In order to improve the general CRI of dichromatic devices such as the PRS-LED, two possibilities can be considered. Firstly, the emission lines can be intentionally broadened, e.g. by compositional grading. Secondly, a second photon-recycling semiconductor can be added thus creating a trichromatic PRS-LED. However, any broadening of the two emission lines or the addition of an emission line will decrease the luminous efficacy and luminous efficiency of the device.

21.11 White LEDs based on dye converters

White LEDs can also be fabricated using organic dye molecules as wavelength converter materials. The dyes can be incorporated in the epoxy encapsulant (Schlotter *et al.*, 1997). Dyes can also be incorporated in optically transparent polymers.

A drawback of organic dyes is their finite lifetime. Dye molecules “bleach out”, i.e. become optically inactive, after a certain number of photon absorption events. Typically a dye molecule is stable for about 10^4–10^6 optical transitions (Jones, 2000). The lack of high molecular stability

of dyes is a serious drawback. The lifetime of dyes is considerably shorter than the lifetime of semiconductor or phosphor wavelength converters.

Dyes have a relatively small difference between the absorption and the emission band (Stokes shift). For example, the Stokes shift for the dye *Coumarin 6* is just 50 nm, as discussed earlier in this chapter. This shift is smaller than the Stokes shift required for dichromatic white LEDs that need typical wavelength shifts of 100 nm or more, as inferred from the separation of complementary wavelengths.

References

Bando K., Noguchi Y., Sakano K., and Shimizu Y. (in Japanese) *Tech. Digest, Phosphor Res. Soc*., *264th Meeting*, November 29 (1996)

CIE *Commission Internationale de l'Eclairage Proceedings, 1931* (Cambridge University Press, Cambridge, 1932)

Goetz W. "White lighting (illumination) with LEDs" *Fifth International Conference on Nitride Semiconductors*, Nara, Japan, May 25–30 (2003)

Guo X., Graff J. W., and Schubert E. F. "Photon-recycling semiconductor light-emitting diode" *IEDM Technical Digest*, **IEDM-99**, 600 (1999)

Guo X., Graff J. W., and Schubert E. F. "Photon-recycling for high brightness LEDs" *Compound Semiconductors* **6**, May/June (2000)

Holcomb M. O., Mueller-Mach R., Mueller G. O., Collins D., Fletcher R. M., Steigerwald D. A., Eberle S., Lim Y. K., Martin P. S., and Krames M. "The LED light bulb: Are we there yet? Progress and challenges for solid-state illumination" *Conference on Lasers and Electro-Optics* (*CLEO*), Baltimore, Maryland, June 1–6 (2003)

Ivey H. F. "Color and efficiency of luminescent light sources" *J. Opt. Soc. Am.* **53**, 1185 (1963)

Jones G., personal communication (2000)

Judd D. B. "Report of US secretariat committee on colorimetry and artificial daylight" in *Proceedings of the Twelfth Session of the CIE, Stockholm* Vol. **1**, p. 11 (Bureau central de la CIE, Paris, 1951)

Justel T., Nikol H., and Ronda C. R. "New developments in the field of luminescent materials for lighting and displays" *Angewandte Chemie (International Edition)* **37**, 3084 (1998)

Karlicek Jr. R. F., personal communication (1999)

Kaufmann U., Kunzer M., Köhler K., Obloh H., Pletschen W., Schlotter P., Schmidt R., Wagner J., Ellens A., Rossner W., and Kobusch M. "Ultraviolet pumped tricolor phosphor blend white emitting LEDs" *Phys. Stat. Sol. (a)* **188**, 143 (2001)

Kim J. K., personal communication (2005)

Kim J. K., Luo H., Schubert E. F., Cho J., Sone C., and Park Y. "Strongly enhanced phosphor efficiency in GaInN white light-emitting diodes using remote phosphor configuration and diffuse reflector cup" *Jpn. J. Appl. Phys. – Express Letter* **44**, L 649 (2005)

Luo H., Kim J. K., Schubert E. F., Cho J., Sone C., and Park Y. "Analysis of high-power packages for phosphor-based white-light-emitting diodes" *Appl. Phys. Lett*. **86**, 243505 (2005)

MacAdam D. L. "Maximum attainable luminous efficiency of various chromaticities" *J. Opt. Soc. Am.* **40**, 120 (1950)

MacAdam D. L. *Color Measurement: Theme and Variations* (Springer, New York, 1985)

Morita D., Yamamoto M., Akaishi K., Matoba K., Yasutomo K., Kasai Y., Sano M., Nagahama S.-I., and Mukai T. "Watt-class high-output-power 365 nm ultraviolet light-emitting diodes" *Jpn. J. Appl. Phys*. **43**, 5945 (2004)

Nakamura S., Senoh M., Iwasa N., Nagahama S., Yamada T., and Mukai T. "Superbright green InGaN single-quantum-well-structure light-emitting diodes" *Jpn. J. Appl. Phys*. (*Lett.*) **34**, L1332 (1995)

Nakamura S. and Fasol G. *The Blue Laser Diode* (Springer, Berlin, 1997)

Narendran N., Gu Y., Freyssinier-Nova J. P., and Zhu Y. "Extracting phosphor-scattered photons to

improve white LED efficiency" *Phys. Stat. Sol. (a)* **202**, R60 (2005)
Narukawa Y. "White light LEDs" *Optics & Photonics News* **15**, No. 4, p. 27 (2004)
Osram-Sylvania Corporation. Data sheet on type 4350 phosphor (2000)
Potdevin A., Chadeyron G., Boyer D., Caillier B., and Mahiou R. "Sol-gel based YAG:Tb^{3+} or Eu^{3+} phosphors for application in lighting sources" *J. Phys. D: Appl. Phys.* **38**, 3251 (2005)
Radkov E., Setlur A., Brown Z., and Reginelli J. "High CRI phosphor blends for near UV LED lamps" *Proc. SPIE* **5530**, 260 (2003)
Radkov E., Bompiedi R., Srivastava A. M., Setlur A. A., and Becker C. "White light with UV LEDs" *Proc. SPIE* **5187**, 171 (2004)
Reeh U., Höhn K., Stath N., Waitl G., Schlotter P., Schneider J., and Schmidt R. "Light-radiating semiconductor component with luminescence conversion element" US Patent 6,576,930 B2 (2003)
Schlotter P., Schmidt R., and Schneider J. "Luminescence conversion of blue light emitting diodes" *Appl. Phys. A* **64**, 417 (1997)
Schlotter P., Baur J., Hielscher C., Kunzer M., Obloh H., Schmidt R., and Schneider J. "Fabrication and characterization of GaN/InGaN/AlGaN double heterostructure LEDs and their application in luminescence conversion LEDs" *Materials Sci. Eng.* **B59**, 390 (1999)
Srivastava A. M. "Phosphors" *Encyclopedia of Physical Science and Technology* 3rd edition **11**, 855 (2004)
Srivastava A. M. and Ronda C. R. "Phosphors" *Interface (The Electrochemical Society)* **12** (2), p. 48 (2003)
Thornton W. A. "Luminosity and color-rendering capability of white light" *J. Opt. Soc. Am.* **61**, 1155 (1971)
Vos, J. J. "Colorimetric and photometric properties of a 2-degree fundamental observer" *Color Res. Appl.* **3**, 125 (1978)
Walter W. "Optimum phosphor blends for fluorescent lamps" *Appl. Opt.* **10**, 1108 (1971)
Wegh R. T., Donker H., Oskam K. D., and Meijerink A. "Visible quantum cutting in $LiGdF_4$:Eu^{3+} through downconversion" *Science* **283**, 664 (1999)